NASA TR R-71

NATIONAL AERONAUTICS AND SPACE ADMINISTRATION

TECHNICAL REPORT
R-71

JET-BOUNDARY CORRECTIONS FOR LIFTING ROTORS CENTERED IN RECTANGULAR WIND TUNNELS

By HARRY H. HEYSON

1960

For sale by the Superintendent of Documents, U.S. Government Printing Office, Washington 25, D.C. Yearly subscription, $15; foreign, $19; single copy price varies according to size --------- Price 45 cents

TECHNICAL REPORT R-71

JET-BOUNDARY CORRECTIONS FOR LIFTING ROTORS CENTERED IN RECTANGULAR WIND TUNNELS

By HARRY H. HEYSON

Langley Research Center
Langley Field, Va.

TECHNICAL REPORT R-71

JET-BOUNDARY CORRECTIONS FOR LIFTING ROTORS CENTERED IN RECTANGULAR WIND TUNNELS

By Harry H. Heyson

SUMMARY

A theoretical analysis provides numerical values of the correction factor. The results indicate that at high speeds the corrections are the same as those for a wing but that at low speeds, for the cases considered, there is a large tunnel-induced upwash at the rotor. Increasing the rotor size decreases the correction factors for wide wind tunnels but has little effect upon the correction factors in deep narrow wind tunnels. The corrections are equivalent to a wind-tunnel-induced rate of climb (or sink), and considerable care will be required in the application to very low speed flight conditions.

INTRODUCTION

With lifting rotors, as with wings, a knowledge of the effect of jet boundaries is necessary in order to correlate successfully wind-tunnel test data with similar data obtained in free flight. Required jet-boundary corrections have been studied extensively for wings (refs. 1 to 3); however, little is known about the corresponding corrections for a lifting rotor. Most investigators, therefore, have been reduced to assuming either that the jet-boundary corrections for a rotor are the same as those for a wing or that these corrections are so small that they may be neglected.

The present paper treats the jet-boundary corrections for a rotor centered in a rectangular wind tunnel. The method used is similar to that used previously for wings; that is, images are arranged around the exterior of the test section in such a manner that the conditions imposed by the jet boundaries are met. The significant difference from a wing investigation is the use of a wake pattern which is more representative of a rotor wake. More specifically, the rotor wake is represented by a skewed elliptic vortex cylinder which, as shown in references 4 and 5, gives a reasonable approximation to the actual flow field of a lifting rotor.

For the limiting case of a vanishingly small rotor, as well as for the images which are far distant from the test section, the rotor wake may be reduced to a simple skewed line of point doublets. This approximation greatly reduces the labor involved in numerical calculations while, at the same time, it preserves the essential feature of the rotor wake, which is the large downwind deflection of the flow.

Numerical results are given for two different wind-tunnel-wall configurations: One is completely closed and the other is closed on the bottom only. The calculated correction factors cover a wide range of wind-tunnel width and height, rotor diameter, and wake skew angle. Several other effects which influence the corrections are treated less completely; for example, the effect of angle of attack is calculated only for a vanishingly small rotor, and the distribution of the interference velocities over the rotor is calculated only for one case.

SYMBOLS

A_R	area of rotor disk, sq ft
A_T	cross-sectional area of wind-tunnel test section, sq ft
$\bar{a}$	vector distance from an arbitrary point in space to vortex element (see fig. 1), ft
B	semiwidth of wind-tunnel test section, ft
C_L	lift coefficient, $\frac{\text{Lift}}{\frac{1}{2}\rho V^2 S}$

C_T thrust coefficient, $\frac{\text{Thrust}}{\rho\pi R^2(\Omega R)^2}$

$d\bar{s}$ vector length of vortex element, ft

H semiheight of wind-tunnel test section, ft

$\bar{i}, \bar{j}, \bar{k}$ unit vectors along x-, y-, and z-axes, respectively

K function related to induced velocity contribution of one image wake

k_L lift coefficient as used in reference 3, $\frac{\text{Lift}}{\rho V^2 S}$

l distance along rotor wake, ft

m, n, p integers (see eq. (19b))

m^* strength of doublet, ft^4/sec

$\bar{q}$ induced velocity vector, ft/sec

R rotor radius, ft

r radial distance from center of rotor, ft

S wing area, sq ft

s vector distance from origin to vortex element in wake, ft

V forward and wind-tunnel velocity, ft/sec

w vertical induced velocity, positive upward, ft/sec

w_0 vertical induced velocity at center of rotor, positive upward, $\frac{-\frac{1}{2}C_T\Omega R}{\sqrt{\mu^2+\lambda^2}}$, ft/sec

w_∞ vertical induced velocity at an arbitrary point near a rotor in free flight, positive upward, ft/sec

Δw vertical interference velocity at center of rotor, positive upward, ft/sec

x, y, z Cartesian coordinates centered in rotor (x measured rearward, y measured laterally at the right, z measured upward), (see fig. 1)

Z height above the ground, ft

α angle of attack of tip-path plane, radians

$\Delta\alpha$ jet-boundary-induced angle, radians

Γ circulation, sq ft/sec

γ wind-tunnel width-height ratio, B/H

δ_w wind-tunnel jet-boundary-correction factor

λ rotor inflow ratio, $\frac{V\sin\alpha + w_0}{\Omega R}$

μ rotor tip-speed ratio, $\frac{V\cos\alpha}{\Omega R}$

ρ mass density of air, slugs/cu ft

σ ratio of rotor diameter to tunnel width, R/B

ϕ_d potential of a single doublet, sq ft/sec

ϕ_∞ potential of a semi-infinite skewed row of doublets, sq ft/sec

χ wake skew angle, $\tan^{-1}\frac{-\mu}{\lambda}$, deg

ψ rotor azimuth angle, measured from downwind position, radians

Ω rotor rotational speed, radians/sec

Note that, contrary to usual practice in rotary-wing studies, all induced and interference velocities are considered herein to be positive when directed upward.

THEORY

INDUCED VELOCITY OF ROTOR IN FREE AIR

Rotary-wing induced-velocity theory is based upon an assumed vortex wake consisting of a skewed elliptical cylinder formed from a uniform distribution of circular vortex rings (fig. 1).

The induced velocities for the rotor wake in free air are found by integrating the Biot-Savart law

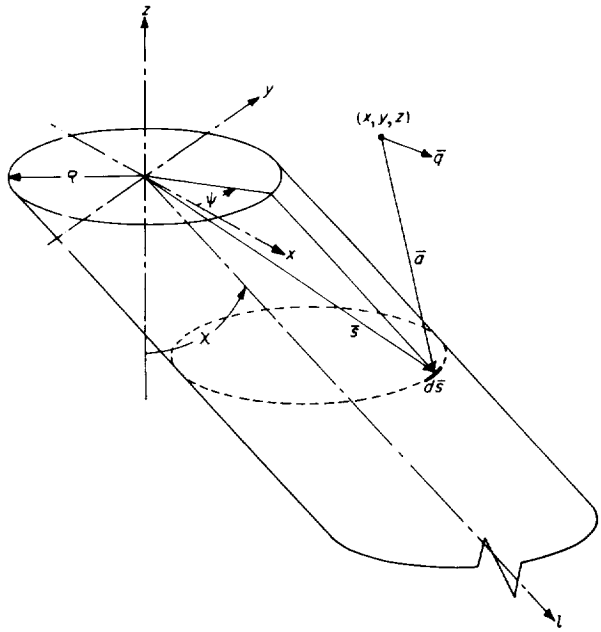

FIGURE 1.—Assumed wake of rotor in free air.

over the wake. Thus,

$$d\bar{q}=\frac{1}{4\pi}\frac{d\Gamma}{dl}\frac{d\bar{s}\times\bar{a}}{|\bar{a}|^3}\,dl \tag{1}$$

where (from fig. 1)

$$\bar{s}=\bar{i}(R\cos\psi+l\sin\chi)+\bar{j}(R\sin\psi)+\bar{k}(-l\cos\chi)$$

$$d\bar{s}=[\bar{i}(-R\sin\psi)+\bar{j}(R\cos\psi)+\bar{k}(0)]d\psi$$

$$\bar{a}=\bar{i}(R\cos\psi+l\sin\chi-x)+\bar{j}(R\sin\psi-y)+\bar{k}(-l\cos\chi-z)$$

so that

$$q=\frac{R}{4\pi}\frac{d\Gamma}{dl}\int_0^{2\pi}\int_0^{\infty}\frac{\begin{vmatrix}\bar{i} & \bar{j} & \bar{k}\\ -\sin\psi & \cos\psi & 0\\ (R\cos\psi+l\sin\chi-x) & (R\sin\psi-y) & (-l\cos\chi-z)\end{vmatrix}}{[(R\cos\psi+l\sin\chi-x)^2+(R\sin\psi-y)^2+(-l\cos\chi-z)^2]^{3/2}}\,dl\,d\psi \tag{2}$$

from which the normal, or $\bar{k}$, component of induced velocity is

$$w_\infty=\frac{R}{4\pi}\frac{d\Gamma}{dl}\int_0^{2\pi}\int_0^{\infty}\frac{x\cos\psi+y\sin\psi-R-l\sin\chi\cos\psi}{[R^2+x^2+y^2+z^2-2R(x\cos\psi+y\sin\psi)+2l(z\cos\chi-x\sin\chi+R\sin\chi\cos\psi)+l^2]^{3/2}}\,dl\,d\psi \tag{3}$$

The integration with respect to l may be accomplished with the aid of items 162 and 170 of reference 6. After substituting limits, equation (3) becomes

$$w_\infty=\frac{R}{4\pi}\frac{d\Gamma}{dl}\int_0^{2\pi}\frac{[(x\cos\psi+y\sin\psi-R)-\sin\chi\cos\psi\sqrt{R^2+x^2+y^2+z^2-2R(x\cos\psi+y\sin\psi)}]d\psi}{[\sqrt{R^2+x^2+y^2+z^2-2R(x\cos\psi+y\sin\psi)}+z\cos\chi-x\sin\chi+R\sin\chi\cos\psi]\sqrt{R^2+x^2+y^2+z^2-2R(x\cos\psi+y\sin\psi)}} \tag{4}$$

which for the special case of $x=y=z=0$ (the center of the rotor) reduces to

$$w_0=-\frac{1}{2}\frac{d\Gamma}{dl} \tag{5}$$

Substituting equation (5) in equation (4) and nondimensionalizing the result with respect to H, the semiheight of the wind tunnel, yield

$$w_\infty=\frac{-\sigma\gamma}{2\pi}w_0\int_0^{2\pi}\frac{\left[\left(\frac{x}{H}\cos\psi+\frac{y}{H}\sin\psi-\sigma\gamma\right)-\sin\chi\cos\psi\sqrt{\sigma^2\gamma^2+\left(\frac{x}{H}\right)^2+\left(\frac{y}{H}\right)^2+\left(\frac{z}{H}\right)^2-2\sigma\gamma\left(\frac{x}{H}\cos\psi+\frac{y}{H}\sin\psi\right)}\right]d\psi}{\left\{\left[\sqrt{\sigma^2\gamma^2+\left(\frac{x}{H}\right)^2+\left(\frac{y}{H}\right)^2+\left(\frac{z}{H}\right)^2-2\sigma\gamma\left(\frac{x}{H}\cos\psi+\frac{y}{H}\sin\psi\right)}+\frac{z}{H}\cos\chi-\frac{x}{H}\sin\chi+\sigma\gamma\sin\chi\cos\psi\right]\sqrt{\sigma^2\gamma^2+\left(\frac{x}{H}\right)^2+\left(\frac{y}{H}\right)^2+\left(\frac{z}{H}\right)^2-2\sigma\gamma\left(\frac{x}{H}\cos\psi+\frac{y}{H}\sin\psi\right)}\right\}} \tag{6}$$

Note that

$$\sigma\gamma=\frac{R}{B}\frac{B}{H}\frac{4\pi R}{4\pi R}\frac{2\gamma}{2\gamma}=\frac{A_R}{A_T}\frac{2\gamma}{\pi}\frac{2}{\sigma\gamma}$$

So that equation (6) may be rewritten as

$$w_\infty=w_0\frac{A_R}{A_T}\left[\frac{-2\gamma}{\pi}K\left(\frac{x}{H},\frac{y}{H},\frac{z}{H}\right)\right] \tag{7a}$$

where

$$K\left(\frac{x}{H},\frac{y}{H},\frac{z}{H}\right)=\frac{1}{\pi\sigma\gamma}\int_0^{2\pi}\frac{\left[\frac{x}{H}\cos\psi+\frac{y}{H}\sin\psi-\sigma\gamma-\sin\chi\cos\psi\sqrt{\sigma^2\gamma^2+\left(\frac{x}{H}\right)^2+\left(\frac{y}{H}\right)^2+\left(\frac{z}{H}\right)^2-2\sigma\gamma\left(\frac{x}{H}\cos\psi+\frac{y}{H}\sin\psi\right)}\right]d\psi}{\left\{\left[\sqrt{\sigma^2\gamma^2+\left(\frac{x}{H}\right)^2+\left(\frac{y}{H}\right)^2+\left(\frac{z}{H}\right)^2-2\sigma\gamma\left(\frac{x}{H}\cos\psi+\frac{y}{H}\sin\psi\right)}+\frac{z}{H}\cos\chi-\frac{x}{H}\sin\chi+\sigma\gamma\sin\chi\cos\psi\right]\sqrt{\sigma^2\gamma^2+\left(\frac{x}{H}\right)^2+\left(\frac{y}{H}\right)^2+\left(\frac{z}{H}\right)^2-2\sigma\gamma\left(\frac{x}{H}\cos\psi+\frac{y}{H}\sin\psi\right)}\right\}} \tag{7b}$$

INDUCED VELOCITY OF A VERY SMALL ROTOR

In the preceding section the field of the rotor was obtained by representing its wake by a skewed, uniform, elliptic cylinder comprised of very closely spaced vortex rings. Each of these rings is exactly equivalent (see ref. 7, for example) to a uniform doublet sheet circumscribed by the ring. Furthermore, the circulation of the vortex ring and the strength of the doublet sheet are uniquely related; that is,

$$\frac{\Gamma}{4\pi}=\frac{-m^*}{\pi R^2} \tag{8}$$

where m^* is the total strength of all the doublets comprising the circular sheet of radius R.

If the rotor is very small (or, more specifically, if the point of interest is far from the rotor) each doublet sheet may be considered as a point doublet, thus giving rise to a wake represented by a skewed semi-infinite line of point doublets, all directed vertically downward (fig. 2).

The potential function for any one of these doublets is

$$\phi_d=\frac{-m^*z}{(x^2+y^2+z^2)^{3/2}} \tag{9}$$

where x, y, and z are measured from the center of the doublet.

For the semi-infinite line of doublets, the potential function ϕ_∞ is

$$\phi_\infty = -\int_0^\infty \frac{\left(\frac{dm^*}{dl}\right)(z+l\cos\chi)dl}{[(x-l\sin\chi)^2+y^2+(z+l\cos\chi)^2]^{3/2}} \tag{10}$$

where x, y, and z are now measured from the end of the doublet row as in figure 2.

Equation (10) may be integrated by means of items 162 and 170 of reference 6. After substituting limits, the result is:

$$\phi_\infty = -\frac{dm^*}{dl}\left[\frac{z+\cos\chi\sqrt{x^2+y^2+z^2}}{(\sqrt{x^2+y^2+z^2}+z\cos\chi-x\sin\chi)\sqrt{x^2+y^2+z^2}}\right] \tag{11}$$

The vertical induced velocity will then be the partial derivative of ϕ_∞ with respect to z, or

$$w_\infty = \frac{\partial\phi_\infty}{\partial z} = -\frac{dm^*}{dl}\left\{\frac{x^2+y^2}{(\sqrt{x^2+y^2+z^2}+z\cos\chi-x\sin\chi)(r^2+y^2+z^2)^{3/2}}\right.$$
$$\left.-\left[\frac{z+\cos\chi\sqrt{x^2+y^2+z^2}}{(\sqrt{x^2+y^2+z^2}+z\cos\chi-x\sin\chi)\sqrt{x^2+y^2+z^2}}\right]^2\right\} \tag{12}$$

In order to relate the strength of the line of doublets to quantities normally associated with a

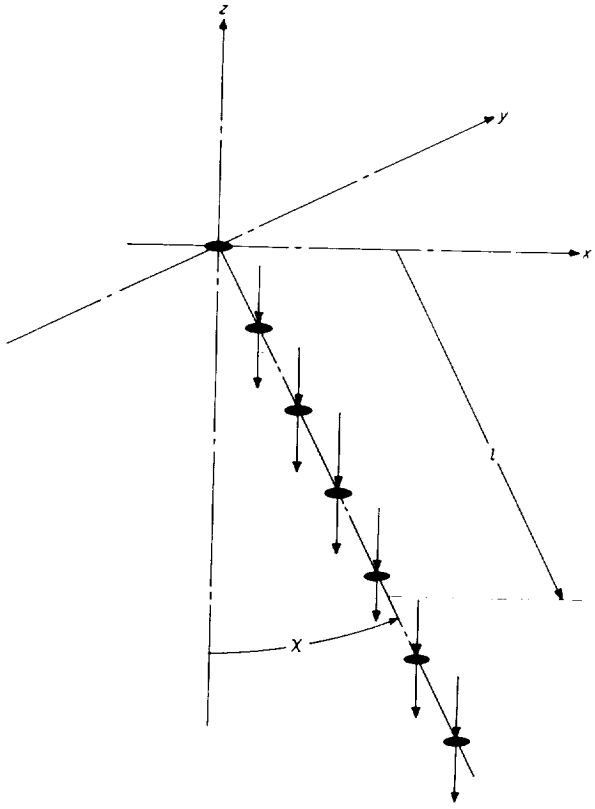

FIGURE 2.—Wake of a very small rotor as represented by a semi-infinite row of vertically directed doublets.

rotor, note that, in consequence of equation (8),

$$\frac{dm^*}{dl}=-\frac{R^2}{4}\frac{d\Gamma}{dl} \tag{13}$$

However, the induced velocity at the center of the rotor is (eq. (5))

$$w_0=-\frac{1}{2}\frac{d\Gamma}{dl} \tag{14}$$

so that

$$\frac{dm^*}{dl}=w_0\frac{R^2}{2} \tag{15}$$

Substituting equation (15) into equation (12) and nondimensionalizing the result with respect to H, the semiheight of the wind tunnel, yield

$$w_\infty=-\frac{w_0R^2}{2H^2}\left\{\frac{\left(\frac{x}{H}\right)^2+\left(\frac{y}{H}\right)^2}{\left[\sqrt{\left(\frac{x}{H}\right)^2+\left(\frac{y}{H}\right)^2+\left(\frac{z}{H}\right)^2}+\frac{z}{H}\cos\chi-\frac{x}{H}\sin\chi\right]\left[\left(\frac{x}{H}\right)^2+\left(\frac{y}{H}\right)^2+\left(\frac{z}{H}\right)^2\right]^{3/2}}\right.$$
$$\left.-\left\{\frac{\frac{z}{H}+\cos\chi\sqrt{\left(\frac{x}{H}\right)^2+\left(\frac{y}{H}\right)^2+\left(\frac{z}{H}\right)^2}}{\left[\sqrt{\left(\frac{x}{H}\right)^2+\left(\frac{y}{H}\right)^2+\left(\frac{z}{H}\right)^2}+\frac{z}{H}\cos\chi-\frac{x}{H}\sin\chi\right]\sqrt{\left(\frac{x}{H}\right)^2+\left(\frac{y}{H}\right)^2+\left(\frac{z}{H}\right)^2}}\right\}^2\right] \tag{16}$$

which, after some manipulation, may be rewritten in the same form as equation (7a); that is

$$w_\infty=w_0\frac{A_R}{A_T}\left[-\frac{2\gamma}{\pi}K\left(\frac{x}{H},\frac{y}{H},\frac{z}{H}\right)\right] \tag{17a}$$

where

$$K\left(\frac{x}{H},\frac{y}{H},\frac{z}{H}\right)=\frac{\left(\frac{x}{H}\right)^2+\left(\frac{y}{H}\right)^2}{\left[\sqrt{\left(\frac{x}{H}\right)^2+\left(\frac{y}{H}\right)^2+\left(\frac{z}{H}\right)^2}+\frac{z}{H}\cos\chi-\frac{x}{H}\sin\chi\right]\left[\left(\frac{x}{H}\right)^2+\left(\frac{y}{H}\right)^2+\left(\frac{z}{H}\right)^2\right]^{3/2}}$$
$$-\left\{\frac{\frac{z}{H}+\cos\chi\sqrt{\left(\frac{x}{H}\right)^2+\left(\frac{y}{H}\right)^2+\left(\frac{z}{H}\right)^2}}{\left[\sqrt{\left(\frac{x}{H}\right)^2+\left(\frac{y}{H}\right)^2+\left(\frac{z}{H}\right)^2}+\frac{z}{H}\cos\chi-\frac{x}{H}\sin\chi\right]\sqrt{\left(\frac{x}{H}\right)^2+\left(\frac{y}{H}\right)^2+\left(\frac{z}{H}\right)^2}}\right\}^2 \tag{17b}$$

SOLID LOWER BOUNDARY

In the case of a rotor the wake is inclined sharply across the airstream and, in general, will intersect the floor of the tunnel at some short distance downstream. In the present analysis the wake is considered to continue downstream coincident with the tunnel floor. In order to satisfy the condition of zero flow through the solid boundary, there will be, among others, a mirror-image wake directly below the boundary. This mirror-image wake also flows along the boundary after it intersects the floor. Since these parts of the two wakes are of equal and opposite strength and coincident, they may be ignored in the calculations, and the wakes may be considered to terminate at the point of intersection.

Consider first the flow caused only by the rotor wake in the test section and by the one image wake

directly below it (fig. 3). By superposition, from either equation (7) or equation (17), the vertical induced velocity is given by

$$w=w_0\frac{A_R}{A_T}\left\{-\frac{2\gamma}{\pi}\left[K\left(\frac{x}{H},\frac{y}{H},\frac{z}{H}\right)\right.\right.$$
$$-K\left(\frac{x}{H}-\tan\chi,\frac{y}{H},\frac{z}{H}+1\right)-K\left(\frac{x}{H},\frac{y}{H},\frac{-z}{H}-2\right)$$
$$\left.\left.+K\left(\frac{x}{H}-\tan\chi,\frac{y}{H},\frac{-z}{H}-1\right)\right]\right\} \qquad (18)$$

where, now, x, y, and z are measured from the end of the upper or "real" wake.

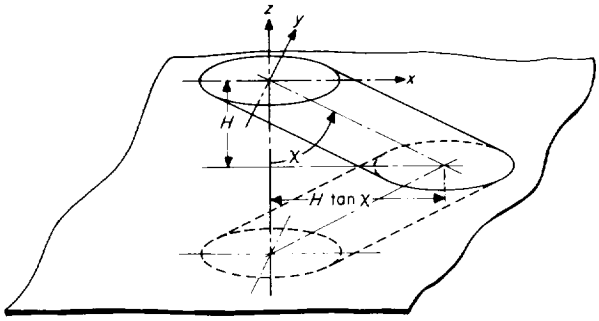

FIGURE 3.—Wake and image wake directly below floor of wind tunnel.

It will be observed that the superpositions used in developing equation (18) require that the rotor has zero angle of attack. The effect of angle of attack will be discussed at length in a subsequent section of this paper.

WIND TUNNEL WITH SOLID LOWER BOUNDARY

The two wind-tunnel configurations considered in this paper have solid lower boundaries. An indication of the complete image system required to represent the boundary conditions for the closed tunnel is shown in figure 4(a) and that for the tunnel which is closed on the bottom only is shown in figure 4(b). It may be seen that these image systems are similar to those for wings. Images are reflected across solid boundaries with opposite sign so as to meet the requirement of zero normal velocity at the boundary, and images are reflected across free boundaries with like sign so as to meet the condition of a continuous pressure gradient across the boundary. It may further be seen that all images occur in sets identical to the simple solid-boundary wake and image discussed in the previous section. Thus, by superposition, from equation (18) (with the following substitutions: $\frac{x}{H}=\frac{x}{H}$; $\frac{y}{H}=\frac{y}{H}-\frac{2mB}{H}=\frac{y}{H}-2m\gamma$; $\frac{z}{H}=\frac{z}{H}-\frac{4nH}{H}=\frac{z}{H}-4n$) the *interference* velocity at the center of the

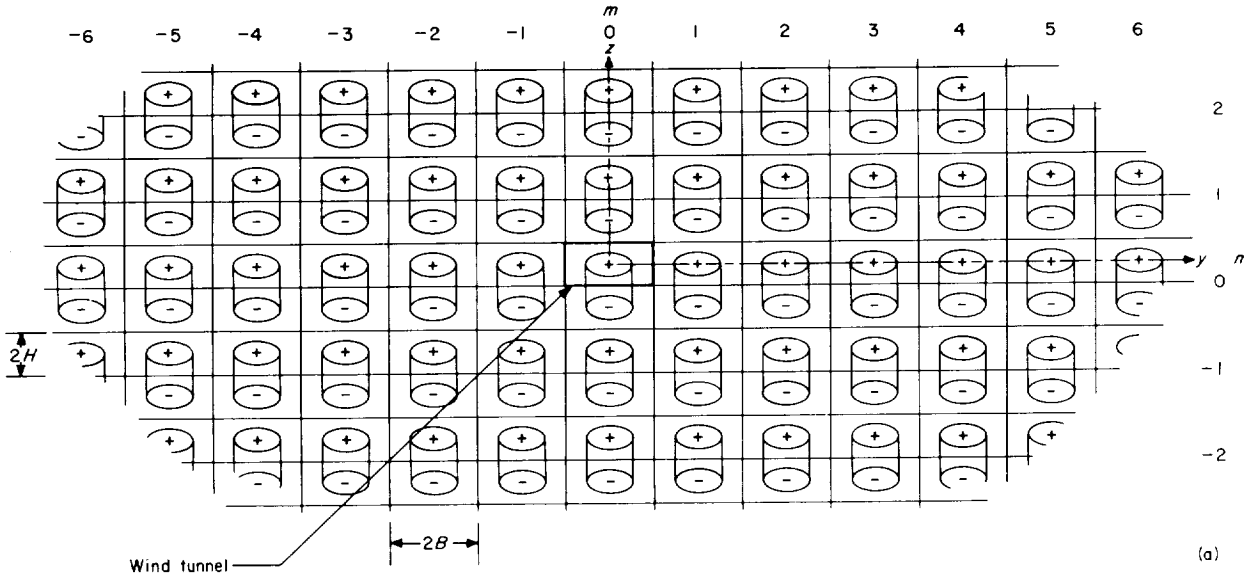

(a) Closed wind tunnel.

FIGURE 4.—Image system representing effect of wind-tunnel boundaries. Plus signs indicate same direction of vorticity as wake in wind tunnel.

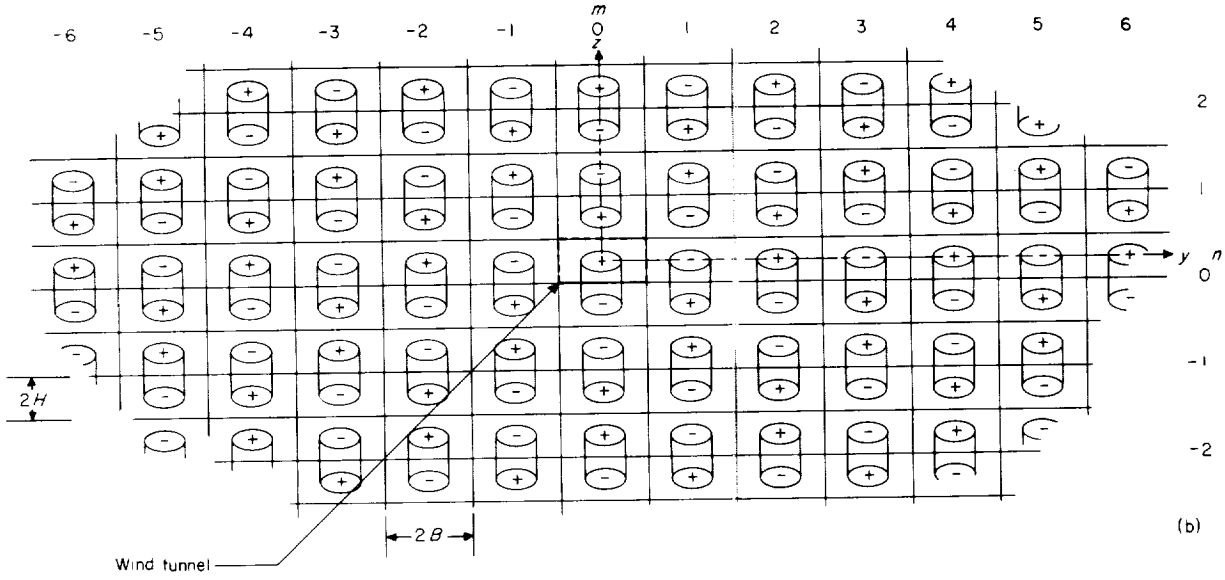

(b) Wind tunnel closed on bottom only.

FIGURE 4.—Concluded.

test section is found to be

$$\Delta w = \delta_w \frac{\Lambda_R}{\Lambda_T} w_0 \tag{19a}$$

where

$$\delta_w = -\frac{2\gamma}{\pi}\left\{ \sum_{\substack{n=-\infty \\ n=m\neq 0}}^{\infty} \sum_{m=-\infty}^{\infty} (-1)^p \left[K\left(\frac{x}{H}, \frac{y}{H}-2m\gamma, \frac{z}{H}-4n\right) \right.\right.$$
$$-K\left(\frac{x}{H}-\tan\chi, \frac{y}{H}-2m\gamma, \frac{z}{H}-4n+1\right)-K\left(\frac{x}{H}, \frac{y}{H}-2m\gamma, -\frac{z}{H}+4n-2\right)$$
$$\left.+K\left(\frac{x}{H}-\tan\chi, \frac{y}{H}-2m\gamma, -\frac{z}{H}+4n-1\right)\right]-K\left(\frac{x}{H}-\tan\chi, \frac{y}{H}, \frac{z}{H}+1\right)$$
$$\left.-K\left(\frac{x}{H}, \frac{y}{H}, -\frac{z}{H}-2\right)+K\left(\frac{x}{H}-\tan\chi, \frac{y}{H}, -\frac{z}{H}-1\right)\right\} \tag{19b}$$

where $p=0$ for the closed tunnel and $p=m+n$ for the tunnel which is closed on the bottom only.

Notice that the terms corresponding to $m=n=0$ are omitted from the summation but are represented separately at the end of equation (19b). These final terms do not include the term representing the semi-infinite rotor wake itself, since it is *only* the *interference* velocity which is of primary concern herein.

When the skew angle χ is 90° the wake progresses directly downstream and never intersects the lower boundary. Thus, for this case, the second, fourth, fifth, and seventh terms on the right-hand side of equation (19b) are zero and may be ignored.

FREE BOUNDARIES AT VERY LOW SPEEDS

It will be noted (ref. 8, for example) that the boundary condition for a free boundary depends upon the induced velocities being small in comparison with the wind-tunnel velocity. For very low speeds (low skew angles) this condition is largely violated since the induced effects may be large

even when the rotor is small. In the limiting case of hovering ($\chi=0$), the wind-tunnel jet does not even exist and the free boundaries will have no effect. Thus, for the wind tunnel considered herein which is closed on the bottom only, the only boundary which contributes an interference velocity in hovering is the tunnel floor. For other very low forward speeds the open boundaries will contribute somewhat to the total interference, although this contribution will not necessarily be that indicated by the calculated corrections. Consequently, for low forward speeds, the interference velocities are assumed herein to lie between those calculated for the complete tunnel and those calculated for the tunnel floor only.

If it may be assumed that the tunnel floor is effectively of infinite width rather than of width $2B$, the correction factor for the floor only may be obtained from equation (19b) by omitting all terms except the last three. At the center of a very small rotor, appendix A shows that the correction factor for the tunnel bottom reduces to the simpler form

$$\delta_w=-\frac{2\gamma}{\pi}\left(\frac{3}{2}\cos^4\chi+\frac{1}{4}\right) \tag{20}$$

The correspondence of the correction factors for the wind-tunnel floor only to ground effect is obvious. This subject is discussed in reference 9.

OPEN LOWER BOUNDARY

If the lower boundary of the jet is free, the errors incurred will be even greater since the wake actually intersects this free boundary. Figure 5 is a dust flow photograph of the flow generated by a rotor at low speed in a completely open wind tunnel. It may be seen that the wake is deflected completely out of the wind tunnel. Thus, with a free lower surface, there is some doubt as to the actual boundary condition required. Under conditions as severe as that shown in figure 5 there is even considerable doubt that the wind-tunnel results can be successfully correlated with any free-flight condition. At moderately large skew angles, the wake will approach the lower surface of the airstream somewhere within the closed return passage. Under these conditions, the effect of finite jet length (ref. 10) would become so large that it could no longer be ignored. At present, however, the inclusion of this effect is considered prohibitively difficult. At very high skew angles, the wind-tunnel results can probably be corrected fairly well by use of the normal corrections for a wing.

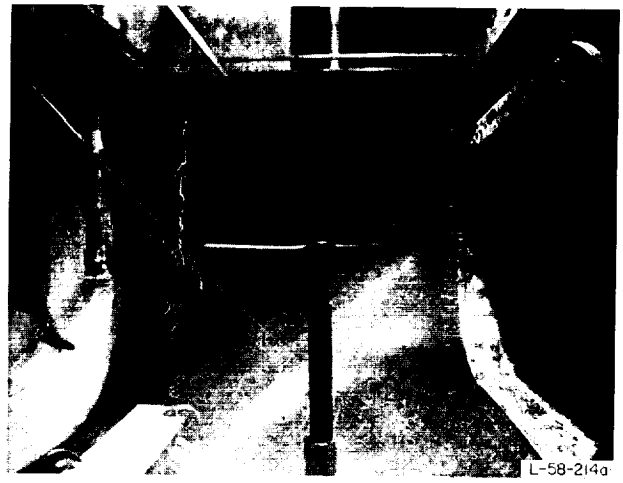

FIGURE 5.—Photograph of flow caused by a rotor at low speed in a completely open wind tunnel.

In view of the uncertainty of the boundary condition on a free lower surface, no such wind-tunnel configurations have been considered in the present investigation.

EFFECT OF ANGLE OF ATTACK

Thus far in the analysis, it has been assumed that the rotor is at zero angle of attack. The analysis for other angles of attack will be restricted herein to the case of a very small rotor since this restriction greatly simplifies the problem.

When the rotor is very small, an angle of attack produces two predominant effects. First, the wake angle with respect to the tunnel axis will now be $\chi-\alpha$ rather than simply χ (fig. 6). The quantity $\chi-\alpha$ may thus be considered as an effective skew angle. Second, the direction of the wake doublets will no longer be vertical since they remain perpendicular to the tip-path plane. This effect may, however, be treated by considering the wake to be a linear combination of a wake of vertical doublets and of a wake of horizontal doublets having strengths proportional to the cosine and sine of α, respectively. The induced velocity for a wake of vertical doublets

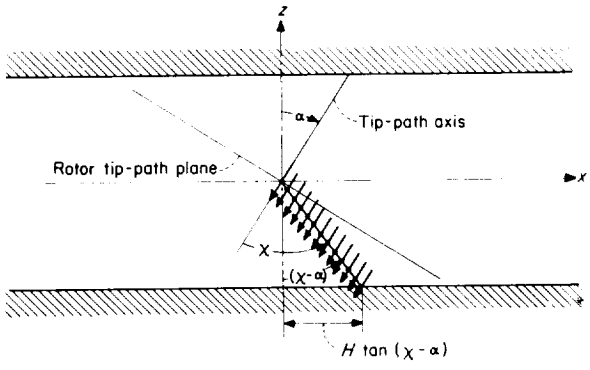

FIGURE 6. - Wake of small rotor operating at angle of attack in wind tunnel.

was derived in a preceding section of this paper. The induced velocity for a wake of horizontal doublets will now be derived.

For a single horizontal forward-directed doublet, the potential ϕ_d is

$$\phi_d = \frac{-m^* x}{(x^2+y^2+z^2)^{3/2}} \tag{21}$$

where x, y, and z are measured from the center of the doublet.

Thus, for a semi-infinite line (fig. 7) of such doublets, the potential ϕ_∞ will be

$$\phi_\infty = -\int_0^\infty \frac{\frac{dm^*}{dl}(x-\sin\chi)dl}{[(x-l\sin\chi)^2+y^2+(z+l\cos\chi)^2]^{3/2}} \tag{22}$$

The vertical induced velocity will then be

$$w_\infty = \frac{\partial\phi_\infty}{\partial z} = \frac{dm^*}{dl}\left[\frac{xz}{(\sqrt{x^2+y^2+z^2}+z\cos\chi-x\sin\chi)(x^2+y^2+z^2)^{3/2}}\right.$$
$$\left.+\frac{(x-\sin\chi\sqrt{x^2+y^2+z^2})(z+\cos\chi\sqrt{x^2+y^2+z^2})}{(\sqrt{x^2+y^2+z^2}+z\cos\chi-x\sin\chi)^2(x^2+y^2+z^2)}\right] \tag{24}$$

Finally, after nondimensionalization (and the use of eq. (13)), equation (24) may be rewritten as

$$w_\infty = w_0\frac{A_R}{A_T}\left[\frac{-2\gamma}{\pi}K\left(\frac{x}{H},\frac{y}{H},\frac{z}{H}\right)\right] \tag{25a}$$

where

$$K\left(\frac{x}{H},\frac{y}{H},\frac{z}{H}\right) = -\left\{\frac{\left(\frac{x}{H}\right)\left(\frac{z}{H}\right)}{\left[\sqrt{\left(\frac{x}{H}\right)^2+\left(\frac{y}{H}\right)^2+\left(\frac{z}{H}\right)^2}+\frac{z}{H}\cos\chi-\frac{x}{H}\sin\chi\right]\left[\left(\frac{x}{H}\right)^2+\left(\frac{y}{H}\right)^2+\left(\frac{z}{H}\right)^2\right]^{3/2}}\right.$$
$$\left.+\frac{\left[\frac{x}{H}-\sin\chi\sqrt{\left(\frac{x}{H}\right)^2+\left(\frac{y}{H}\right)^2+\left(\frac{z}{H}\right)^2}\right]\left[\frac{z}{H}+\cos\chi\sqrt{\left(\frac{x}{H}\right)^2+\left(\frac{y}{H}\right)^2+\left(\frac{z}{H}\right)^2}\right]}{\left[\sqrt{\left(\frac{x}{H}\right)^2+\left(\frac{y}{H}\right)^2+\left(\frac{z}{H}\right)^2}+\frac{z}{H}\cos\chi-\frac{x}{H}\sin\chi\right]^2\left[\left(\frac{x}{H}\right)^2+\left(\frac{y}{H}\right)^2+\left(\frac{z}{H}\right)^2\right]}\right\} \tag{25b}$$

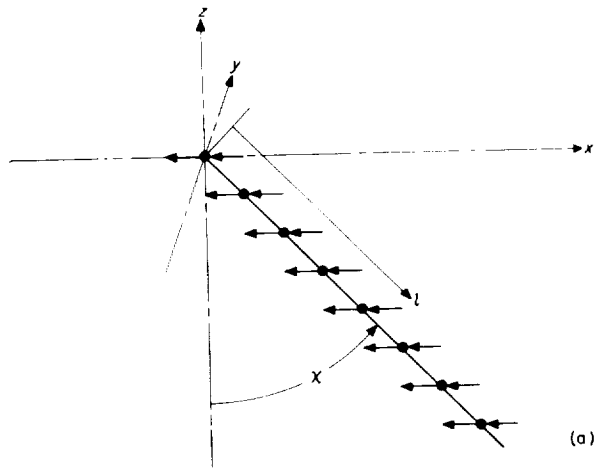

(a) Wake in free air.

FIGURE 7. - Wake of horizontal doublets.

where x, y, and z are now measured from the start of the line of doublets.

Equation (22) may be integrated by means of items 162 and 170 of reference 6. After substituting the limits of integration, the result is

$$\phi_\infty = \frac{-\frac{dm^*}{dl}(x-\sin\chi\sqrt{x^2+y^2+z^2})}{(\sqrt{x^2+y^2+z^2}+z\cos\chi-x\sin\chi)\sqrt{x^2+y^2+z^2}} \tag{23}$$

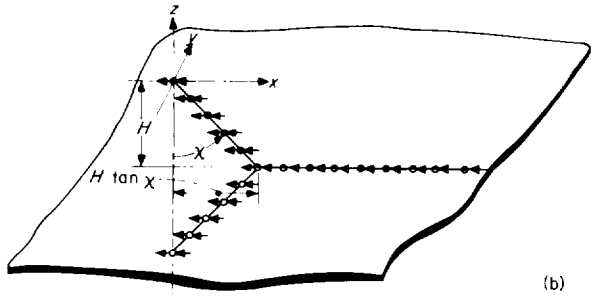

(b) Wake and image directly below floor of wind tunnel.

FIGURE 7.—Concluded.

Figure 7(b) shows the combination of horizontal doublet wake and images which satisfies the condition of a solid floor below the rotor. It will be observed that the effects of the real and image wakes trailing along the floor do not cancel for this case. (Note that sufficient tunnel velocity is assumed so that the wake does trail rearward.) Instead, the effects of these wakes now add. If it is observed that the wake along the floor is identical to the wake at $\chi=90°$ (except for being displaced downward and rearward), the contribution of the two wakes along the floor, in terms of K, may be found directly from equation (25b) as

$$2K|_{\chi=90°}\left(\frac{x}{H}-\tan\chi,\frac{y}{H},\frac{z}{H}+1\right)$$

$$=-2\left\{\frac{\left(\frac{x}{H}-\tan\chi\right)\left(\frac{z}{H}+1\right)}{\left[\sqrt{\left(\frac{x}{H}-\tan\chi\right)^2+\left(\frac{y}{H}\right)^2+\left(\frac{z}{H}+1\right)^2}-\frac{x}{H}+\tan\chi\right]\left[\left(\frac{x}{H}-\tan\chi\right)^2+\left(\frac{y}{H}\right)^2+\left(\frac{z}{H}+1\right)^2\right]^{3/2}}\right.$$

$$\left.+\frac{\left[\frac{x}{H}-\tan\chi-\sqrt{\left(\frac{x}{H}-\tan\chi\right)^2+\left(\frac{y}{H}\right)^2+\left(\frac{z}{H}+1\right)^2}\right]\left(\frac{z}{H}+1\right)}{\left[\sqrt{\left(\frac{x}{H}-\tan\chi\right)^2+\left(\frac{y}{H}\right)^2+\left(\frac{z}{H}+1\right)^2}-\frac{x}{H}+\tan\chi\right]^2\left[\left(\frac{x}{H}-\tan\chi\right)^2+\left(\frac{y}{H}\right)^2+\left(\frac{z}{H}+1\right)^2\right]}\right\} \quad (26)$$

The use of equation (26) then alters the expression for the correction factor (see eq. (19b)) to the form

$$\delta_u=-\frac{2\gamma}{\pi}\left\{\sum_{\substack{n=-\infty\\ n=m\neq 0}}^{\infty}\sum_{m=-\infty}^{\infty}(-1)^p\left[K\left(\frac{x}{H},\frac{y}{H}-2m\gamma,\frac{z}{H}-4n\right)-K\left(\frac{x}{H}-\tan\chi,\frac{y}{H}-2m\gamma,\frac{z}{H}-4n+1\right)\right.\right.$$

$$-K\left(\frac{x}{H},\frac{y}{H}-2m\gamma,-\frac{z}{H}+4n-2\right)+K\left(\frac{x}{H}-\tan\chi,\frac{y}{H}-2m\gamma,-\frac{z}{H}+4n-1\right)$$

$$\left.+2K|_{\chi=90°}\left(\frac{x}{H}-\tan\chi,\frac{y}{H}-2m\gamma,\frac{z}{H}-4n+1\right)\right]-K\left(\frac{x}{H}-\tan\chi,\frac{y}{H},\frac{z}{H}+1\right)-K\left(\frac{x}{H},\frac{y}{H},-\frac{z}{H}-2\right)$$

$$\left.+K\left(\frac{x}{H}-\tan\chi,\frac{y}{H},-\frac{z}{H}-1\right)+2K|_{\chi=90°}\left(\frac{x}{H}-\tan\chi,\frac{y}{H},\frac{z}{H}+1\right)\right\} \quad (27)$$

where, again, $p=0$ for the closed tunnel and $p=m+n$ for the tunnel which is closed on the bottom only. When the skew angle is 90°, the wake never intersects the wind-tunnel floor, so that the second, fourth, fifth, sixth, eighth, and ninth terms on the right-hand side of equation (27) are zero and may be neglected.

Values of the jet-boundary-correction factor can be obtained by inserting the values of K obtained from equations (25b) and (26) into equation (27).

The correction factors for the wind-tunnel floor only, which involve the last four terms of equation (27), may be expressed in simpler form (appendix B) in this case also; that is,

$$\delta_w=\frac{2\gamma}{\pi}\left(\sin\chi\cos^3\chi-\frac{1}{2}\sin^3\chi\cos\chi-\frac{1}{4}\tan\frac{\chi}{2}-2\cos^3\chi\right) \tag{28}$$

NUMERICAL CALCULATIONS

The equations for the wind-tunnel jet-boundary-correction factors (as given by eqs. (7b), (17b), (19b), and (25b)) were programed for use on a high-speed automatic computing machine (IBM 704 electronic data processing machine). The summations were carried out until additional terms were of the order of 0.00001 of the sum of the last three terms of equation (19b). This occasionally required terms with values of m or n as great as 12. For the small rotor ($\sigma=0$), each combination of γ and χ required approximately 30 seconds of computing time.

For finite-size rotors ($\sigma\neq0$), the values of K (eq. (7b)) were obtained by computing 240 values of the integrand around the azimuth and then integrating by means of Simpson's rule. All terms of the summation for which the absolute values of both m and n were less than or equal to 2 were computed by means of equation (7). The effect of images farther removed from the origin than this was computed by assuming that the rotor was small (eq. (17)), since at these distances the difference between the two procedures should be negligible. Rather than recompute the effect of the distant images, their contribution to δ_w was merely saved from the $\sigma=0$ calculations and then added manually to the correction for the more centrally located images.

The capacity of the computing machine made it possible, even for finite-size rotors, to compute the correction factor for the closed tunnel, the tunnel closed on the bottom only, and the tunnel floor only in parallel with each other. A total of approximately 5 minutes was required to compute all three numerical results for each combination of γ, σ, and χ. For the special case of $\chi=90°$, where many terms of equation (19b) are always zero, this time was reduced to approximately 3 minutes.

The calculated correction factors for $0.5\leqq\gamma\leqq2.0$, $0\leqq\sigma\leqq0.95$, and $0\leqq\chi\leqq90°$ are presented in tables I to IV.

DISCUSSION

COMPARISON WITH WINGS

It is observed (fig. 4) that for a very small rotor at $\chi=90°$, the complete system of wake images is reduced to a system of semi-infinite vertically directed line doublets (which are identical to the vortex doublets of ref. 1) lying along the center lines of the tunnel images. Since the image systems for the wing and for the rotor at $\chi=90°$ are identical, the calculated correction factors for the wing and for the rotor should also be identical. Note, however, that the present results are expressed in terms of the rotor induced velocity w_0. Since at $\chi=90°$, $w_0=-\frac{C_L}{4}=-\frac{k_L}{2}$, there will be a constant factor of -4 or -2 between the present results and those of references 1, 2, and 3.[1]

The calculated correction factors from reference 3, in terms of the present definition, are given in table V, where they may be compared with the results of the present calculation. Such small differences as are shown are merely a measure of the accuracy of the computing procedure.

Since the wake of a wing is very similar to that of a rotor at high forward speeds, it would be expected that the correction factors for a finite-size rotor, in the limiting case of $\chi=90°$, would be identical to those for an elliptically loaded wing. Table VI shows a comparison between the present

[1] Reference 3 (see also ref. 2) called attention to certain errors in the original version of reference 1, in consequence of which an errata sheet was appended to reference 1. Major revisions were made before reference 1 was incorporated into the Eighteenth Annual Report of the NACA (1932). The numerical values of the correction factor for the closed-on-bottom-only wind tunnel, in particular, were completely recomputed. The new values, however, were apparently recalculated from the equations of reference 3 without regard to the use of k_L rather than C_L in that paper. Thus, even in the revised version of reference 1, the correction factors for the closed-on-bottom-only wind tunnel are incorrect by a factor of 2.

results and those for a wing (ref. 11). It will be observed that the correction factors for the wing and rotor, in general, follow the same trends, but that there are differences which increase as the size of the rotor increases. The major reason for these differences is that the correction factors for the wing were computed on the basis of an *average* interference across the span, whereas the corrections for the rotor were obtained by computing the interference at the rotor center *only*. The distribution of the interference velocity over the rotor will be discussed subsequently.

EFFECT OF WAKE SKEW ANGLE

Figure 8 shows the manner in which the jet-boundary corrections for a small rotor vary with wake skew angle. In general, for both wind-tunnel-wall configurations investigated, the interference velocities, which are identical to those of a wing at $\chi = 90°$, rapidly change to indicate a large induced upwash as the skew angle approaches zero. The change with skew angle is greatest for the wind tunnels with the largest width-height ratio. The reason for this change is primarily a greatly increased effect of the tunnel floor. This effect may be seen in figure 8(b) where the wind-tunnel correction factors closely approach the correction factors for the tunnel floor only as the skew angle approaches zero.

In free flight, the wake skew angle increases rapidly from zero in hovering. For a typical, lightly loaded helicopter rotor, skew angles of 80° to 90° are obtained at tip-speed ratios of the order of 0.10 to 0.15. Thus, for wind-tunnel tests at cruising and high-speed flight conditions (high skew angles), the wind-tunnel corrections for a rotor are essentially the same as those for a wing. In hovering, and in the transition speed range (low skew angles), however, the jet-boundary corrections will be much larger and will change rapidly with forward velocity.

EFFECT OF WIDTH-HEIGHT RATIO

For the two wind-tunnel configurations examined, figure 9 shows that there is no width-height ratio which yields a zero-correction wind tunnel for all rotor flight conditions. For high-skew-angle flight conditions, the wide tunnels are probably superior since the correction factors are somewhat smaller. For tests at very low speeds, however, the situation is reversed, and it may be preferable to have a narrow deep test section. This is particularly true for low-speed static-stability tests of large rotors, since the variation in the correction factors with speed for a wide tunnel may be large enough to produce serious errors in the stability derivatives with respect to velocity.

EFFECT OF ROTOR SIZE

The calculated jet-boundary-correction factors for rotors with finite size are shown graphically in figures 10 and 11 as a function of the ratio of rotor diameter to tunnel width σ and in figures 12 and 13 as a function of wake skew angle. Examination of these figures indicates that the correction factors are influenced to a large degree by the ratio of rotor diameter to tunnel width and that the degree of influence is largely dependent upon both the wake skew angle and the wind-tunnel width-height ratio. In general, the following trends may be observed. For wind tunnels which have greater width than height, increased rotor size entails major reductions in the correction factor. This reduction is greatest at the low skew angles associated with hovering and transitional flight. The reduction of the correction factor decreases as the width of the tunnel decreases, until at values of γ on the order of 0.5 the effect of rotor size on the correction factor is very small and in some cases negligible.

EFFECT OF ANGLE OF ATTACK

It was pointed out in a previous section that the effect of angle of attack could, in the case of a very small rotor ($\sigma=0$), be accounted for by using an effective wake skew angle $\chi-\alpha$ and by including the interference caused by a wake of suitably selected horizontal doublets. Figure 14 (see also table IV) presents the jet-boundary-correction factors for a wake of horizontal forward-directed doublets of unit strength.

It will be observed that the correction factors for the horizontal doublet wake are of the same order of magnitude and show the same trends with skew angle as the correction factors previously presented for the vertical doublet wake. A comparison of the correction factors for the various wind-tunnel configurations indicates that, as before, the wind-tunnel floor is responsible for the major portion of the correction.

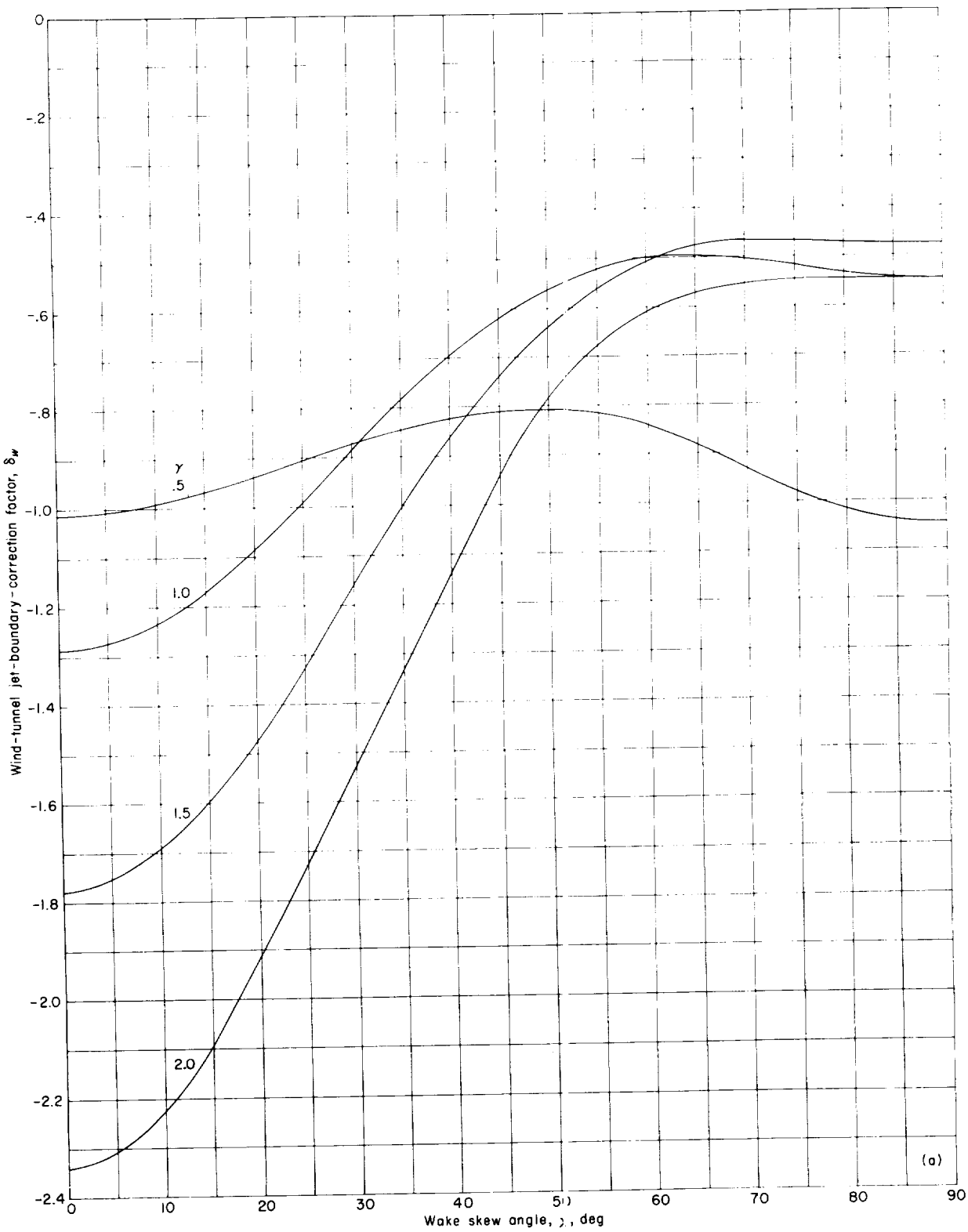

(a) Closed wind tunnels.

FIGURE 8.—Wind-tunnel jet-boundary-correction factors for a small rotor as a function of wake skew angle.

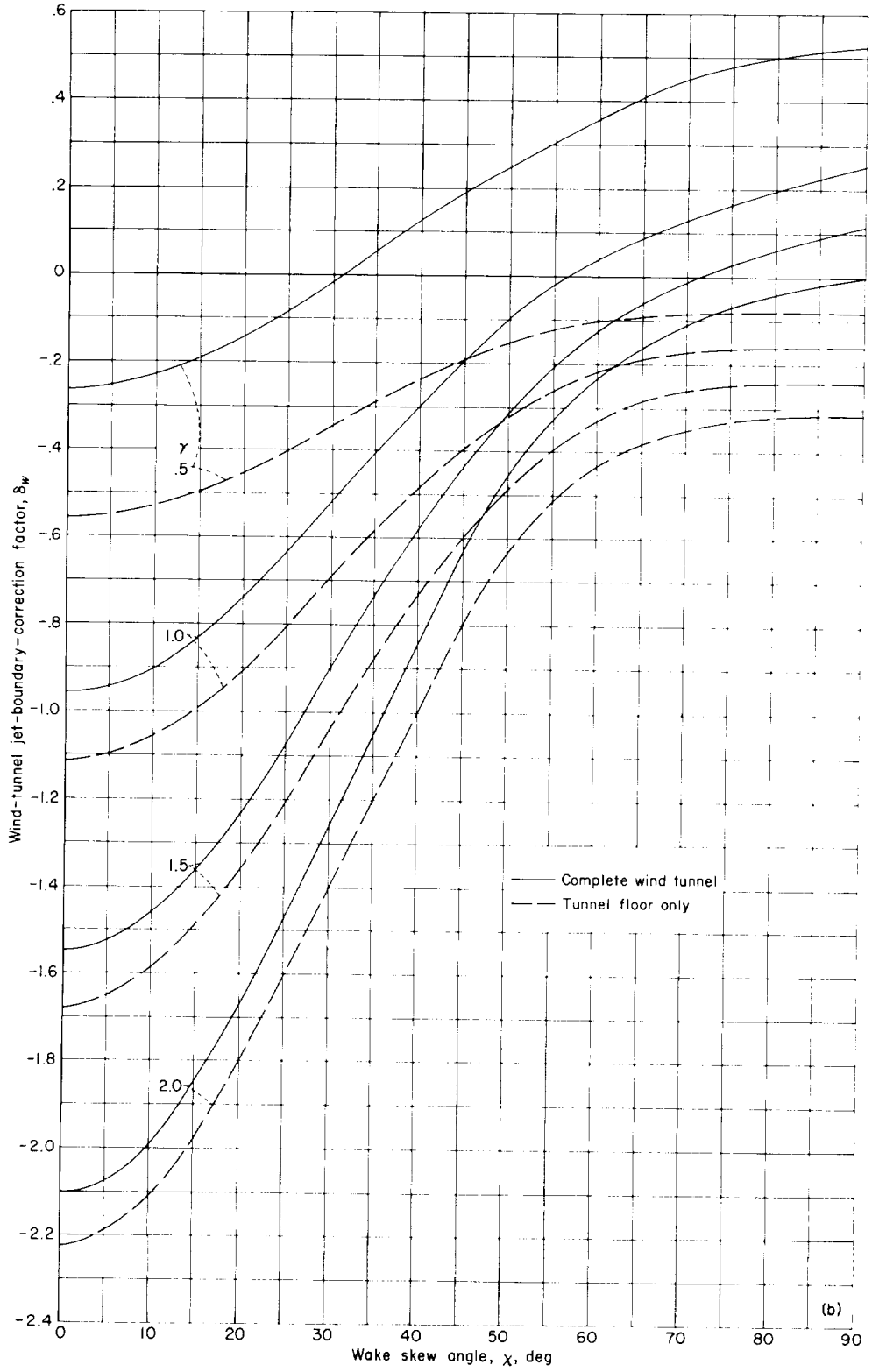

(b) Wind tunnels closed on bottom only.

FIGURE 8.—Concluded.

578834—61——3

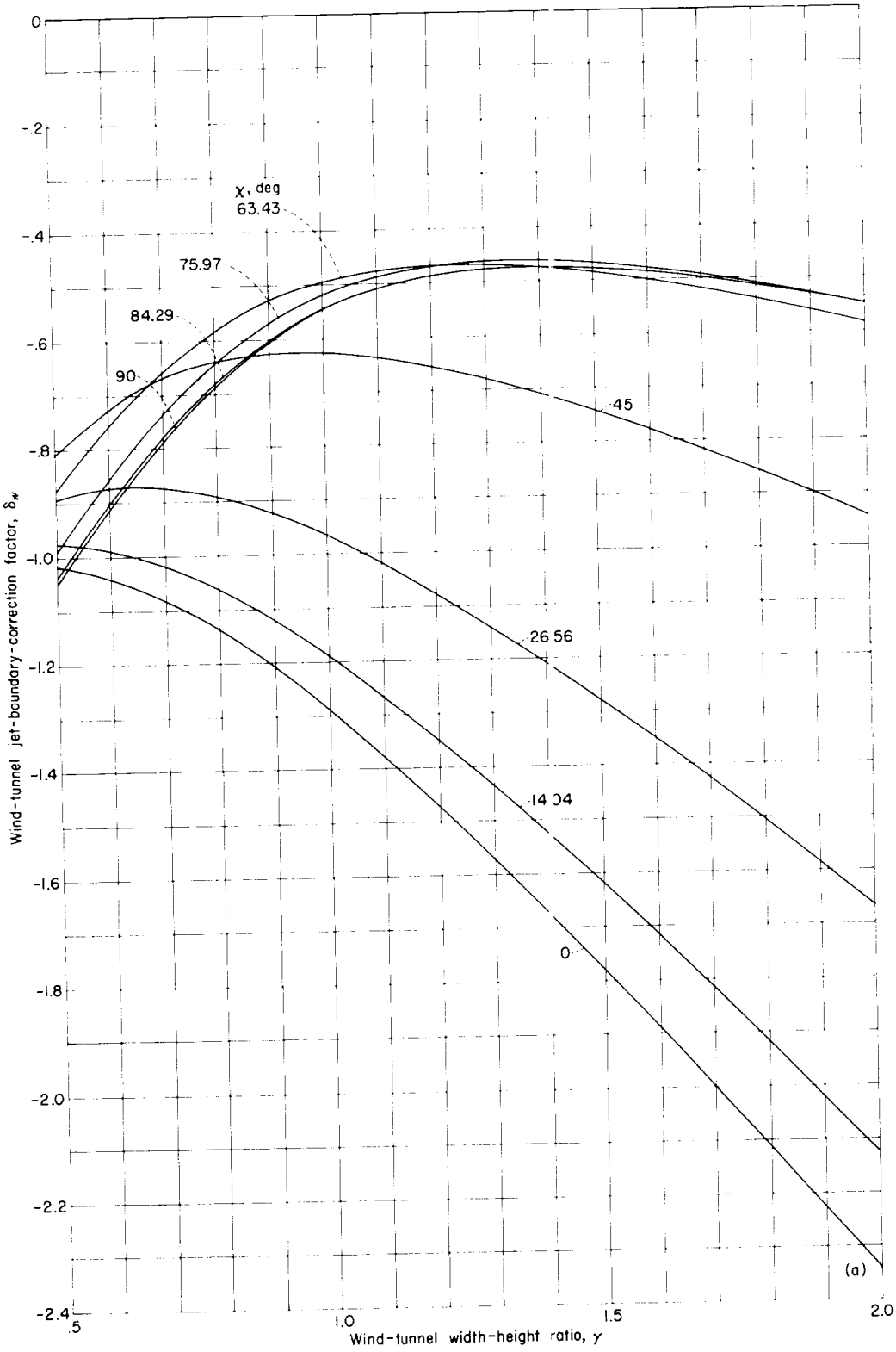

(a) Closed wind tunnels.

FIGURE 9.—Wind-tunnel jet-boundary-correction factors for a small rotor as a function of tunnel width-height ratio.

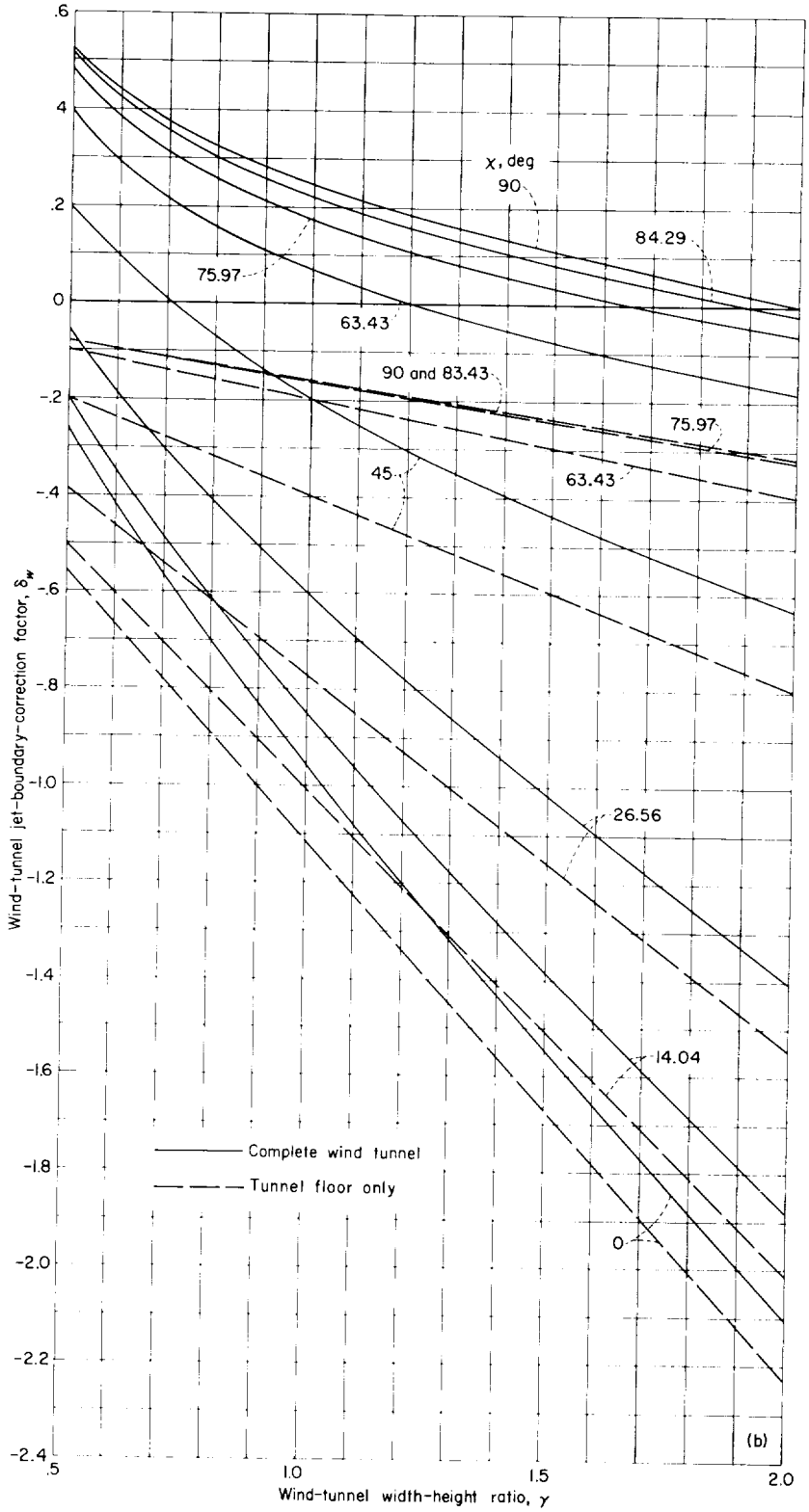

(b) Wind tunnels closed on bottom only.

FIGURE 9.—Concluded.

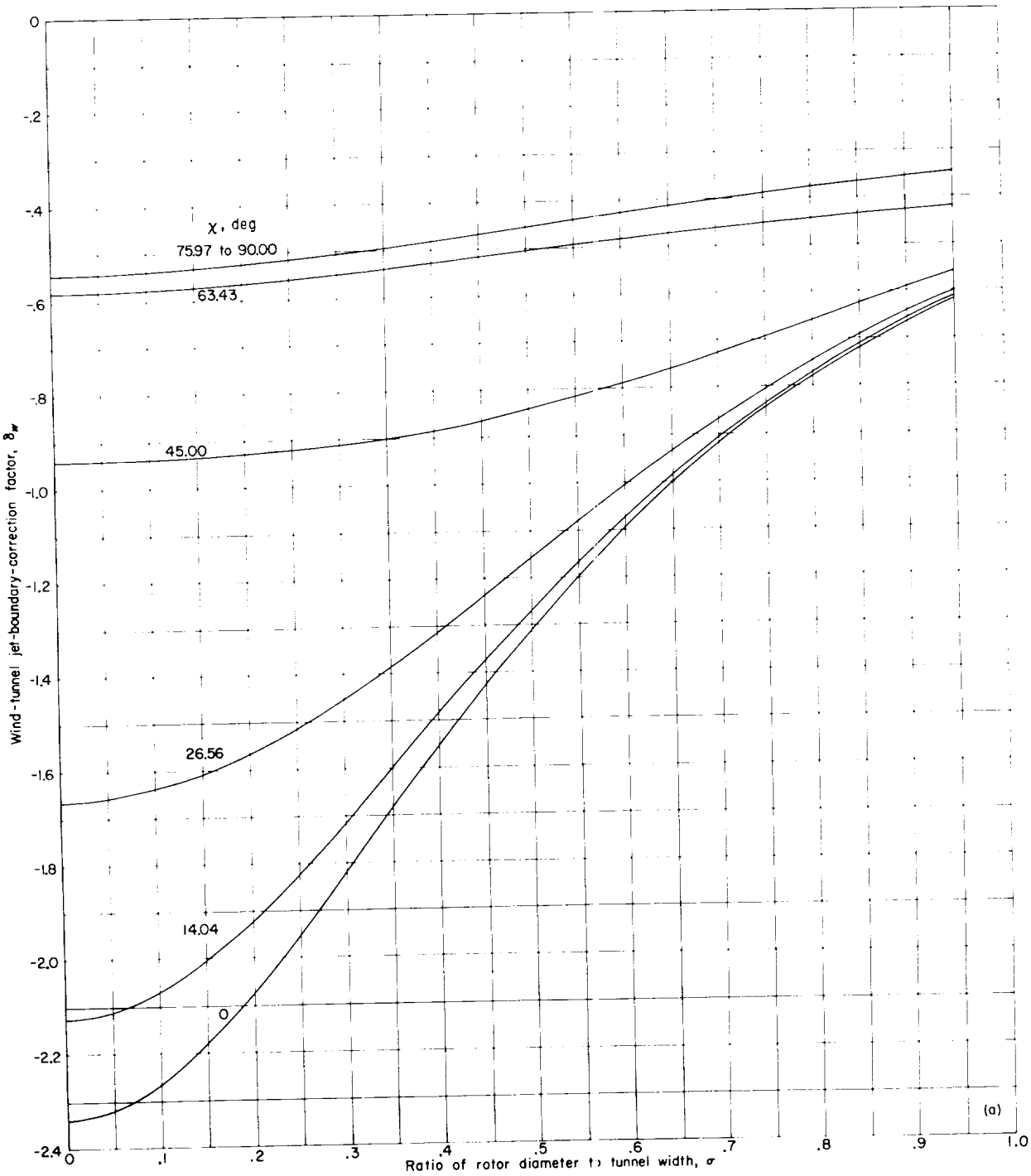

(a) $\gamma = 2.0$.

FIGURE 10.—Effect of ratio of rotor diameter to tunnel width σ on wind-tunnel jet-boundary-correction factors for closed rectangular wind tunnels with rotor mounted on wind-tunnel center line.

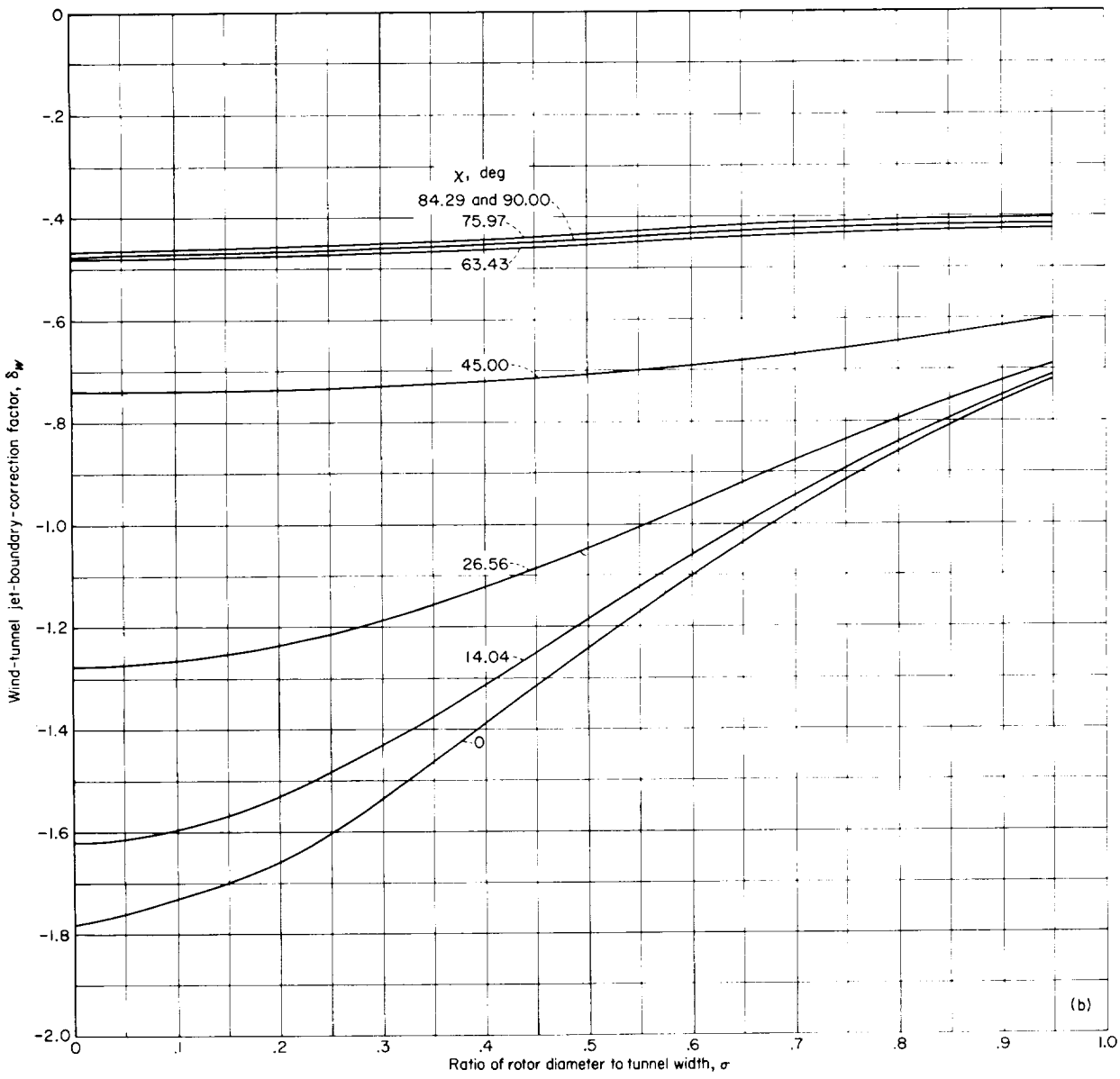

(b) $\gamma = 1.5$.

FIGURE 10.—Continued.

The interference correction factors, for both horizontal and vertical doublet wakes, have been combined, as previously discussed, to obtain the correction factors for rotors operating at tip-path-plane angles of attack of $\pm 5°$ and $\pm 10°$. These correction factors for $\gamma = 1.0$ are shown in figure 15 as a function of the effective skew angle $\chi - \alpha$. It is evident that angle of attack has a significant effect upon the correction factor. However, for the angles used in figure 15, which are typical of rotor tests, it appears that the changes due to angle of attack should be small enough that the present simple treatment will suffice even when the rotor is reasonably large.

Figure 15(c) is of particular interest because of its close relation to the treatment of ground effect in reference 9. Here, angle of attack alters the correction factors by an almost constant percentage which is approximately equal to twice the angle of attack in degrees.

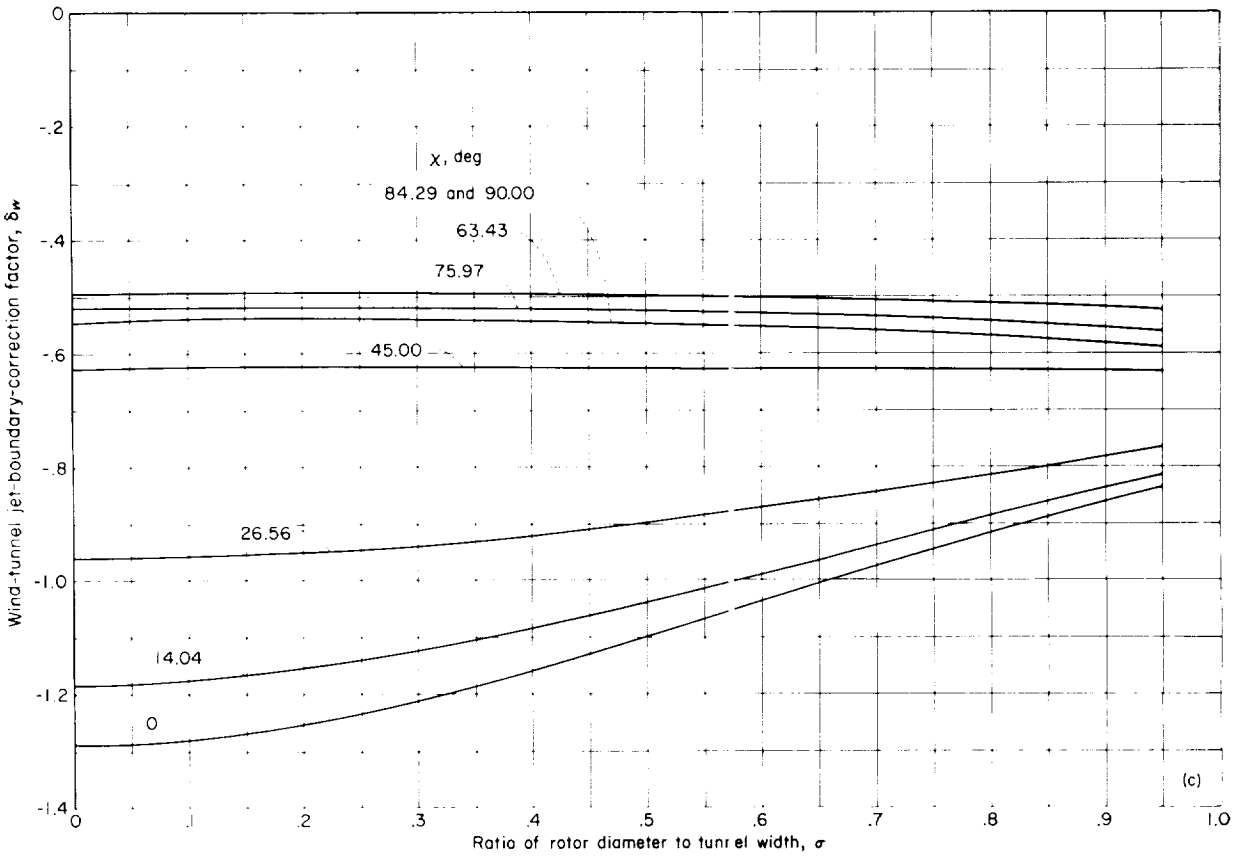

(c) $\gamma = 1.0$.

FIGURE 10.—Continued.

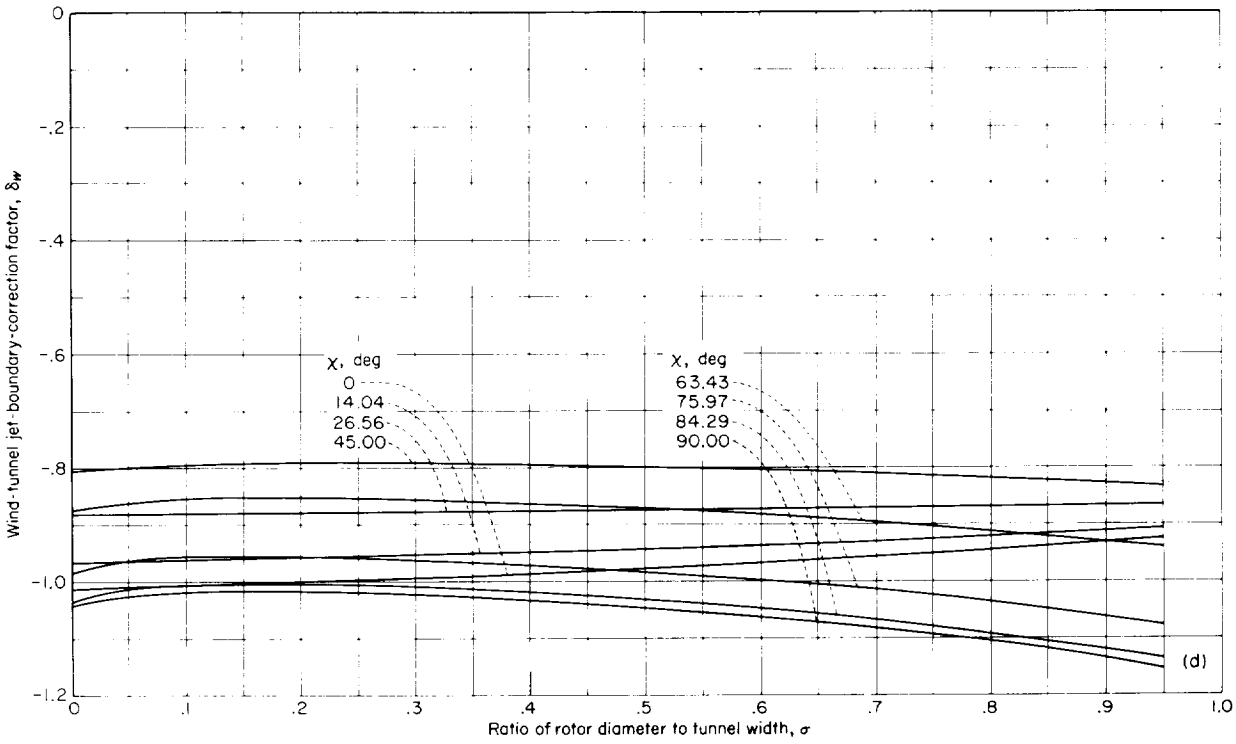

(d) $\gamma=0.5$.

FIGURE 10.—Concluded.

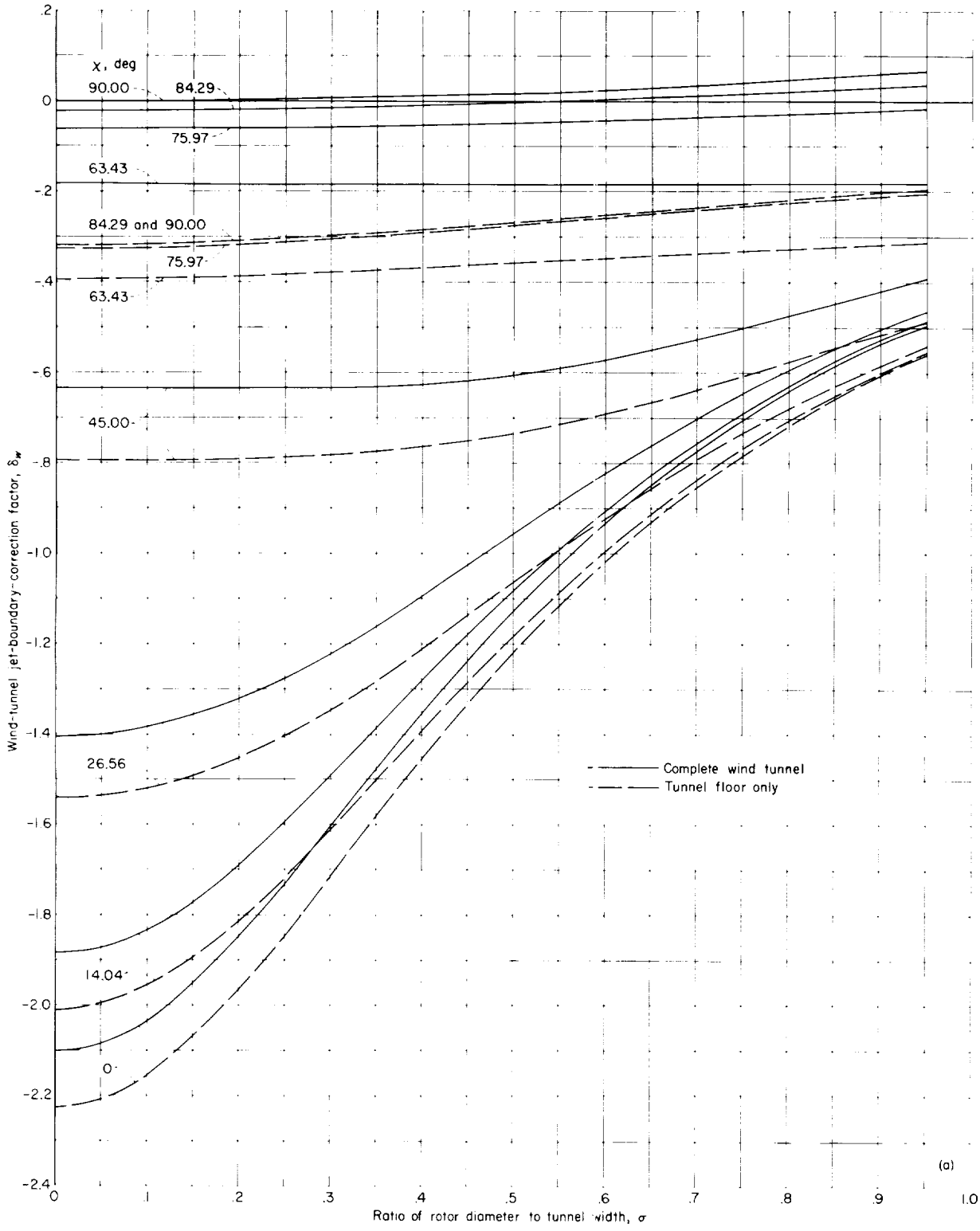

(a) $\gamma = 2.0$.

FIGURE 11.—Effect of ratio of rotor diameter to tunnel width σ on wind-tunnel jet-boundary-correction factors for rectangular wind tunnels closed on bottom only with rotor mounted on wind-tunnel center line.

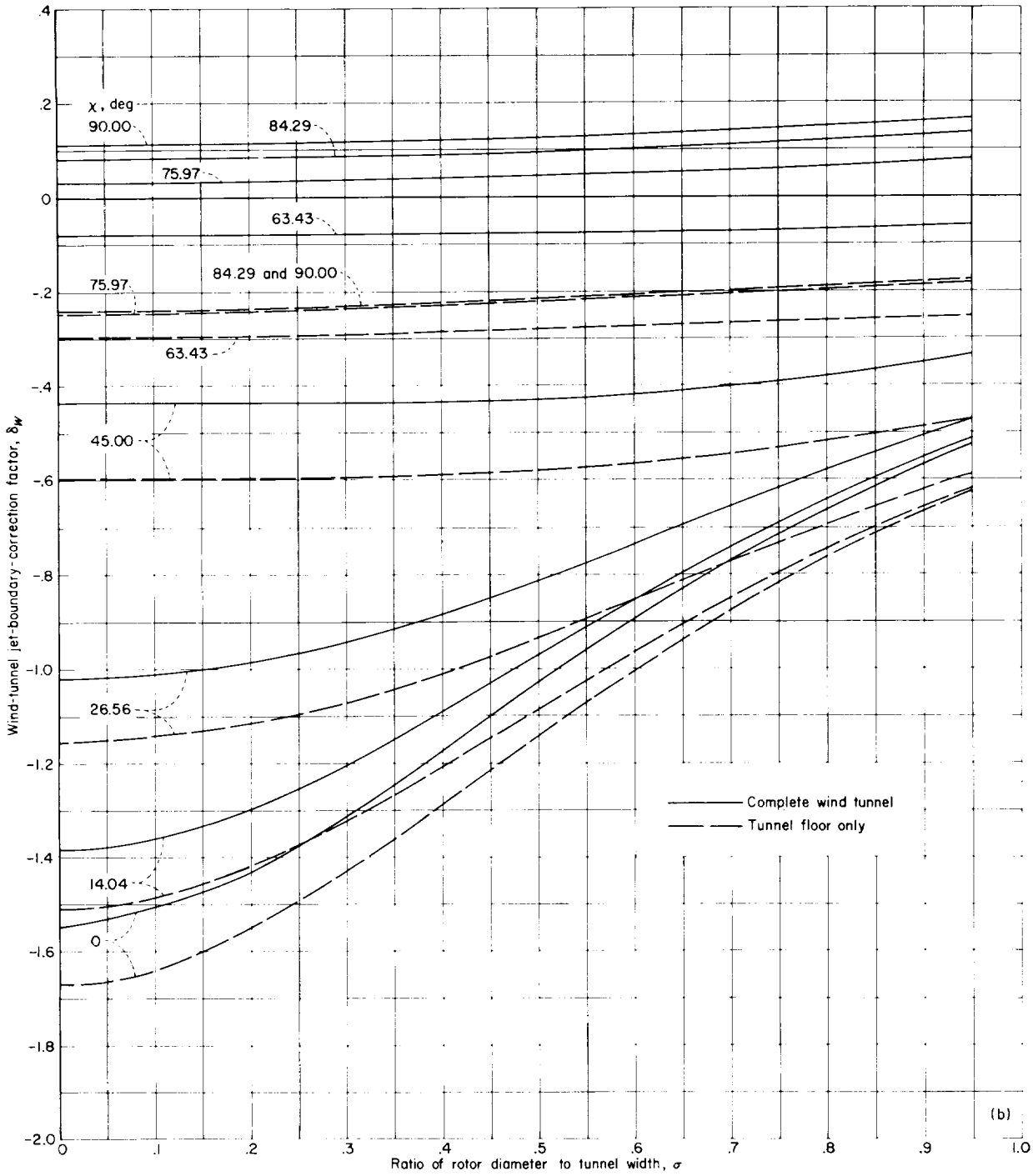

(b) $\gamma = 1.5$.

FIGURE 11.—Continued.

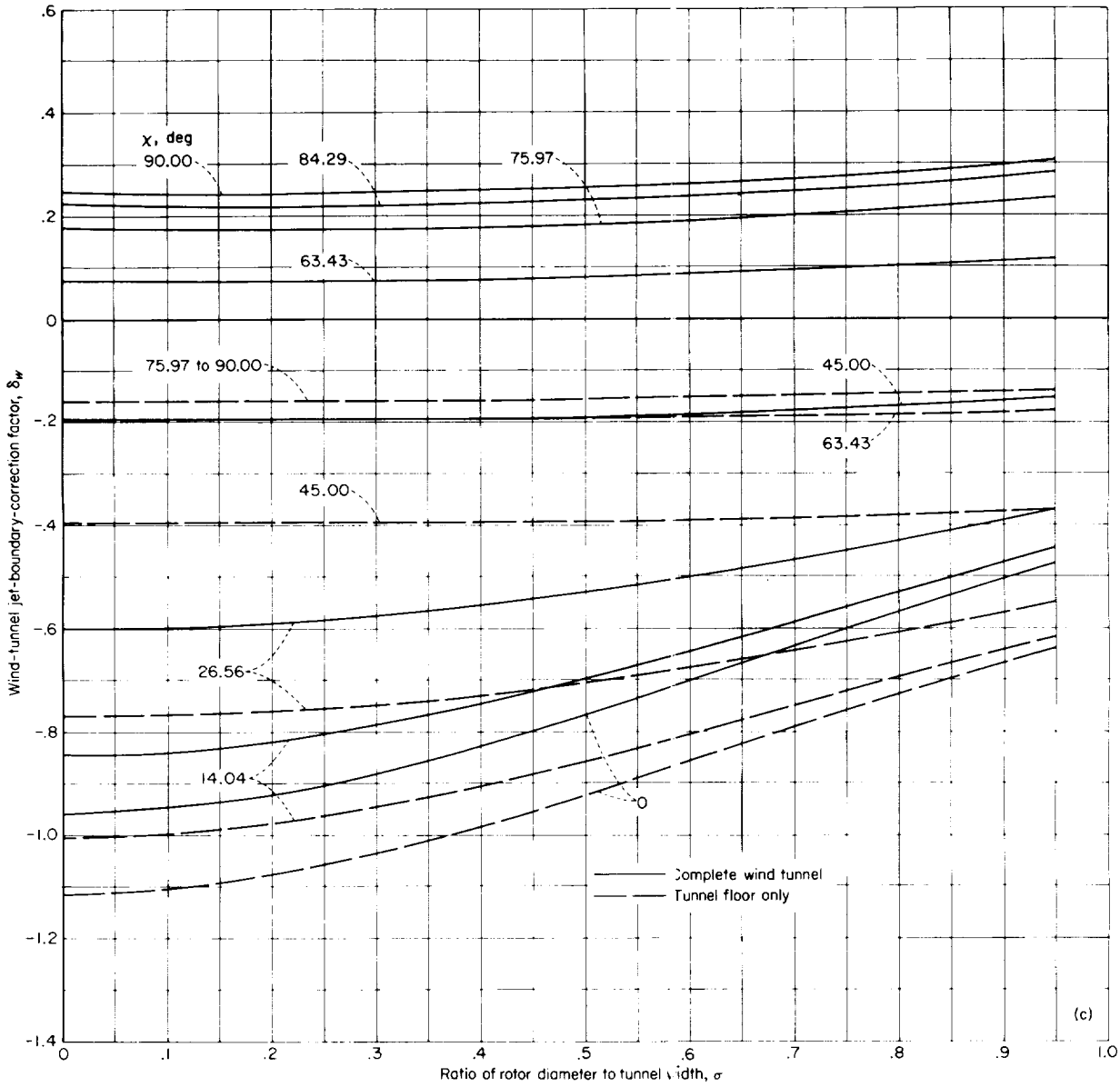

(c) $\gamma = 1.0$.

FIGURE 11.— Continued.

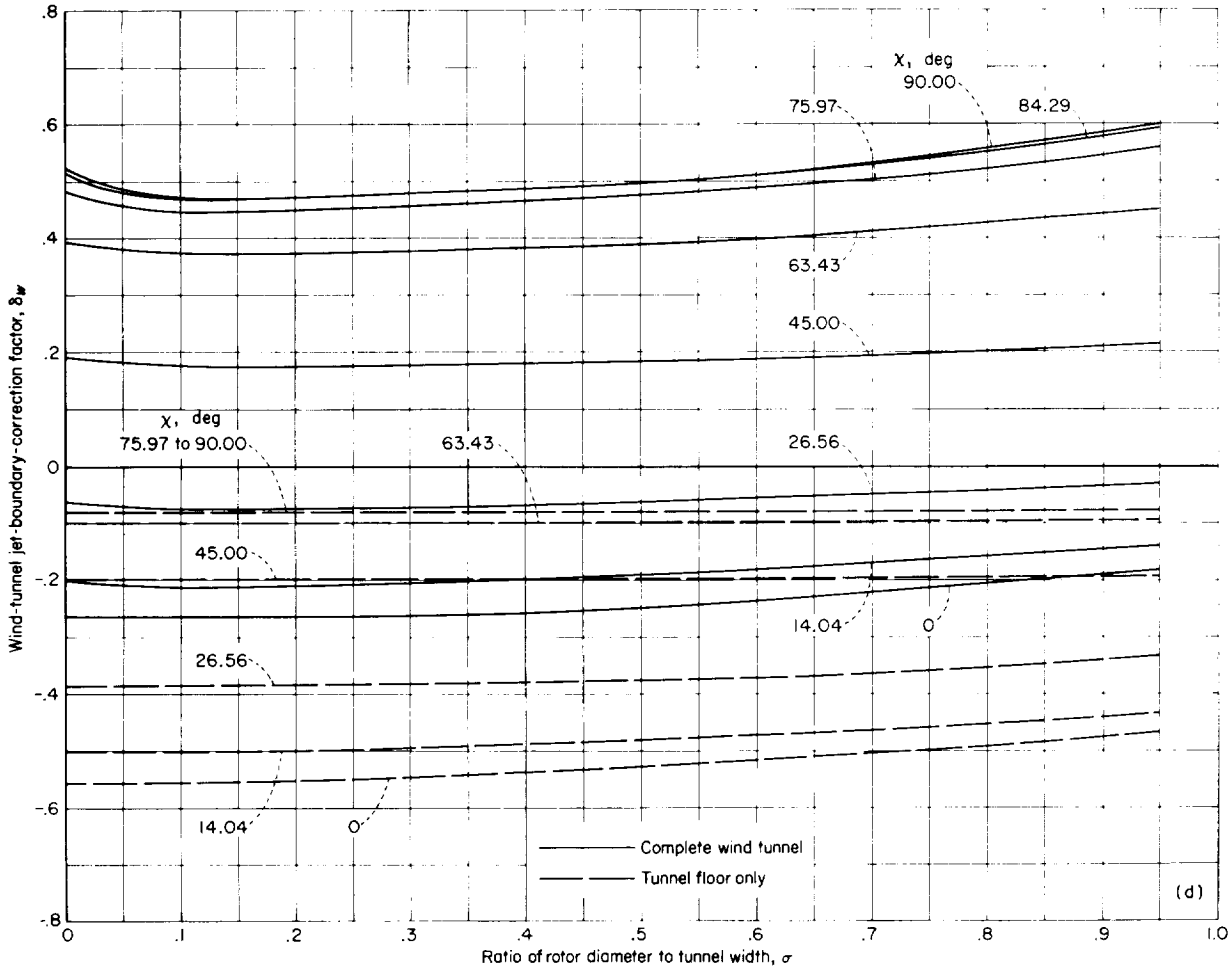

(d) $\gamma = 0.5$.

FIGURE 11.—Concluded.

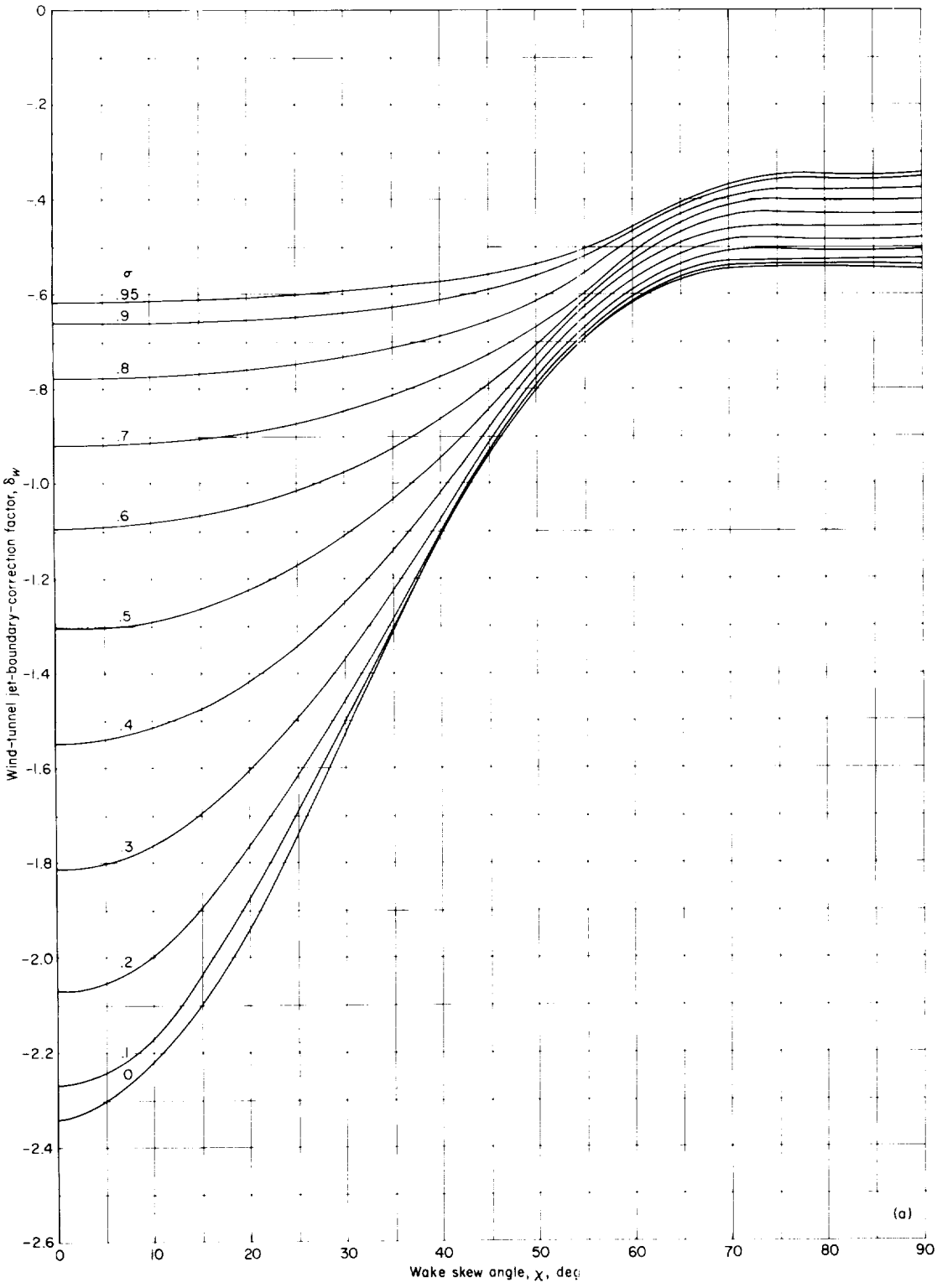

(a) $\gamma = 2.0$.

FIGURE 12.—Effect of skew angle χ on wind-tunnel jet-boundary-correction factors for closed rectangular wind tunnels with rotor mounted on wind-tunnel center line.

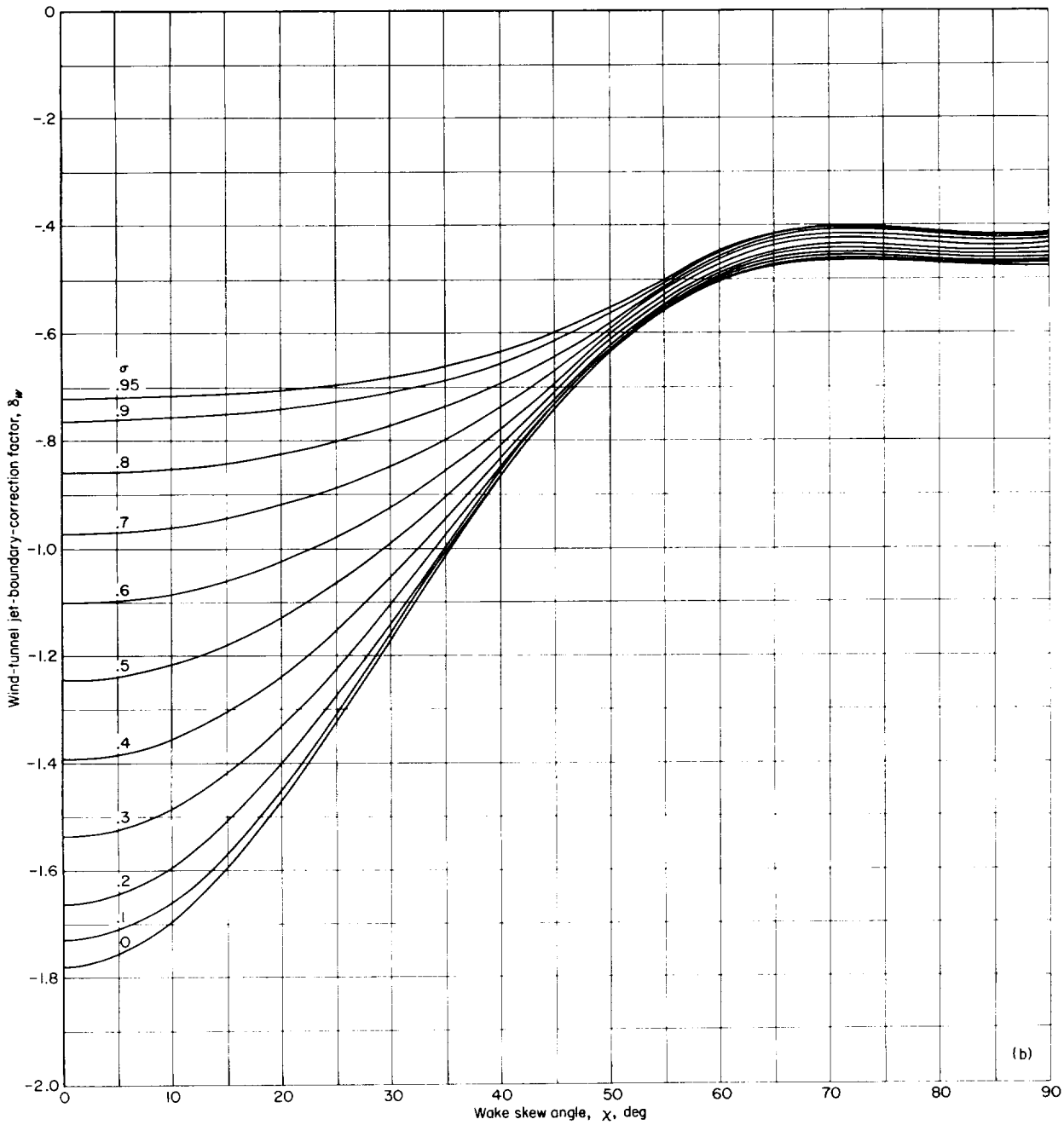

(b) $\gamma = 1.5$.

FIGURE 12.—Continued.

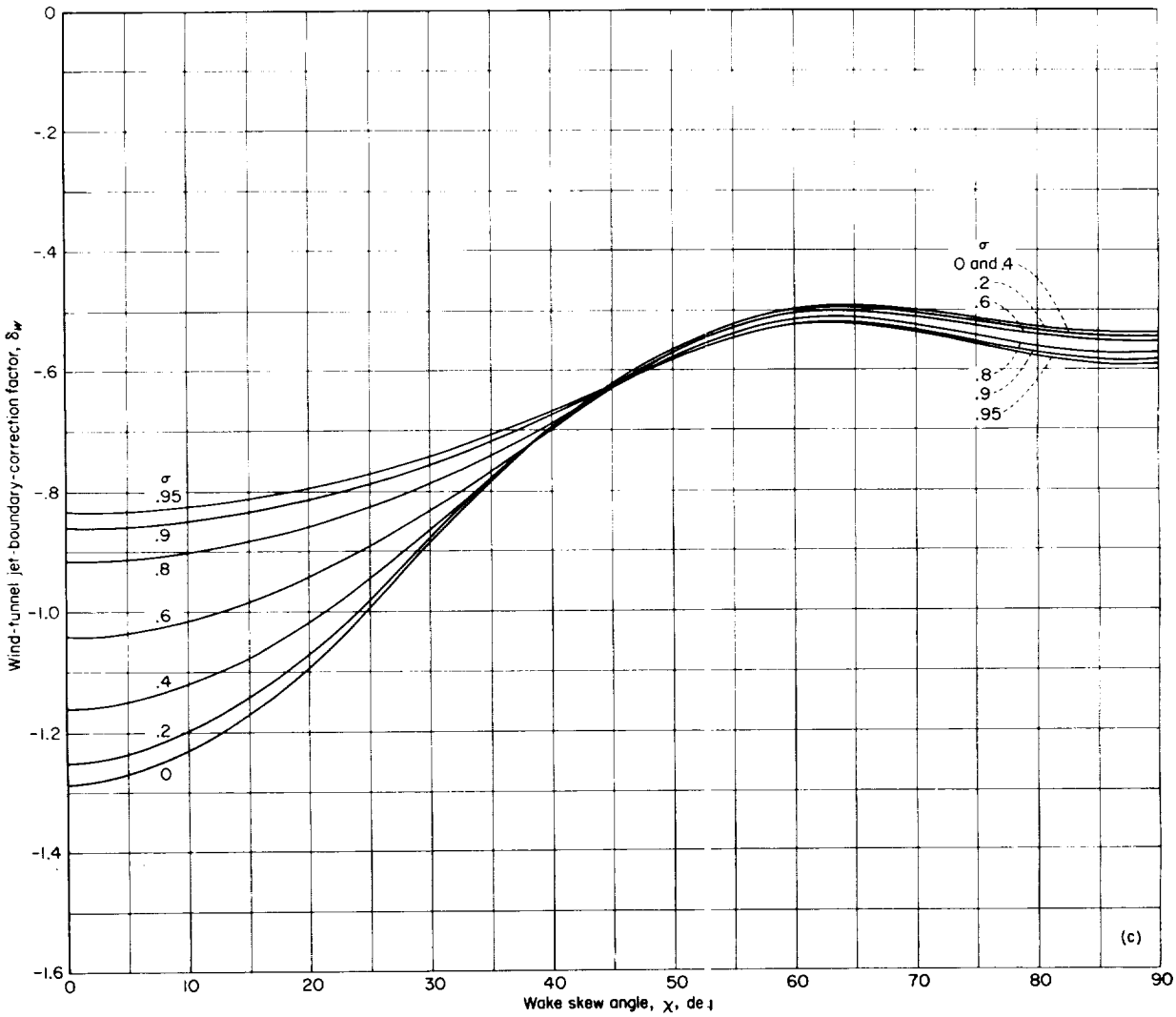

(c) $\gamma = 1.0$.

FIGURE 12.—Continued.

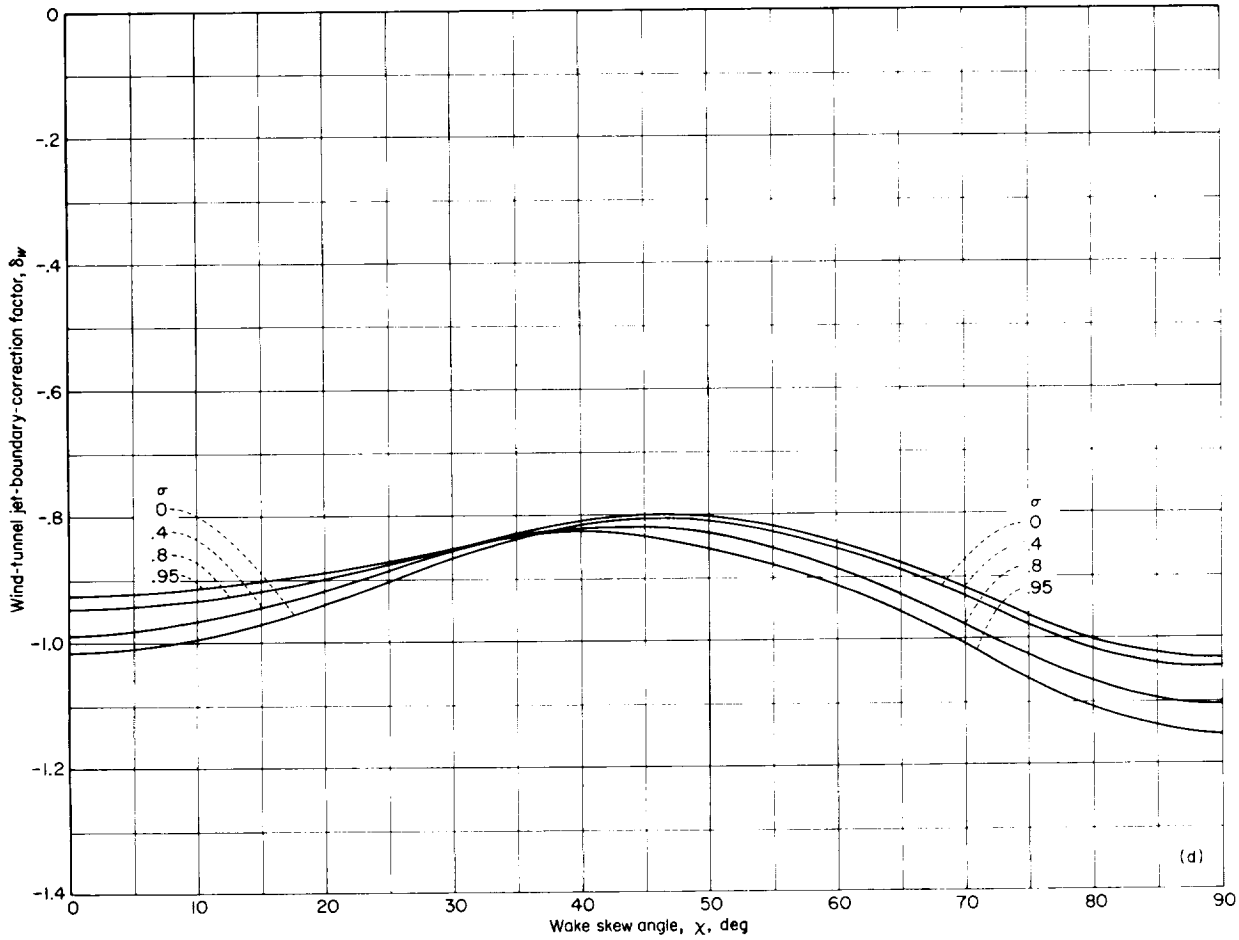

(d) $\gamma = 0.5$.

FIGURE 12.—Concluded.

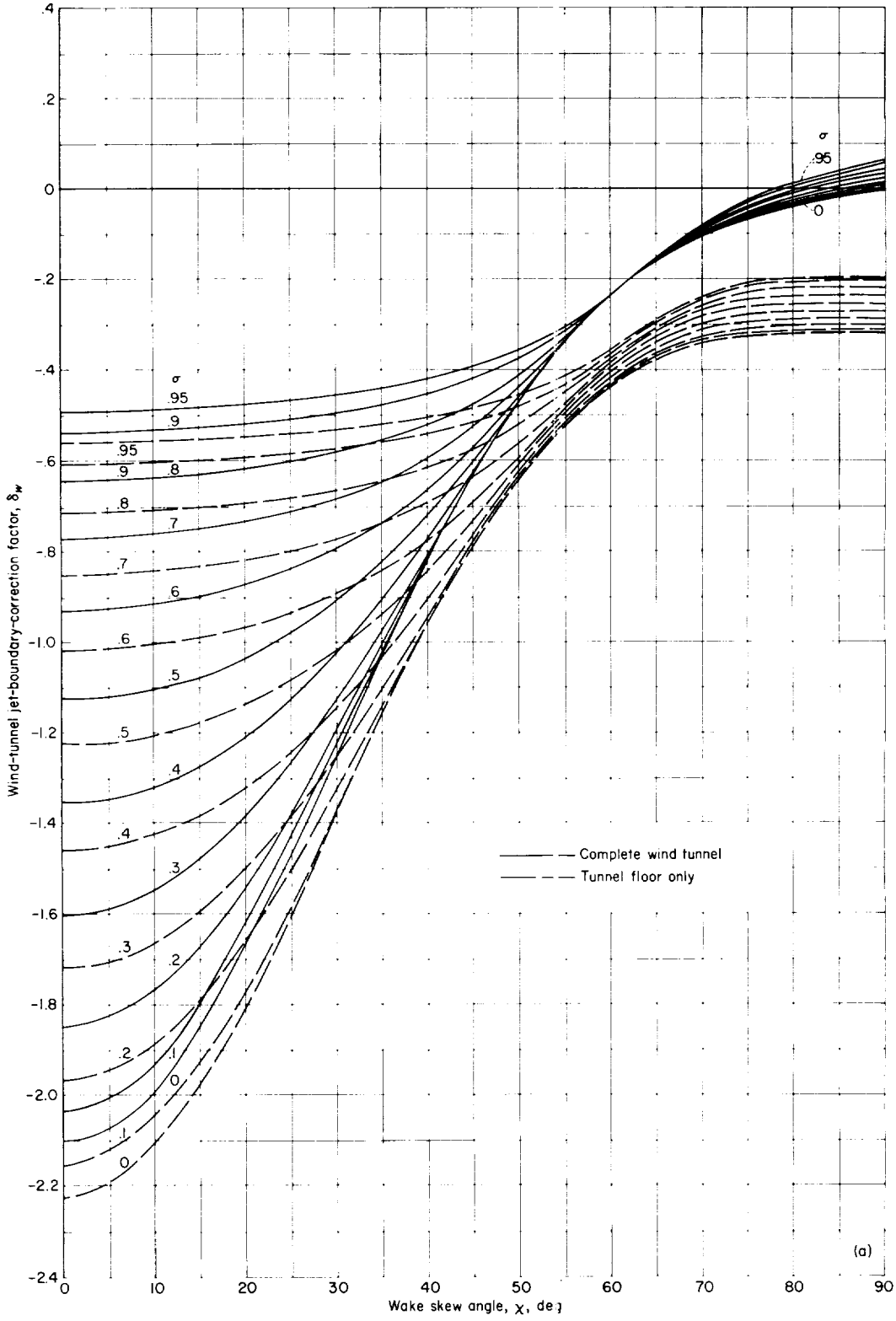

(a) $\gamma = 2.0$.

FIGURE 13.- Effect of skew angle χ on wind-tunnel jet-boundary-correction factors for rectangular wind tunnels closed on bottom only with rotor mounted on wind-tunnel center line.

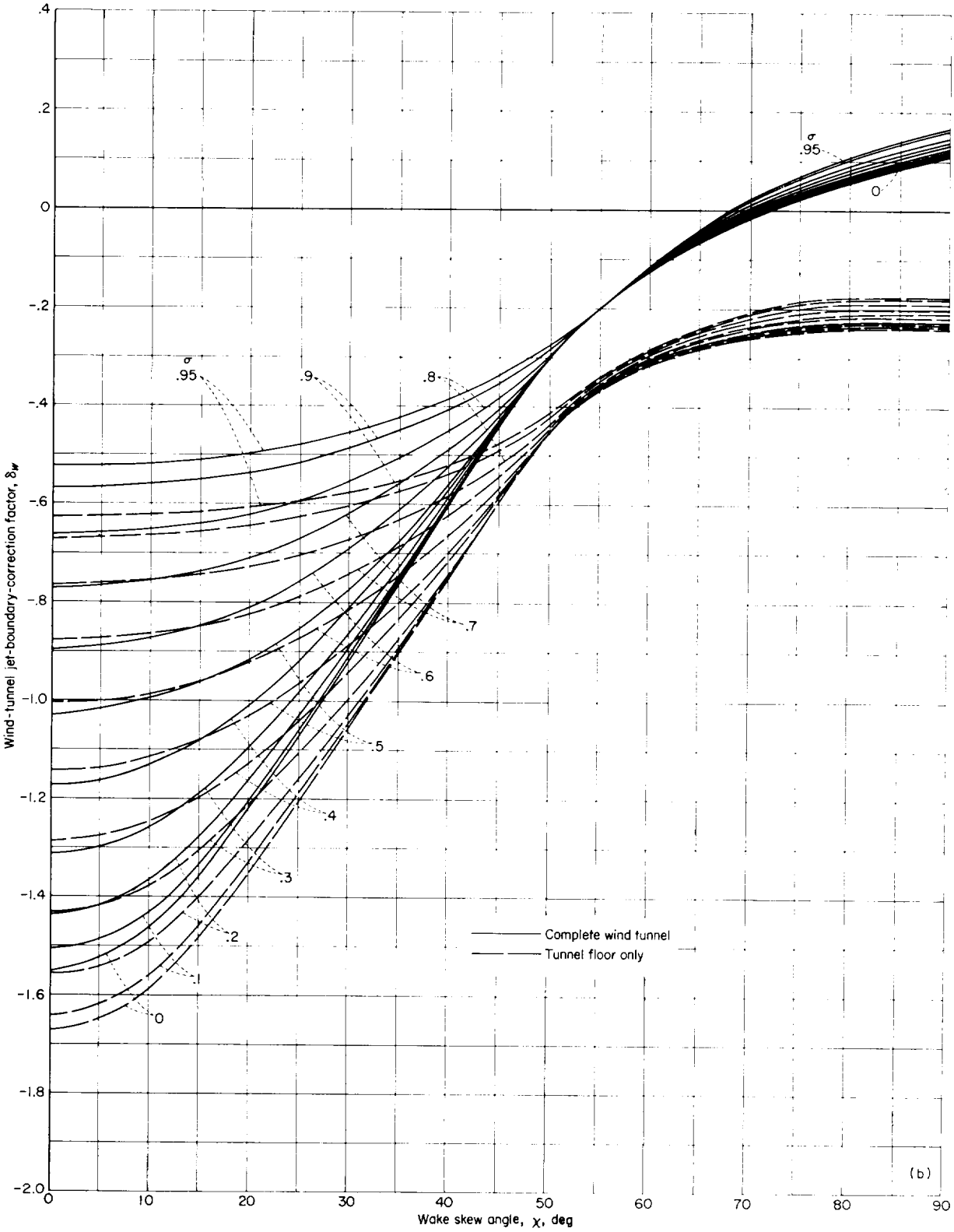

(b) $\gamma = 1.5$.

FIGURE 13.—Continued.

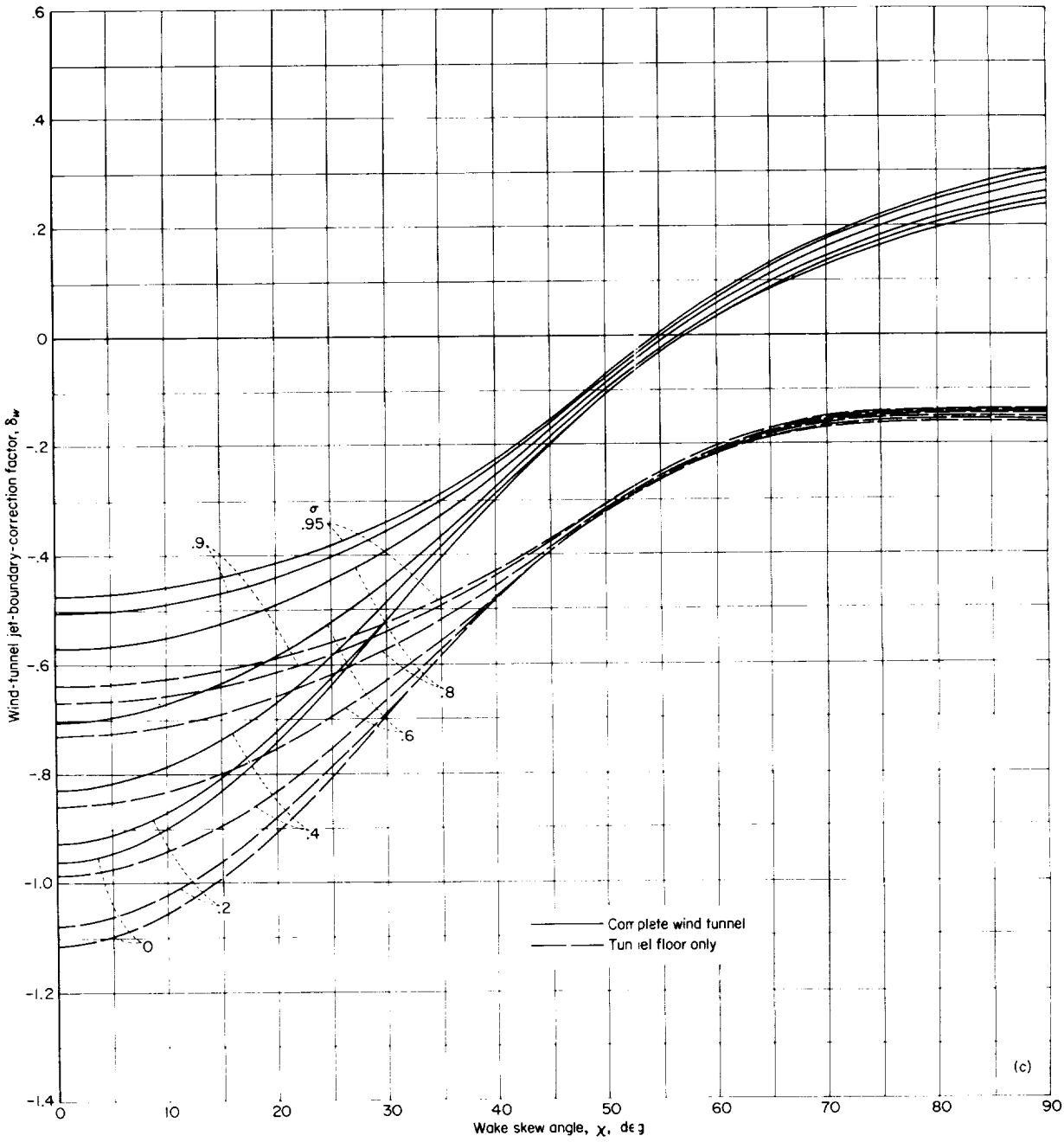

(c) $\gamma = 1.0$.

FIGURE 13. Continued.

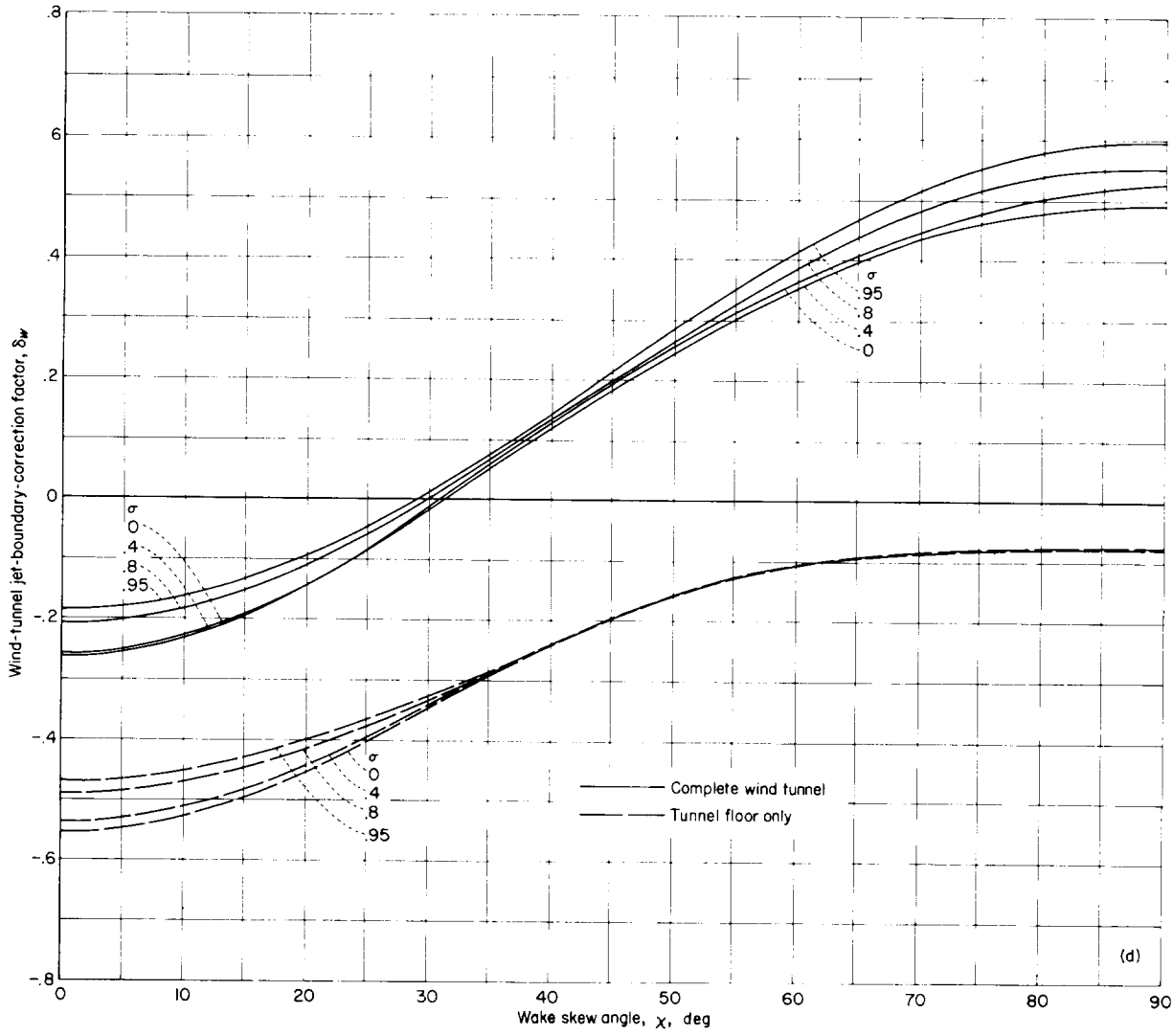

(d) $\gamma = 0.5$.

FIGURE 13.—Concluded.

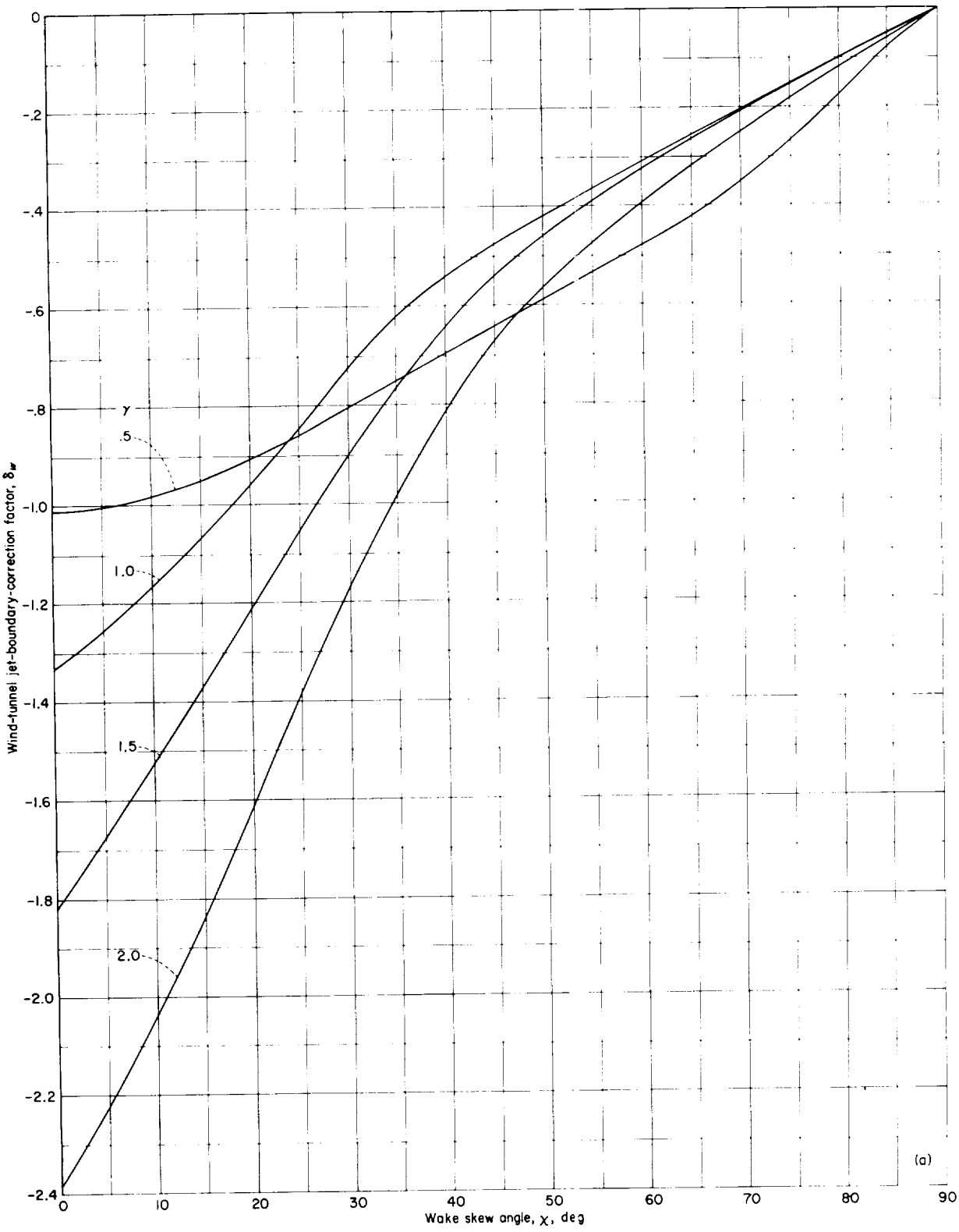

(a) Closed wind tunnels.

FIGURE 14.- Wind-tunnel jet-boundary-correction factors for a wake of horizontal doublets.

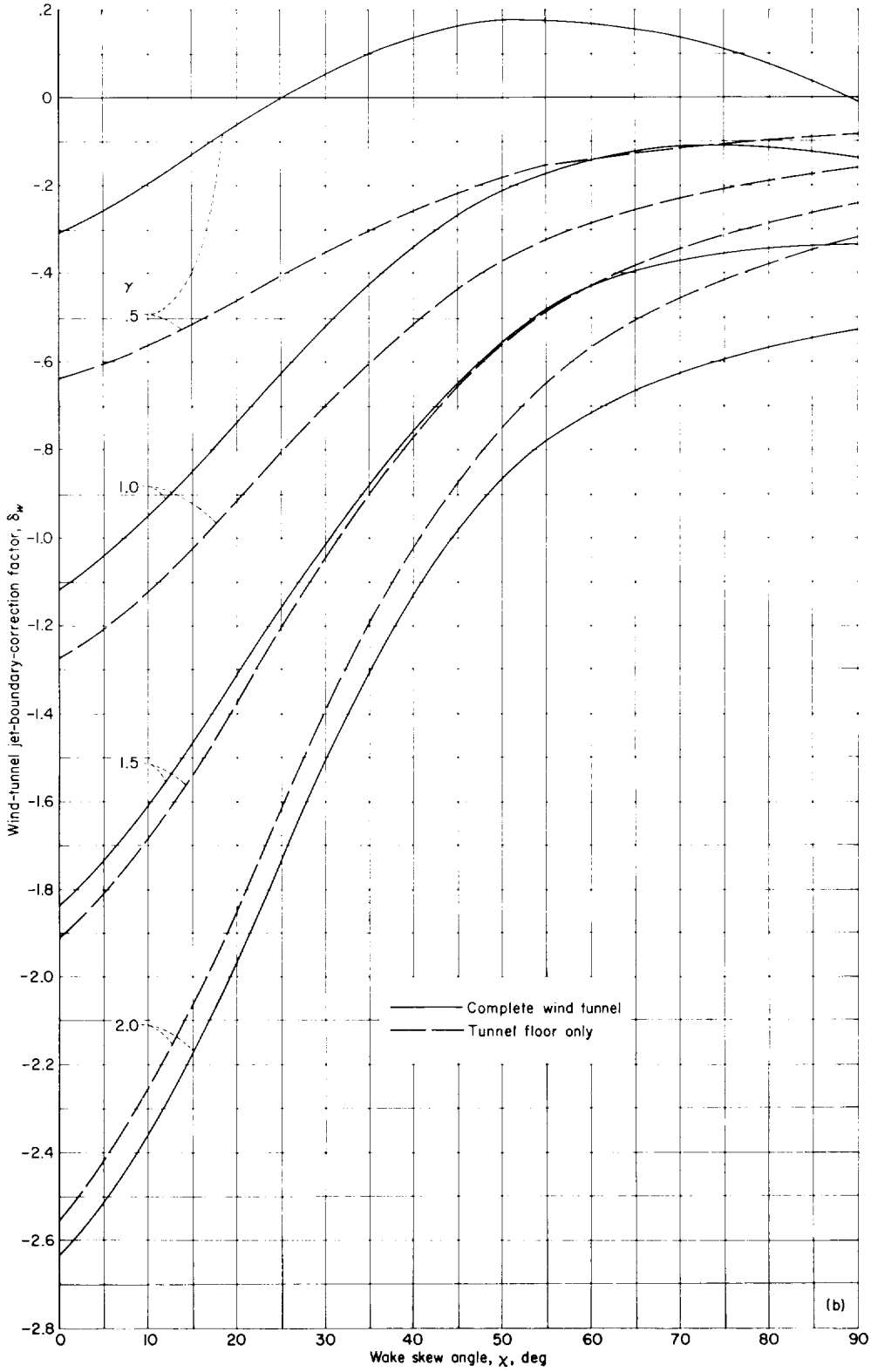

(b) Wind tunnels closed on bottom only.

FIGURE 14.—Concluded.

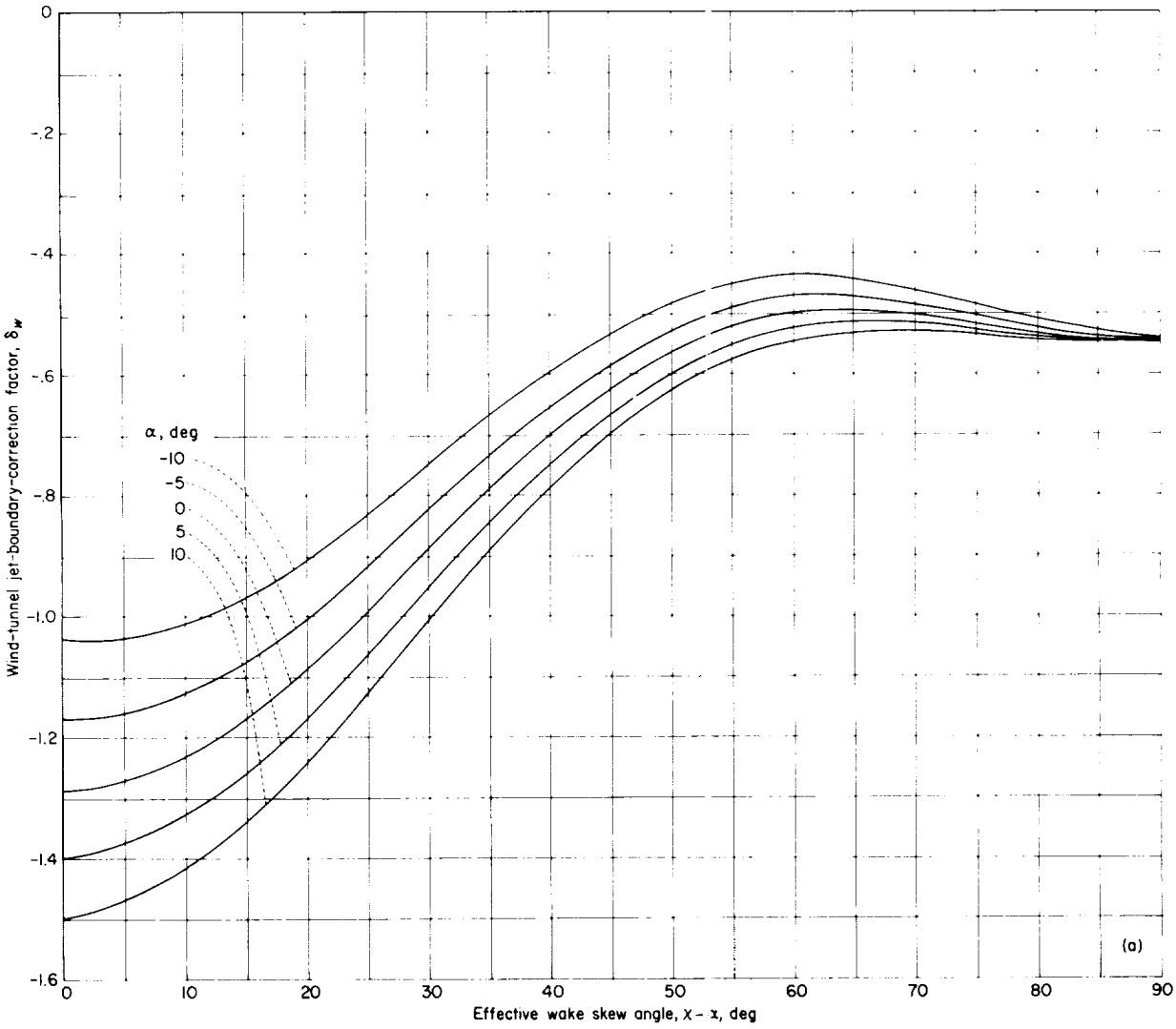

(a) Closed wind tunnel.

FIGURE 15.—Effect of angle of attack on wind-tunnel jet-boundary-correction factor. $\gamma = 1.0$.

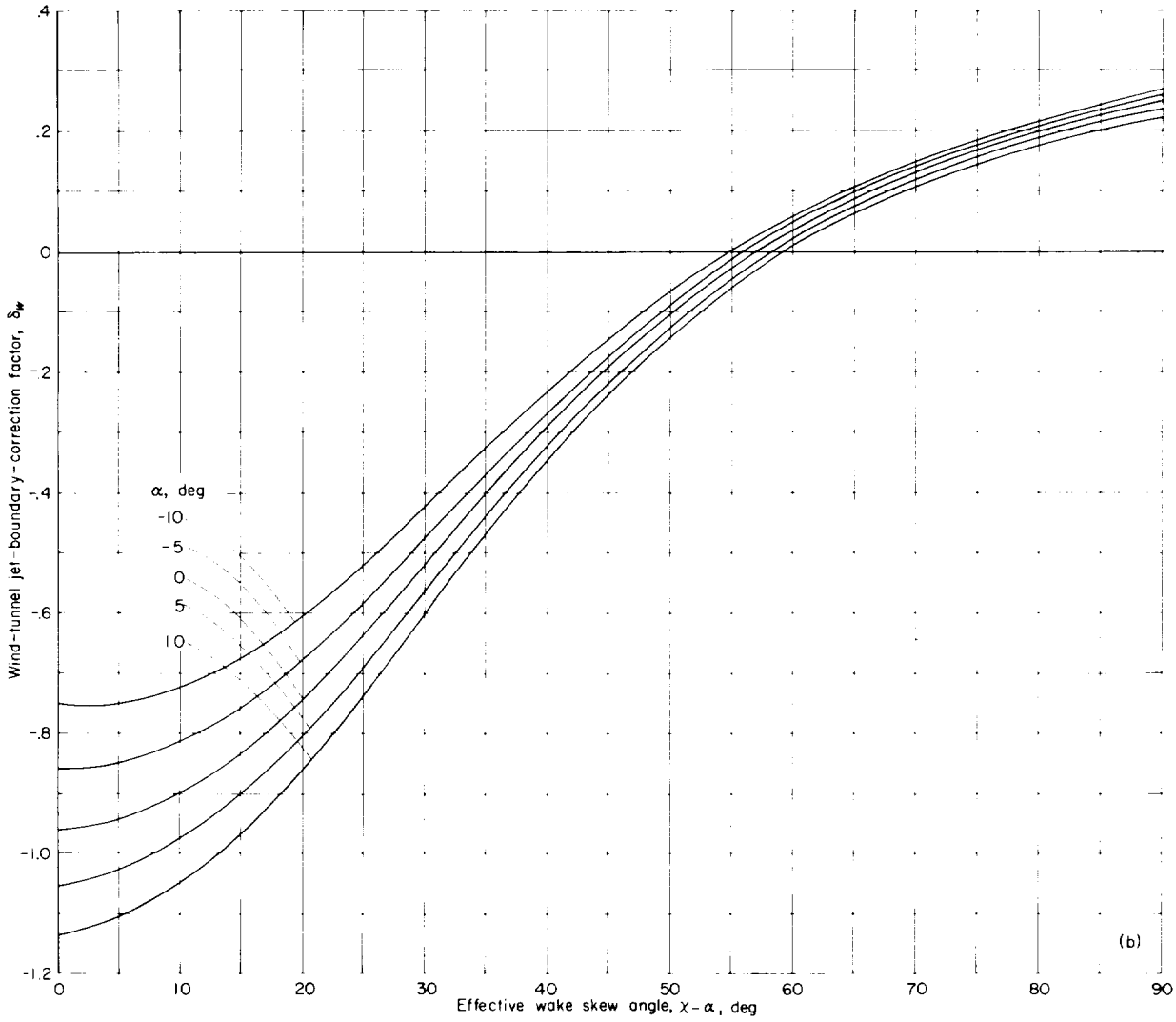

(b) Wind tunnel closed on bottom only.

FIGURE 15.- -Continued.

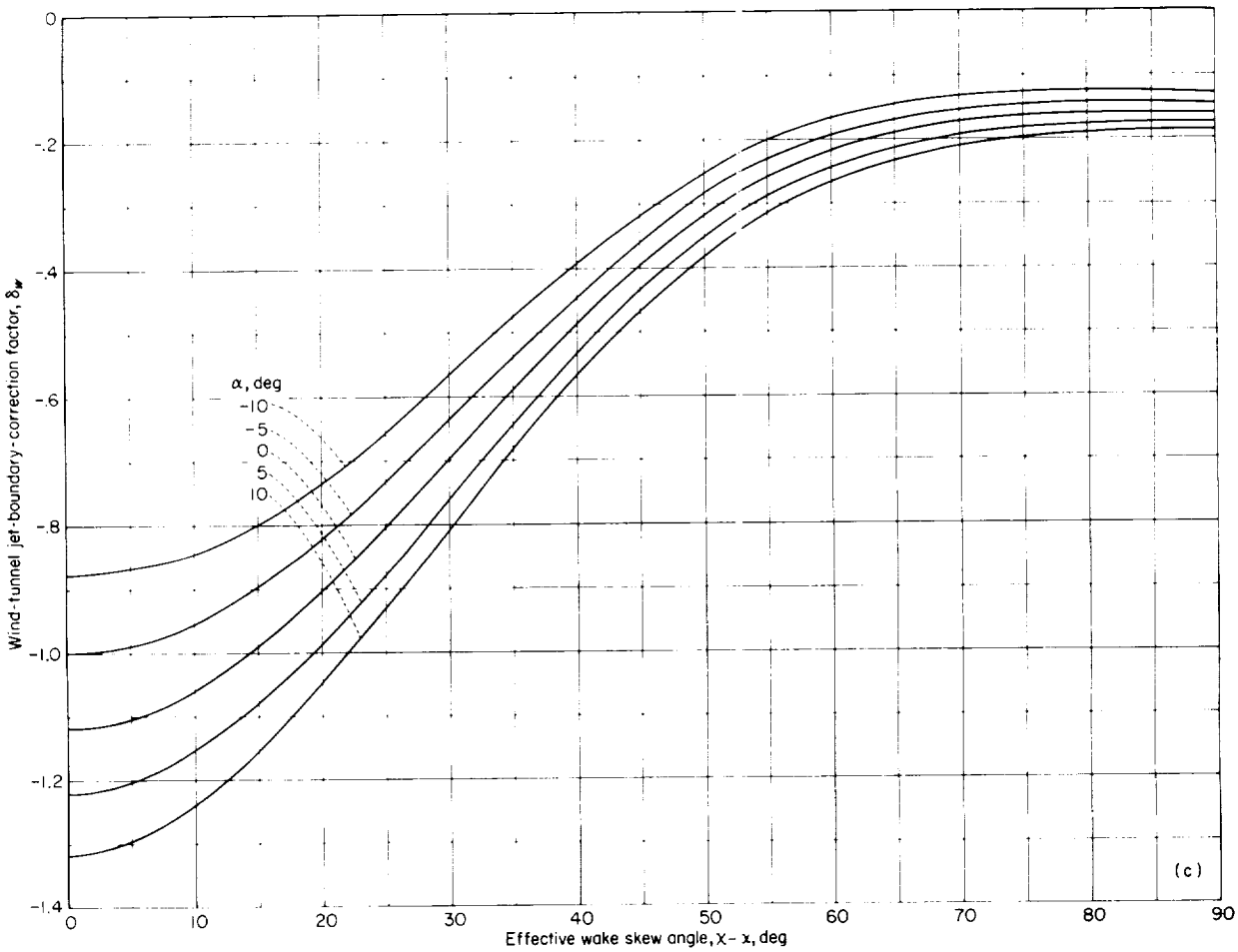

(c) Wind-tunnel floor only.

FIGURE 15.—Concluded.

DISTRIBUTION OF INTERFERENCE VELOCITY

Figures 16 and 17 show the distribution of the tunnel-induced interference velocity along the major axes of the rotor disk for a case in which $\gamma=2.0$ and $\sigma=0.4$. The interference velocity is presented directly and was obtained by noting that the area ratio A_R/A_T in equation (19a) is given by

$$\frac{A_R}{A_T}=\frac{\pi R^2}{4BH}=\frac{\pi}{4}\sigma^2\gamma \tag{29}$$

The interference velocity varies widely over the rotor disk. In particular, the peak interference along the lateral axis is experienced at the center of the rotor, and at all skew angles the interference decreases toward the sides of the rotor. The interference velocity distribution is not as simple along the longitudinal axis. Here the peak interference occurs at the center of the rotor only when the skew angle is zero. As the skew angle increases, the point of maximum interference shifts further rearward until, for skew angles of 45° or more, the interference velocity increases monotonically from the leading edge to the trailing edge of the rotor disk. The peak value of interference is, however, always found to occur very near a value of x/H of $\tan\chi$. $\left(\text{Note that } \frac{x}{H}=\sigma\gamma\frac{x}{R} \text{ or, in this particular example, } \frac{x}{H}=0.8\frac{x}{R}.\right)$

The differences between the local interference velocity and the value at the center of the rotor indicate that some error has been incurred by using only the interference at the center of the

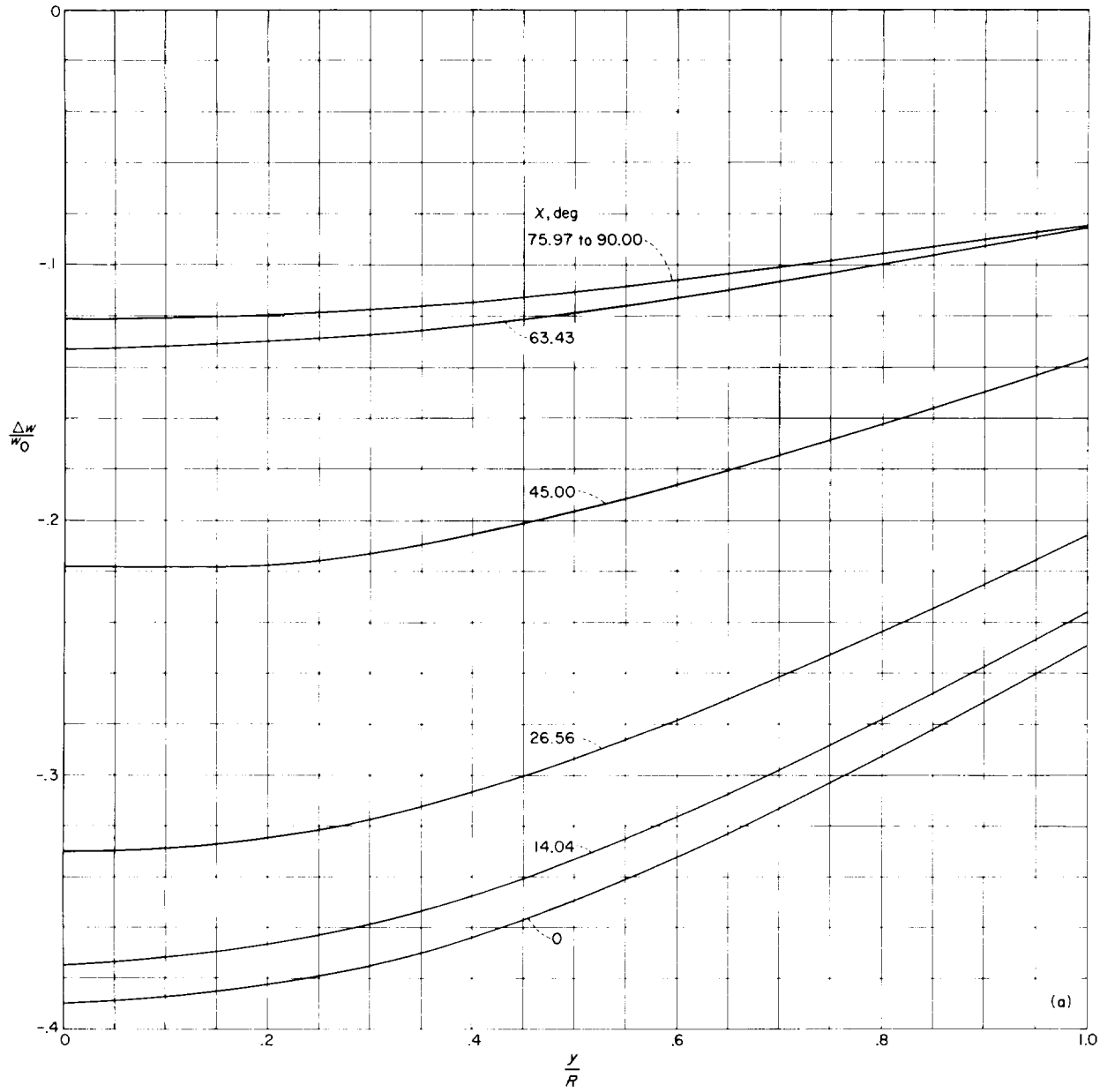

(a) Closed wind tunnel.

FIGURE 16.—Distribution of jet-boundary-induced interference velocity on lateral axis of rotor. $\gamma=2.0$; $\sigma=0.4$.

rotor in determining the jet-boundary correction. This is illustrated by figure 18 in which, for this case ($\sigma=0.4$, $\gamma=2.0$), the correction factor based on the average interference velocity is compared with that computed using only the central interference velocity. It may be seen that the use of an average value of interference velocity significantly reduces the size of the jet-boundary correction at low skew angles but that there is little difference at higher skew angles. Since, for $\sigma=0$, the interference velocity at the center is identically equal to the average interference velocity, it may be observed that the error caused by using only the central interference velocity will decrease with decreasing rotor size.

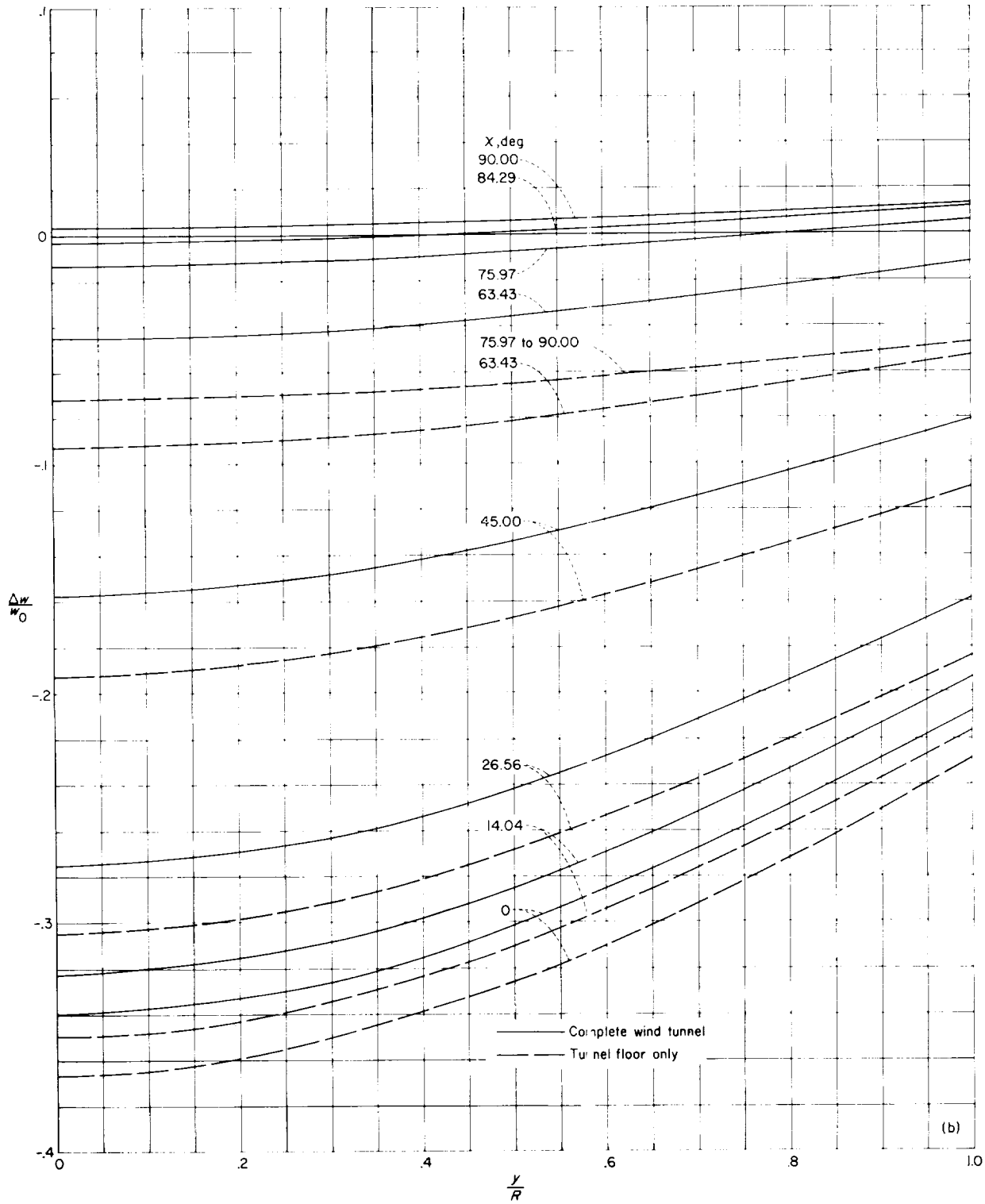

(b) Wind tunnel closed on bottom only.

FIGURE 16.—Concluded.

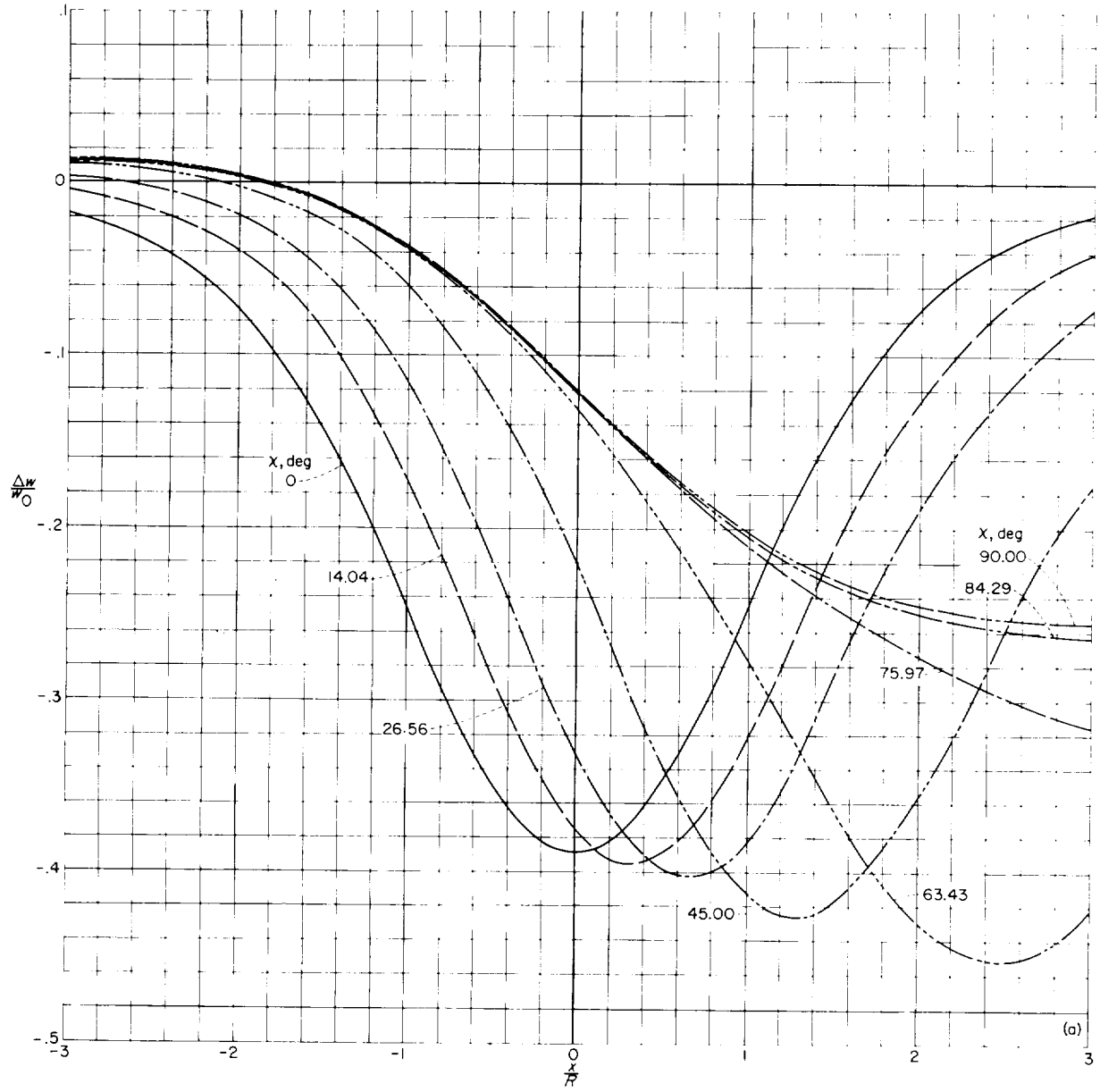

(a) Closed wind tunnel.

FIGURE 17.—Distribution of jet-boundary-induced interference velocity on longitudinal axis of rotor. $\gamma=2.0$; $\sigma=0.4$.

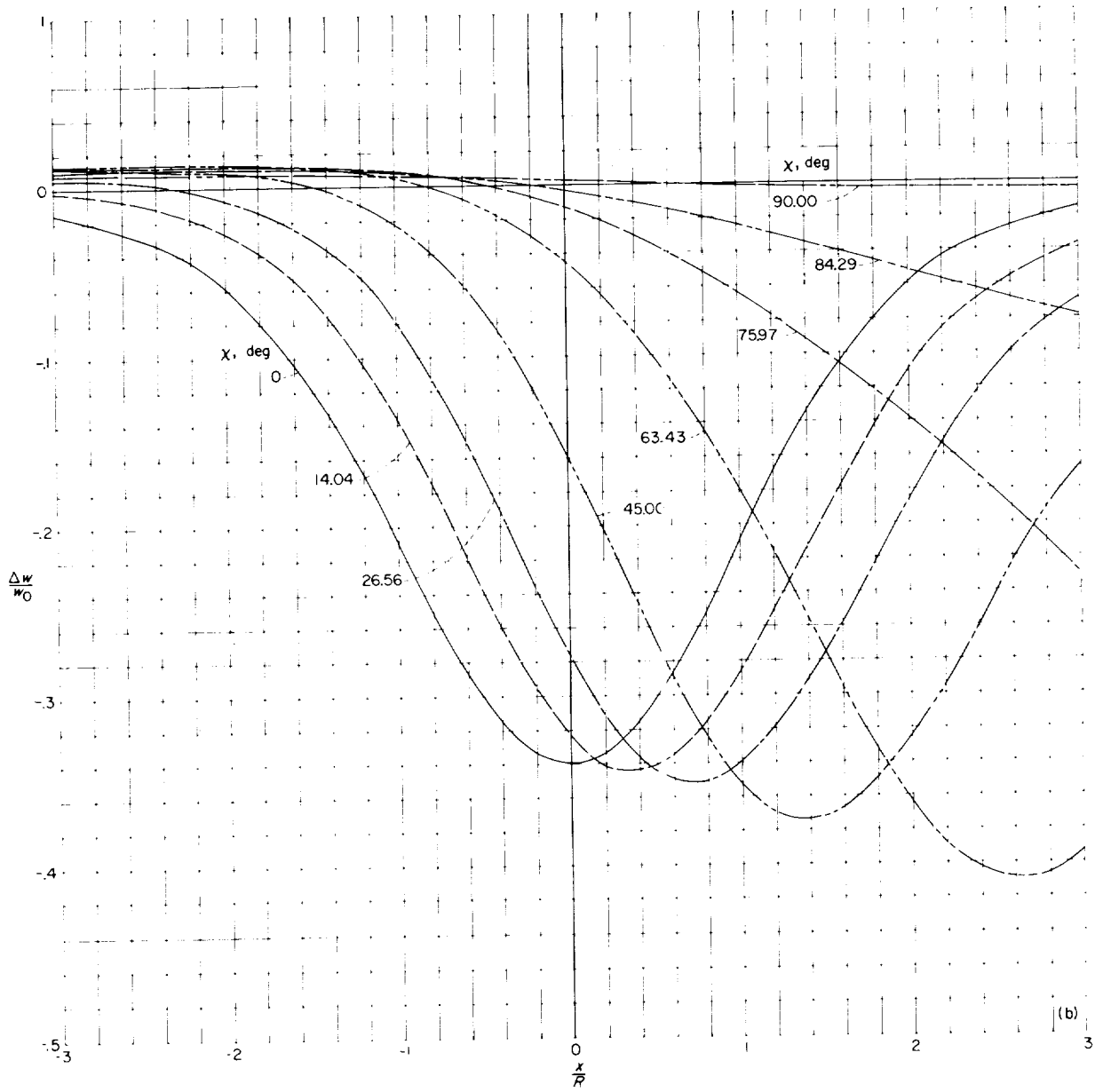

(b) Wind tunnel closed on bottom only.

FIGURE 17. Continued.

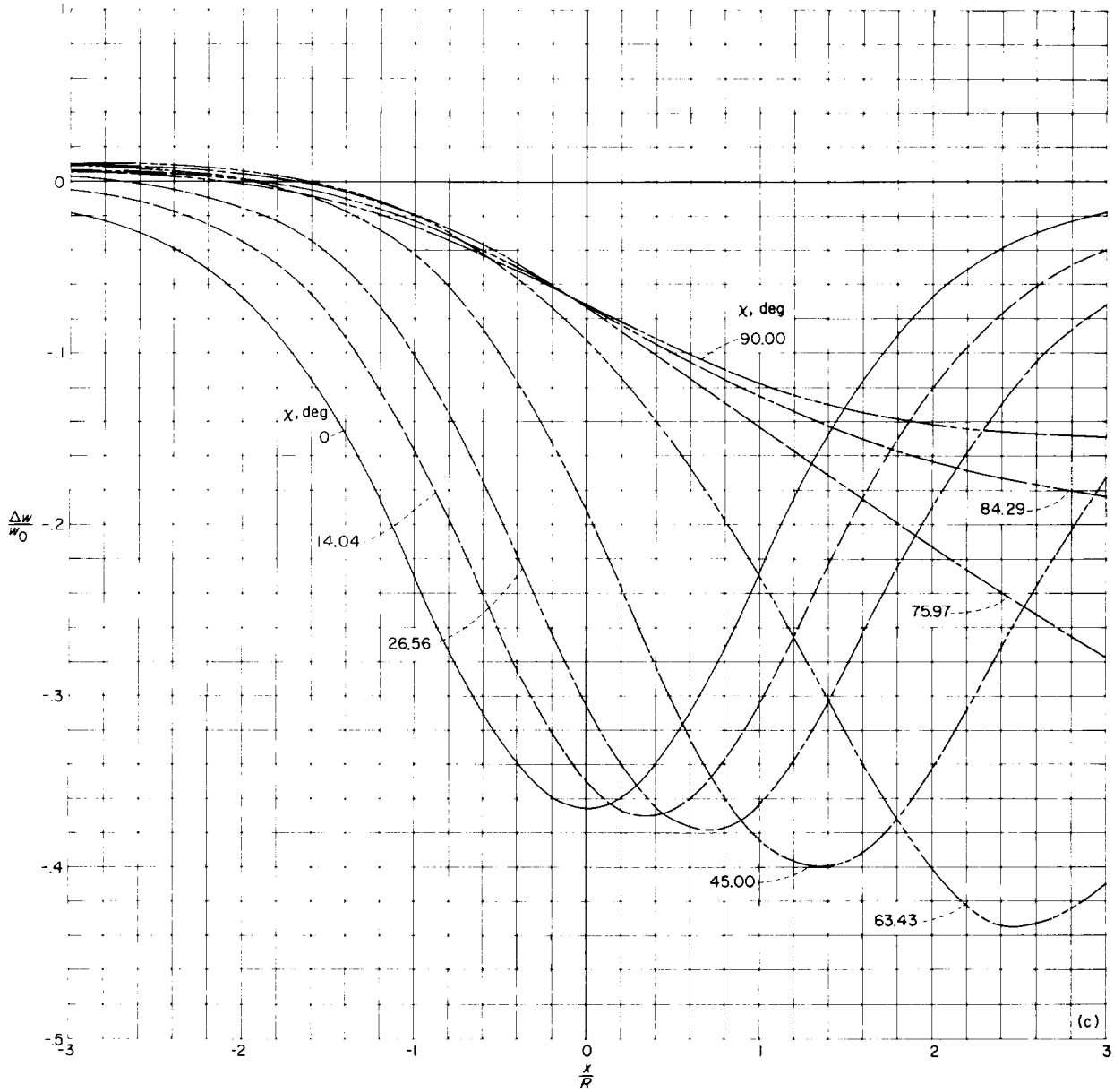

(c) Wind-tunnel floor only.

FIGURE 17.—Concluded.

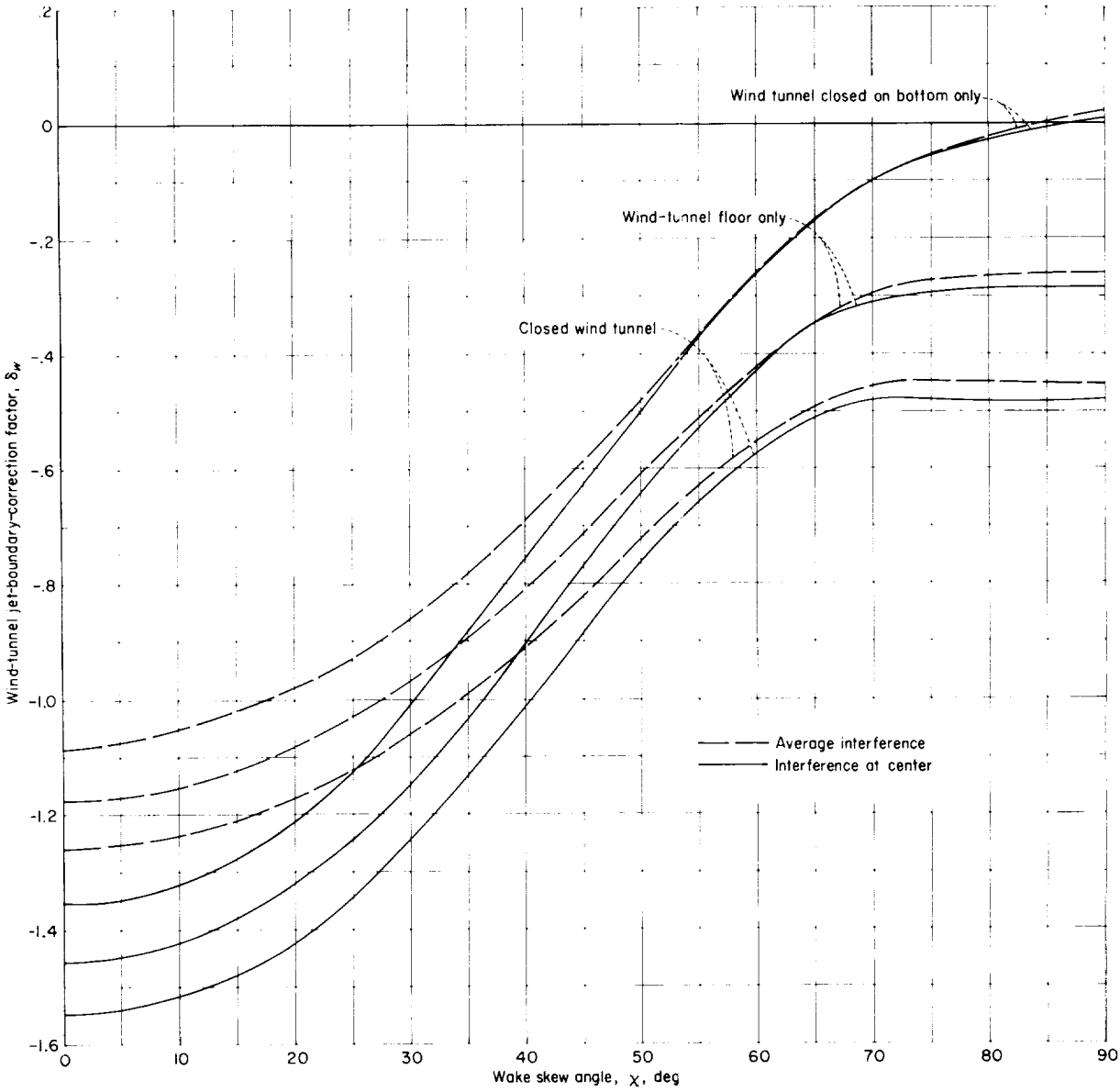

FIGURE 18.—Comparison of average jet-boundary interference with that found at rotor center. $\gamma=2.0$; $\sigma=0.4$.

TANDEM ROTORS

With tandem rotors the wind-tunnel boundaries induce an interference velocity over each rotor which is due only to the presence of the individual rotor in the wind tunnel. In addition, an interference velocity at the front rotor is induced by the tunnel boundaries because of the presence of the rear rotor. Likewise, there is a correction upon the rear rotor because of the presence of the front rotor. For example, when considering equally loaded, nonoverlapped, tandem rotors, the total average interference velocity at the front rotor is the sum (fig. 17) of the average interference over $-1 \leqq \frac{x}{R} \leqq 1$ and the average interference over $-3 \leqq \frac{x}{R} \leqq -1$, whereas the average interference velocity at the rear rotor is the sum of the average interferences over $-1 \leqq \frac{x}{R} \leqq 1$ and

$1 \leqq \frac{x}{R} \leqq 3$. The interference at the rear rotor (fig. 19) is therefore much greater than that for a single rotor, and it reaches a maximum at a skew angle of the order of 55°. The interference at the front rotor is somewhat greater than that for a single rotor; however, it rapidly approaches the single-rotor interference as the skew angle increases.

EFFECT OF DISK LOAD DISTRIBUTION

The entire analysis presented herein has been confined to the case of a uniformly loaded rotor. The additional consideration of nonuniform disk loading would greatly increase the difficulty of obtaining numerical results and therefore has not been attempted.

Some insight into the magnitude of the effect of nonuniform disk loading can, however, be obtained from previous work on wings in the wind tunnel and on rotors hovering in ground effect. Since a uniformly loaded rotor in high-speed flight ($\chi=90°$) is equivalent to an elliptically loaded wing, the magnitude of the effect of changes in load distribution should be essentially the same. It is clear (refs. 11 and 12) that the effect of changing from elliptic to uniform loading is small and that it may be accounted for simply by assuming that the wing has a somewhat shortened span. The same treatment should be sufficient for the rotor as well, provided that χ is near 90°.

Reference 13 treats the case of uniformly and nonuniformly loaded rotors hovering ($\chi=0°$) in ground effect. The calculated results are exactly equivalent to those of the present paper for the case of the wind-tunnel floor only. The height above the ground Z/R in reference 13 is identical to $1/\sigma\gamma$ in the present paper and the *interference* velocities may be obtained by subtracting the induced velocities at infinite height above the ground from those at any given value of Z/R. When treated in this manner, the calculated results of reference 13 appear as shown in figure 20(a), where the interference velocities for both uniform and triangular disk loading are presented as a function of radius.

Figure 20(a) shows that the distribution of the interference velocity over the rotor disk is greatly affected by changes in disk load distribution when $\sigma\gamma$ is greater than 1. Thus, corrections to detailed measurements of rotor-blade pressure-distribution measurements, for example, might be severely affected by the assumption of uniform loading. For simpler measurements, such as the overall forces developed by the rotor, the results can probably be corrected adequately by the use of only the average interference velocity over the entire rotor disk. These average velocities are shown in figure 20(b) where it may be seen that the effect of changes in disk load distribution is small.

APPLICATION OF RESULTS

For a wing, the characteristics in the wind tunnel are identical to those of the same wing operating at a different angle of attack in free air. This interpretation is not adequate in the present case since, in hovering and at very low speeds, the characteristics of the rotor are affected primarily by the change in inflow rather than by the change in effective angle of attack. It is for this reason that the correction factor is defined herein in terms of the induced velocity.

One interpretation of the present results is that the interference velocity represents a change in rate of climb (or sink) between the corresponding wind-tunnel and free-air flight conditions. This interpretation is valid throughout the entire speed range of a rotor. In the limiting case of hovering, it is the only possible interpretation, and considerable care will be required in correlating the results from flight and wind-tunnel tests. At high speeds, however, the concept of a change in rate of climb is identical to the concept of a change in angle of attack. Thus, at high forward speeds, it is permissible to use the correction as a change in angle of attack given by

$$\Delta\alpha=\tan^{-1}\frac{\Delta w}{V} \tag{30}$$

It may be noted that mathematically the wind-tunnel corrections for a wing approach infinity as the velocity approaches zero solely because $\Delta\alpha$ is taken as $\Delta w/V$ rather than $\tan^{-1}\frac{\Delta w}{V}$. This presents no real difficulty in itself since the representation of the wake, which passes directly downstream, is hopelessly inadequate long before the small-angle assumption introduces significant errors.

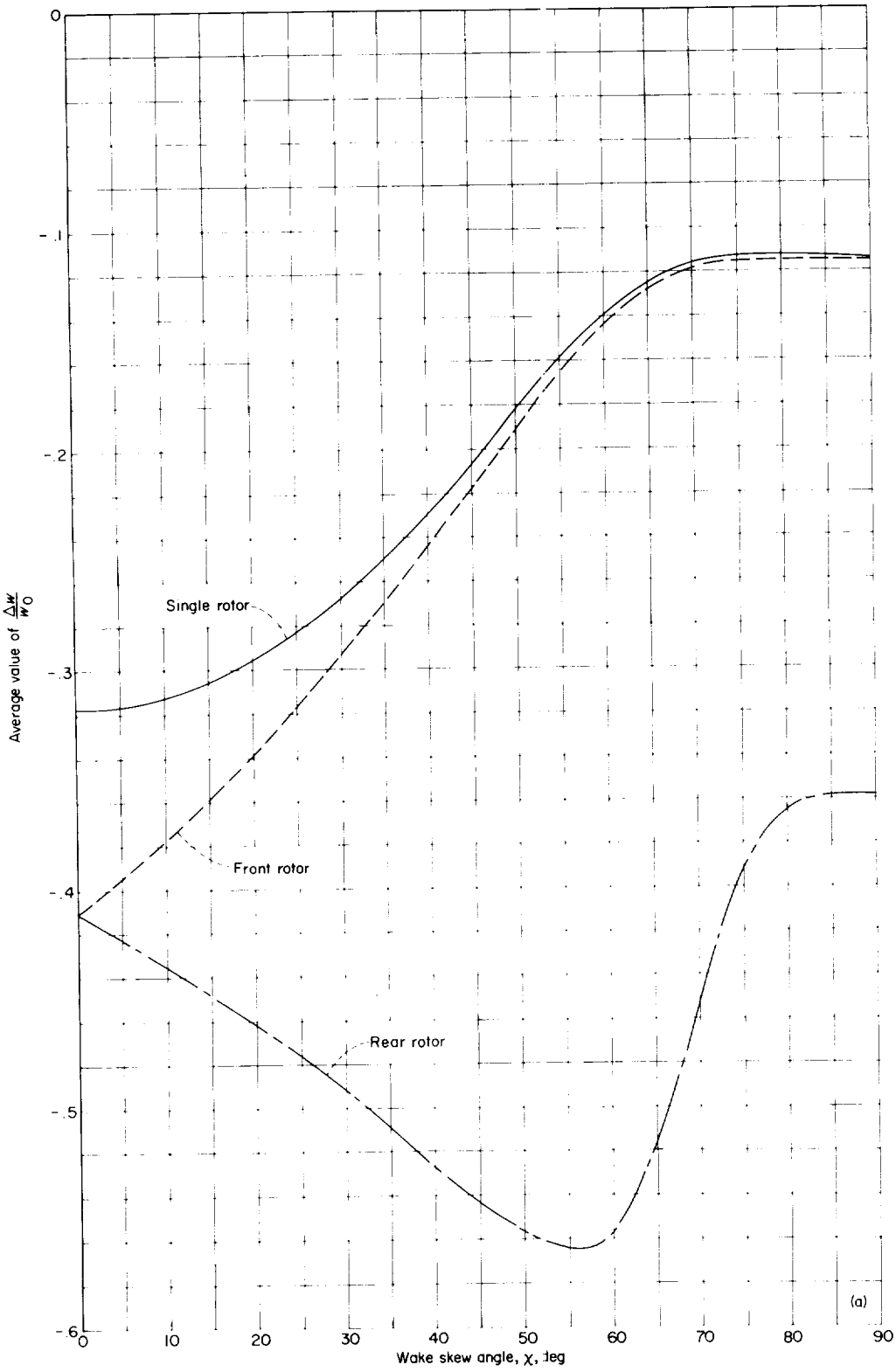

(a) Closed wind tunnel.

FIGURE 19.—Average jet-boundary interference for equally loaded, nonoverlapped, tandem rotors. $\gamma=2.0$; $\sigma=0.4$.

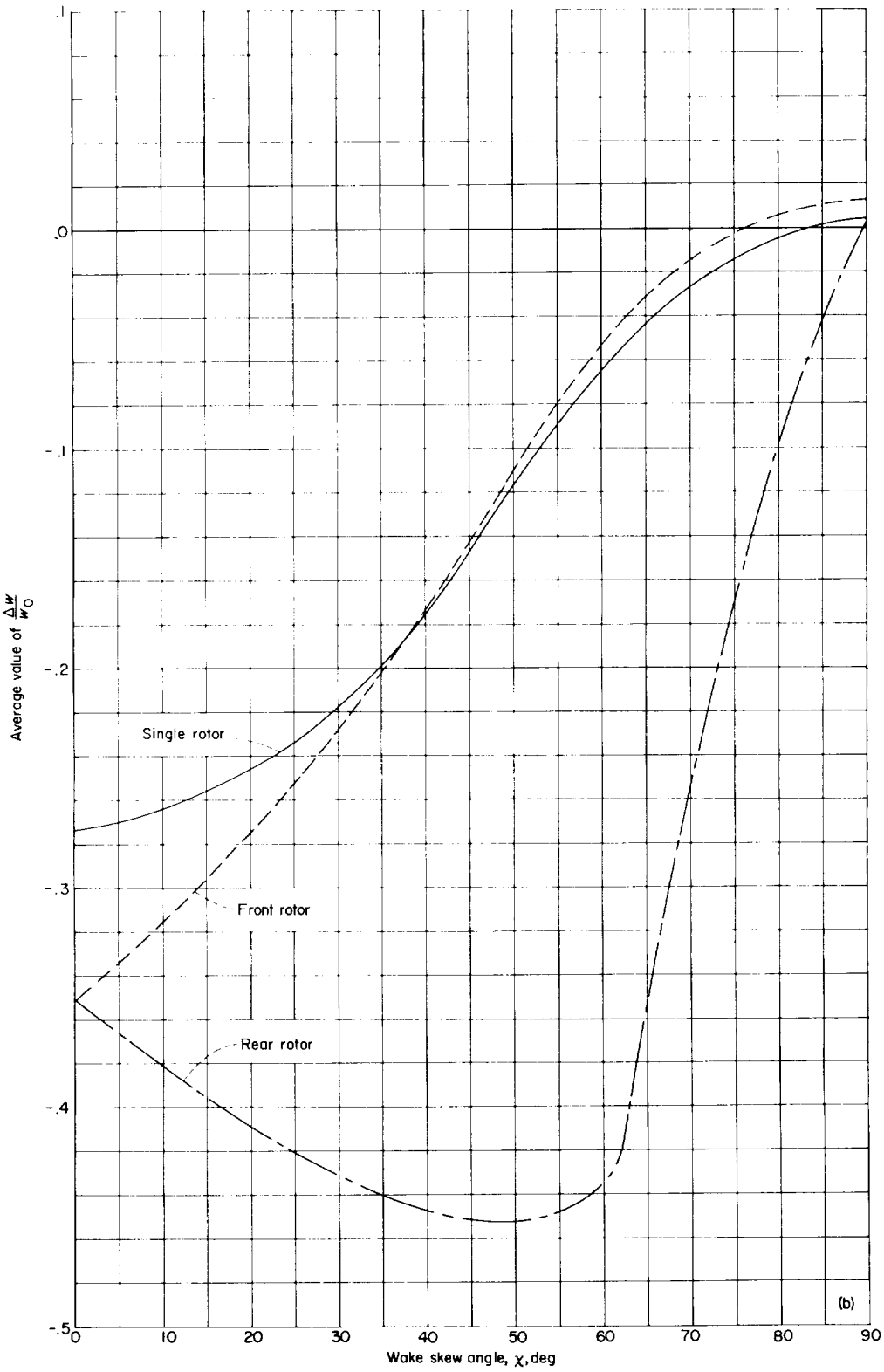

(b) Wind tunnel closed on bottom only.

FIGURE 19.—Continued.

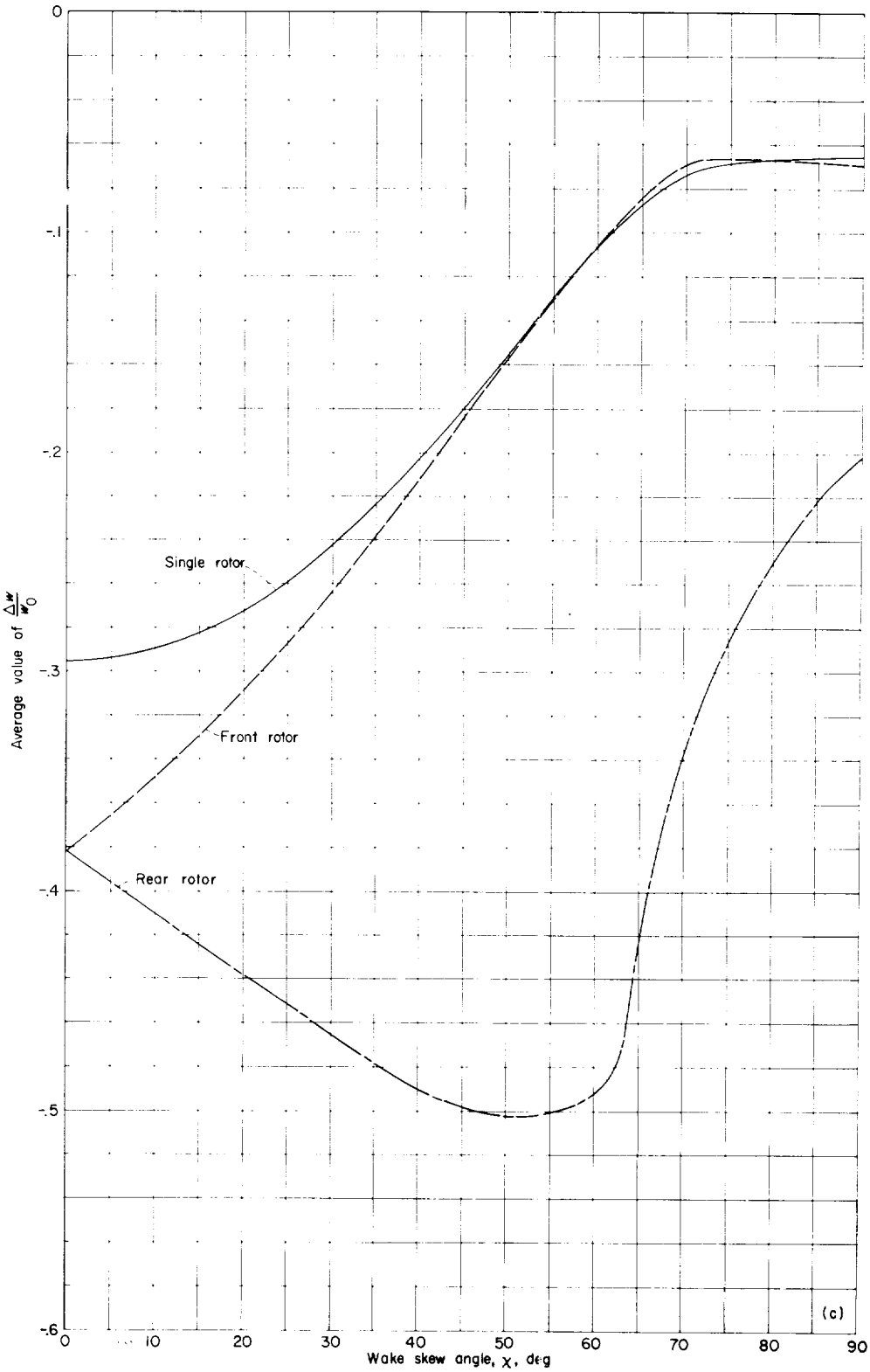

(c) Wind-tunnel floor only.

FIGURE 19.—Concluded.

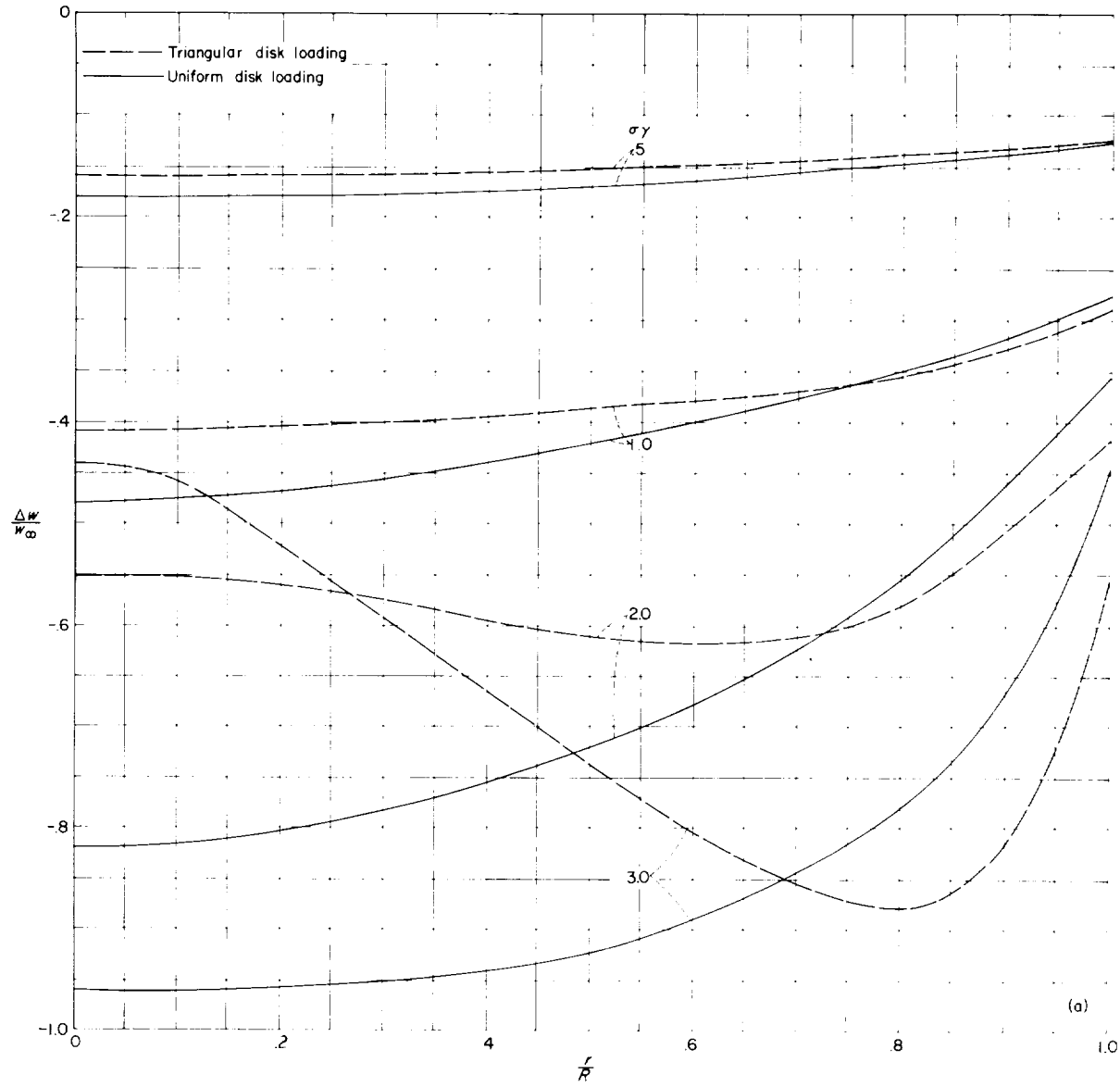

(a) Distribution of interference velocities over rotor disk.

FIGURE 20.—Effect of disk load distribution on interference from wind-tunnel floor only. $\chi = 0°$.

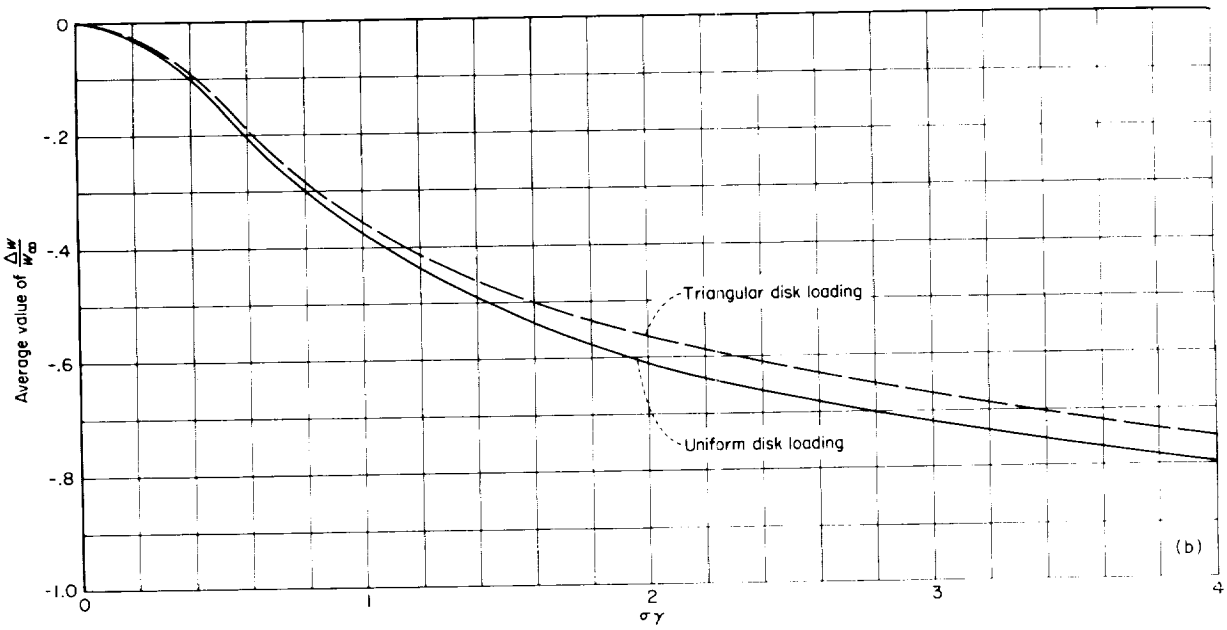

(b) Average interference velocity.

FIGURE 20.—Concluded.

EFFECT OF OFFCENTER POSITIONS OF ROTOR

The calculations presented in this paper have been restricted to the case of a rotor centered in the wind tunnel. It has been shown that for a wing (ref. 12, for example) the correction factors will be altered by locating the wing either above or below the wind-tunnel center line. Similar effects may be expected for a rotor. For the case of $\chi=90°$, these effects are, of course, identical to those already available for wings. For example, the symmetry of the wake in the wind tunnel causes the correction factor to be the same for symmetrical locations above or below the center line. For skew angles other than 90°, the wake of a rotor eventually passes close to the floor regardless of whether it is above or below the wind-tunnel center line; consequently, the correction factors will differ for locations above and below the wind-tunnel center line. Since at very low speeds the tunnel floor alone accounts for the major part of the interference, it would be expected that the interference will be less for locations above the center line (farther from the floor), and greater for locations below the center line (nearer the floor).

APPLICATION TO WINGS

The correspondence between the corrections for wings and rotors, particularly for $\sigma=0$ where a knowledge of the shape of the lifting mechanism is immaterial, leads to several interesting conclusions regarding jet-boundary corrections for wings.

First, note (fig. 8) that the correction factors are altered only slightly by wake skew angles in the range $75°<\chi<90°$. These skew angles correspond to the maximum wake deflections that are attainable with simple wings. The very small effect of these small wake deflections is the reason that it has not been found necessary to account for the actual wake deflection when computing the correction factors for wings.

Second, note that if a larger wake deflection is attained, then there may be considerable change in the jet-boundary correction. Such large deflections are indeed encountered in low-speed wind-tunnel tests of most vertical-take-off-and-landing aircraft. In such cases, it may be preferable to use the present results by finding an effective skew angle based on total lift rather than to attempt to account for the corrections on the basis of the jet-

boundary-induced interference velocities computed for a wing with no wake deflection.

CONCLUSIONS

This study of the jet-boundary corrections for lifting rotors centered in rectangular wind tunnels has provided numerical values of the jet-boundary-correction factor. Study of these numerical values indicates the following conclusions:

1. At high speeds (wake skew angles near 90°), the jet-boundary corrections for a rotor are the same as those for a wing.

2. At very low speeds (low skew angles), the corrections are largely determined by the wind-tunnel floor; in the cases considered there is a large tunnel-induced upwash at the rotor.

3. Increasing the rotor size decreases the jet-boundary-correction factors for wide wind tunnels but has little effect if the ratio of width to height is significantly less than 1.0. The effect of rotor size is greatest at the low skew angles which represent hovering and transition flight.

4. There is no wind-tunnel width-height ratio among the cases considered which results in a zero-correction wind tunnel throughout the entire speed range.

5. The wind-tunnel-induced interference velocity will be highly nonuniform over the rotor disk if the rotor is large with respect to the wind-tunnel width. The nonuniformity along the longitudinal axis causes major increases in the corrections at the rear rotor of tandem helicopters.

6. The wind-tunnel corrections are more appropriately considered as a change in rate of climb rather than a change in angle of attack. Considerable care will be required in the application of these corrections at very low forward speeds.

LANGLEY RESEARCH CENTER,
NATIONAL AERONAUTICS AND SPACE ADMINISTRATION,
LANGLEY FIELD, VA., *January 11, 1960.*

APPENDIX A

CORRECTION FACTOR FOR A WAKE OF VERTICAL DOUBLETS ABOVE A SOLID LOWER BOUNDARY

The jet-boundary-correction factor for a wake of vertical doublets above a solid lower boundary is given by the last three terms of equation (19b) as

$$\delta_w = -\frac{2\gamma}{\pi}\left[-K\left(\frac{x}{H}-\tan\chi,\ \frac{y}{H},\ \frac{z}{H}+1\right)-K\left(\frac{x}{H},\ \frac{y}{H},-\frac{z}{H}-2\right)+K\left(\frac{x}{H}-\tan\chi,\ \frac{y}{H},-\frac{z}{H}-1\right)\right] \tag{A1}$$

where, from equation (17b),

$$K\left(\frac{x}{H},\ \frac{y}{H},\frac{z}{H}\right)=\frac{\left(\frac{x}{H}\right)^2+\left(\frac{y}{H}\right)^2}{\left[\sqrt{\left(\frac{x}{H}\right)^2+\left(\frac{y}{H}\right)^2+\left(\frac{z}{H}\right)^2}+\frac{z}{H}\cos\chi-\frac{x}{H}\sin\chi\right]\left[\left(\frac{x}{H}\right)^2+\left(\frac{y}{H}\right)^2+\left(\frac{z}{H}\right)^2\right]^{3/2}}$$

$$-\left\{\frac{\frac{z}{H}+\cos\chi\sqrt{\left(\frac{x}{H}\right)^2+\left(\frac{y}{H}\right)^2+\left(\frac{z}{H}\right)^2}}{\left[\sqrt{\left(\frac{x}{H}\right)^2+\left(\frac{y}{H}\right)^2+\left(\frac{z}{H}\right)^2}+\frac{z}{H}\cos\chi-\frac{x}{H}\sin\chi\right]\sqrt{\left(\frac{x}{H}\right)^2+\left(\frac{y}{H}\right)^2+\left(\frac{z}{H}\right)^2}}\right\}^2 \tag{A2}$$

Only the center of the rotor is considered herein; therefore, $x=y=z=0$ in equation (A1). Then substituting equation (A2) into equation (A1) gives

$$\delta_w=-\frac{2\gamma}{\pi}\left\{\frac{-\tan^2\chi}{(\sqrt{1+\tan^2\chi}+\cos\chi+\tan\chi\sin\chi)(1+\tan^2\chi)^{3/2}}+\left[\frac{1+\cos\chi\sqrt{1+\tan^2\chi}}{(\sqrt{1+\tan^2\chi}+\cos\chi+\tan\chi\sin\chi)\sqrt{1+\tan^2\chi}}\right]^2-0\right.$$

$$+\left[\frac{-2+2\cos\chi}{(2-2\cos\chi)(2)}\right]^2+\frac{\tan^2\chi}{(\sqrt{1+\tan^2\chi}-\cos\chi+\tan\chi\sin\chi)(1+\tan^2\chi)^{3/2}}$$

$$\left.-\left[\frac{-1+\cos\chi\sqrt{1+\tan^2\chi}}{(\sqrt{1+\tan^2\chi}-\cos\chi+\tan\chi\sin\chi)\sqrt{1+\tan^2\chi}}\right]^2\right\} \tag{A3}$$

Equation (A3) may be considerably simplified by noting the identity $\sqrt{1+\tan^2\chi}=\frac{1}{\cos\chi}$. Thus,

$$\delta_w=-\frac{2\gamma}{\pi}\left[\frac{-\frac{\sin^2\chi}{\cos^2\chi}}{\left(\frac{1+\cos^2\chi+\sin^2\chi}{\cos\chi}\right)\frac{1}{\cos^3\chi}}+\left(\frac{2}{\frac{1+\cos^2\chi+\sin^2\chi}{\cos^2\chi}}\right)^2+\frac{1}{4}+\frac{\frac{\sin^2\chi}{\cos^2\chi}}{\left(\frac{1-\cos^2\chi+\sin^2\chi}{\cos\chi}\right)\frac{1}{\cos^3\chi}}\right] \tag{A4}$$

or

$$\delta_w=-\frac{2\gamma}{\pi}\left(-\frac{1}{2}\sin^2\chi\cos^2\chi+\cos^4\chi+\frac{1}{4}+\frac{1}{2}\cos^2\chi\right) \tag{A5}$$

and, finally,

$$\delta_w=-\frac{2\gamma}{\pi}\left(\frac{3}{2}\cos^4\chi+\frac{1}{4}\right) \tag{A6}$$

APPENDIX B

CORRECTION FACTOR FOR A WAKE OF HORIZONTAL DOUBLETS ABOVE A SOLID LOWER BOUNDARY

The jet-boundary-correction factor for a wake of horizontal doublets above a solid lower boundary is given by the last four terms of equation (27) as

$$\delta_w=-\frac{2\gamma}{\pi}\left[-K\left(\frac{x}{H}-\tan\chi,\frac{y}{H},\frac{z}{H}+1\right)-K\left(\frac{x}{H},\frac{y}{H},-\frac{z}{H}-2\right)\right.$$
$$\left.+K\left(\frac{x}{H}-\tan\chi,\frac{y}{H},-\frac{z}{H}-1\right)+2K\Big|_{\chi=\pi/2}\left(\frac{x}{H}-\tan\chi,\frac{y}{H},\frac{z}{H}+1\right)\right] \quad \text{(B1)}$$

where, from equation (25b),

$$K\left(\frac{x}{H},\frac{y}{H},\frac{z}{H}\right)=-\left\{\frac{\left(\frac{x}{H}\right)\left(\frac{z}{H}\right)}{\left[\sqrt{\left(\frac{x}{H}\right)^2+\left(\frac{y}{H}\right)^2+\left(\frac{z}{H}\right)^2}+\frac{z}{H}\cos\chi-\frac{x}{H}\sin\chi\right]\left[\left(\frac{x}{H}\right)^2+\left(\frac{y}{H}\right)^2+\left(\frac{z}{H}\right)^2\right]^{3/2}}\right.$$
$$\left.+\frac{\left[\frac{x}{H}-\sin\chi\sqrt{\left(\frac{x}{H}\right)^2+\left(\frac{y}{H}\right)^2+\left(\frac{z}{H}\right)^2}\right]\left[\frac{z}{H}+\cos\chi\sqrt{\left(\frac{x}{H}\right)^2+\left(\frac{y}{H}\right)^2+\left(\frac{z}{H}\right)^2}\right]}{\left[\sqrt{\left(\frac{x}{H}\right)^2+\left(\frac{y}{H}\right)^2+\left(\frac{z}{H}\right)^2}+\frac{z}{H}\cos\chi-\frac{x}{H}\sin\chi\right]^2\left[\left(\frac{x}{H}\right)^2+\left(\frac{y}{H}\right)^2+\left(\frac{z}{H}\right)^2\right]}\right\} \quad \text{(B2)}$$

Since only the center of the rotor is considered herein, $x=y=z=0$ in equation (B1). Now substitute equation (B2) into equation (B1) to obtain

$$\delta_w=\frac{2\gamma}{\pi}\left[\frac{\tan\chi}{(\sqrt{1+\tan^2\chi}+\cos\chi+\tan\chi\sin\chi)(1+\tan^2\chi)^{3/2}}+\frac{(\tan\chi+\sin\chi\sqrt{1+\tan^2\chi})(1+\cos\chi\sqrt{1+\tan^2\chi})}{(\sqrt{1+\tan^2\chi}+\cos\chi+\tan\chi\sin\chi)^2(1+\tan^2\chi)}\right.$$
$$+\frac{2\sin\chi(-2+2\cos\chi)}{(2-2\cos\chi)^2(4)}+\frac{\tan\chi}{(\sqrt{1+\tan^2\chi}-\cos\chi+\tan\chi\sin\chi)(1+\tan^2\chi)^{3/2}}$$
$$\left.-\frac{2\tan\chi}{(\sqrt{1+\tan^2\chi}+\tan\chi)(1+\tan^2\chi)^{3/2}}-\frac{2(\tan\chi+\sqrt{1+\tan^2\chi})}{(\sqrt{1+\tan^2\chi}+\tan\chi)^2(1+\tan^2\chi)}\right] \quad \text{(B3)}$$

Simplifying equation (B3) yields

$$\delta_w=\frac{2\gamma}{\pi}\left(\frac{1}{2}\sin\chi\cos^3\chi+\sin\chi\cos^3\chi-\frac{1}{4}\frac{\sin\chi}{1-\cos\chi}+\frac{1}{2}\frac{\cos^3\chi}{\sin\chi}-2\cos^3\chi\right) \quad \text{(B4)}$$

or, noting that $\frac{\sin\chi}{1-\cos\chi}=\frac{1+\cos\chi}{\sin\chi}$, yields

$$\delta_w=\frac{2\gamma}{\pi}\left(\sin\chi\cos^3\chi-\frac{1}{2}\sin^3\chi\cos\chi-\frac{1}{4}\tan\frac{\chi}{2}-2\cos^3\chi\right) \quad \text{(B5)}$$

REFERENCES

1. Theodorsen, Theodore: The Theory of Wind-Tunnel Wall Interference. NACA Rep. 410, 1931.
2. Theodorsen, Theodore, and Silverstein, Abe: Experimental Verification of the Theory of Wind-Tunnel Boundary Interference. NACA Rep. 478, 1934.
3. Rosenhead, L.: Interference Due to Walls of a Wind-Tunnel. Proc. Roy. Soc. (London), ser. A, vol. 142, Oct. 2, 1933, pp. 308–320.
4. Heyson, Harry H.: Preliminary Results From Flow-Field Measurements Around Single and Tandem Rotors in the Langley Full-Scale Tunnel. NACA TN 3242, 1954.
5. Heyson, Harry H., and Katzoff, S.: Induced Velocities Near a Lifting Rotor With Nonuniform Disk Loading. NACA Rep. 1319, 1957. (Supersedes NACA TN 3690 by Heyson and Katzoff and TN 3691 by Heyson.)
6. Peirce, B. O.: A Short Table of Integrals. Third rev. ed., Ginn and Co., 1929, p. 24.
7. Prandtl, L., and Tietjens, O. G. (L. Rosenhead, trans.): Fundamentals of Hydro- and Aeromechanics. Dover Pub., Inc., 1957, pp. 200–207.
8. Prandtl, L., and Tietjens, O. G. (J. P. Den Hartog, trans.): Applied Hydro- and Aeromechanics. Dover Pub., Inc., 1957, pp. 222–224.
9. Heyson, Harry H.: Ground Effect for Lifting Rotors in Forward Flight. NASA TN D-234, 1960.
10. Katzoff, S., Gardner, Clifford S., Diesendruck, Leo, and Eisenstadt, Bertram J.: Linear Theory of Boundary Effects in Open Wind Tunnels With Finite Jet Lengths. NACA Rep. 976, 1950. (Supersedes NACA TN 1826.)
11. Glauert, H.: The Interference on the Characteristics of an Aerofoil in a Wind Tunnel of Rectangular Section. R. & M. No. 1459, British A.R.C., 1932.
12. Silverstein, Abe, and White, James A.: Wind-Tunnel Interference With Particular Reference to Off-Center Positions of the Wing and to the Downwash at the Tail. NACA Rep. 547, 1936.
13. Heyson, Harry H.: An Evaluation of Linearized Vortex Theory as Applied to Single and Multiple Rotors Hovering In and Out of Ground Effect. NASA TN D–43, 1959.

TABLE I

JET-BOUNDARY-CORRECTION FACTORS FOR CLOSED RECTANGULAR WIND TUNNELS

(a) $\gamma = 2.0$

Skew angle, χ, deg	Correction factor for σ of —										
	0	0.1	0.2	0.3	0.4	0.5	0.6	0.7	0.8	0.9	0.95
0	−2. 341	−2. 268	−2. 073	−1. 817	−1. 551	−1. 306	−1. 096	−0. 921	−0. 778	−0. 663	−0. 614
14. 04	−2. 126	−2. 070	−1. 921	−1. 713	−1. 486	−1. 273	−1. 072	−. 907	−. 770	−. 658	−. 611
26. 56	−1. 664	−1. 638	−1. 569	−1. 456	−1. 314	−1. 158	−1. 006	−. 867	−. 746	−. 644	−. 600
45. 00	−. 941	−. 937	−. 929	−. 912	−. 886	−. 846	−. 792	−. 728	−. 659	−. 591	−. 559
63. 43	−. 581	−. 576	−. 566	−. 549	−. 528	−. 506	−. 483	−. 463	−. 444	−. 428	−. 420
75. 97	−. 543	−. 536	−. 524	−. 506	−. 481	−. 454	−. 427	−. 400	−. 375	−. 352	−. 344
84. 29	−. 546	−. 537	−. 525	−. 507	−. 483	−. 456	−. 430	−. 402	−. 378	−. 356	−. 348
90. 00	−. 545	−. 534	−. 523	−. 504	−. 480	−. 454	−. 427	−. 401	−. 377	−. 355	−. 348

(b) $\gamma = 1.5$

Skew angle, χ, deg	Correction factor for σ of —										
	0	0.1	0.2	0.3	0.4	0.5	0.6	0.7	0.8	0.9	0.95
0	−1. 780	−1. 729	−1. 662	−1. 536	−1. 390	−1. 242	−1. 100	−0. 972	−0. 859	−0. 763	−0. 720
14. 04	−1. 619	−1. 596	−1. 530	−1. 432	−1. 314	−1. 187	−1. 063	−. 947	−. 843	−. 752	−. 712
26. 56	−1. 274	−1. 264	−1. 235	−1. 187	−1. 123	−1. 046	−. 963	−. 878	−. 796	−. 721	[illegible]
45. 00	−. 739	−. 737	−. 734	−. 729	−. 721	−. 710	−. 693	−. 672	−. 645	−. 614	−. 599
63. 43	−. 482	−. 479	−. 475	−. 469	−. 462	−. 454	−. 445	−. 438	−. 431	−. 427	−. 426
75. 97	−. 467	−. 462	−. 458	−. 452	−. 444	−. 435	−. 426	−. 417	−. 409	−. 404	−. 402
84. 29	−. 475	−. 469	−. 465	−. 459	−. 451	−. 443	−. 434	−. 426	−. 420	−. 416	−. 415
90. 00	−. 476	−. 467	−. 463	−. 457	−. 450	−. 441	−. 433	−. 425	−. 419	−. 416	−. 415

TABLE I.—Concluded

JET-BOUNDARY-CORRECTION FACTORS FOR CLOSED RECTANGULAR WIND TUNNELS

(c) $\gamma = 1.0$

Skew angle, χ, deg	Correction factor for σ of—						
	0	0.2	0.4	0.6	0.8	0.9	0.95
0	−1.288	−1.253	−1.160	−1.039	−0.916	−0.860	−0.833
14.04	−1.184	−1.157	−1.087	−.991	−.888	−.838	−.815
26.56	−.961	−.949	−.919	−.872	−.812	−.781	−.765
45.00	.625	−.624	−.626	−.628	−.629	−.629	−.629
63.43	−.494	−.493	−.496	−.501	−.511	−.519	−.523
75.97	−.520	−.519	−.522	−.530	−.544	−.554	−.560
84.29	.543	−.539	−.544	−.553	−.570	−.582	−.589
90.00	−.545	−.533	−.543	−.552	−.569	−.582	−.589

(d) $\gamma = 0.5$

Skew angle, χ, deg	Correction factor for σ of						
	0	0.2	0.4	0.6	0.8	0.9	0.95
0	−1.016	−1.004	−0.988	−0.969	−0.946	−0.933	−0.926
14.04	−.975	−.958	−.951	−.938	−.922	−.912	−.907
26.56	−.892	−.877	−.876	−.874	−.870	−.868	−.867
45.00	−.807	−.792	−.797	−.806	−.819	−.828	−.832
63.43	−.876	−.856	−.866	−.884	−.912	−.930	−.941
75.97	−.986	−.960	−.974	−.999	−1.037	−1.063	−1.078
84.29	−1.037	1.002	−1.021	−1.049	−1.092	1.121	−1.137
90.00	−1.046	−1.018	−1.034	−1.062	−1.106	−1.135	−1.153

TABLE II

JET-BOUNDARY-CORRECTION FACTORS FOR RECTANGULAR WIND TUNNELS CLOSED ON BOTTOM ONLY

(a) $\gamma = 2.0$

Skew angle, χ, deg	Correction factor for σ of										
	0	0.1	0.2	0.3	0.4	0.5	0.6	0.7	0.8	0.9	0.95
0	−2.103	−2.038	−1.849	−1.605	−1.354	−1.126	−0.932	−0.773	−0.643	−0.538	−0.493
14.04	−1.882	−1.832	−1.692	−1.497	−1.285	−1.088	−.905	−.755	−.631	−.530	−.486
26.56	−1.404	−1.385	−1.323	−1.225	−1.099	−.960	−.826	−.703	−.597	−.506	−.465
45.00	−.633	−.634	−.635	−.634	−.627	−.607	−.573	−.528	−.475	−.419	−.392
63.43	−.181	−.181	−.181	−.181	.182	−.182	−.183	−.184	−.184	−.182	.180
75.97	−.062	−.061	−.060	−.057	−.053	−.048	−.043	−.036	−.028	−.019	−.014
84.29	−.022	−.021	−.019	.016	−.012	−.006	.001	.010	.020	.031	.037
90.00	0	0	.003	.006	.011	.017	.025	.035	.046	.058	.065

(b) $\gamma = 1.5$

Skew angle, χ, deg	Correction factor for σ of										
	0	0.1	0.2	0.3	0.4	0.5	0.6	0.7	0.8	0.9	0.95
0	−1.549	−1.504	−1.435	−1.313	−0.173	−1.030	−0.894	−0.771	−0.662	−0.568	−0.525
14.04	−1.382	−1.360	−1.298	−1.204	−1.091	−.970	−.852	−.741	−.641	−.551	−.511
26.56	−1.021	−1.013	−.987	−.943	−.884	−.814	−.736	−.656	−.579	−.506	
45.00	−.435	−.436	−.436	−.436	−.434	−.429	−.419	−.403	−.380	−.351	−.335
63.43	−.079	−.079	−.078	−.078	−.077	−.075	−.073	−.070	.066	−.062	−.060
75.97	.033	.033	.034	.037	.040	.044	.050	.057	.065	.075	.080
84.29	.083	.083	.084	.087	.090	.096	.102	.110	.119	.131	.137
90.00	.112	.111	.113	.116	.120	.125	.132	.140	.150	.161	.168

TABLE II.—Concluded

JET-BOUNDARY-CORRECTION FACTORS FOR RECTANGULAR WIND TUNNELS CLOSED ON BOTTOM ONLY

(c) $\gamma=1.0$

Skew angle, χ, deg	Correction factor for σ of						
	0	0.2	0.4	0.6	0.8	0.9	0.95
0	−0. 960	−0. 927	−0. 829	−0. 702	−0. 569	−0. 505	−0. 474
14. 04	−. 847	−. 822	−. 748	−. 645	−. 531	−. 474	−. 446
26. 56	−. 601	−. 591	−. 557	−. 502	−. 430	−. 390	−. 370
45. 00	−. 195	−. 196	−. 193	−. 185	−. 170	−. 159	−. 153
63. 43	. 072	. 070	. 075	. 085	. 099	. 109	. 115
75. 97	. 174	. 170	. 178	. 190	. 210	. 223	. 231
84. 29	. 224	. 217	. 224	. 237	. 258	. 272	. 281
90. 00	. 250	. 241	. 228	. 261	. 282	. 296	. 304

(d) $\gamma=0.5$

Skew angle, χ, deg	Correction factor for σ of						
	0	0.2	0.4	0.6	0.8	0.9	0.95
0	−0. 265	−0. 267	−0. 259	−0. 236	−0. 208	−0. 192	−0. 184
14. 04	−. 201	−. 210	−. 199	−. 182	−. 159	−. 147	−. 140
26. 56	−. 061	−. 072	−. 066	−. 056	−. 042	−. 034	−. 030
45. 00	. 192	. 176	. 181	. 189	. 201	. 209	. 213
63. 43	. 395	. 374	. 383	. 400	. 425	. 442	. 451
75. 97	. 482	. 451	. 464	. 487	. 521	. 545	. 559
84. 29	. 514	. 473	. 487	. 511	. 550	. 577	. 592
90. 00	. 524	. 475	. 489	. 514	. 553	. 580	. 596

TABLE III

JET-BOUNDARY-CORRECTION FACTORS δ_w FOR WIND-TUNNEL FLOOR ONLY

(a) $\gamma = 2.0$

Skew angle, χ, deg	Correction factor for σ of —										
	0	0.1	0.2	0.3	0.4	0.5	0.6	0.7	0.8	0.9	0.95
0	−2. 228	−2. 157	−1. 968	−1. 718	−1. 459	−1. 223	−1. 021	−0. 853	−0. 717	−0. 607	−0. 560
14. 04	−2. 010	−1. 957	−1. 813	−1. 612	−1. 392	−1. 187	−. 995	−. 838	−. 707	−. 600	−. 555
26. 56	−1. 541	−1. 519	−1. 453	−1. 348	−1. 214	−1. 067	−. 923	−. 793	−. 679	−. 582	−. 539
45. 00	−. 796	−. 795	−. 791	−. 783	−. 766	−. 736	−. 692	−. 637	−. 576	−. 514	−. 484
63. 43	−. 395	−. 393	−. 387	−. 379	−. 369	−. 358	−. 348	−. 338	−. 328	−. 318	−. 313
75. 97	−. 325	−. 323	−. 315	−. 305	−. 291	−. 276	−. 259	−. 242	−. 226	−. 210	−. 203
84. 29	−. 318	−. 316	−. 309	−. 299	−. 285	−. 269	−. 252	−. 235	−. 218	−. 202	−. 194
90. 00	−. 318	−. 316	−. 309	−. 298	−. 285	−. 269	−. 252	−. 235	−. 218	−. 202	−. 194

(b) $\gamma = 1.5$

Skew angle, χ, deg	Correction factor for σ of—										
	0	0.1	0.2	0.3	0.4	0.5	0.6	0.7	0.8	0.9	0.95
0	−1. 671	−1. 641	−1. 555	−1. 431	1. 288	−1. 142	−1. 003	−0. 877	−0. 765	−0. 669	−0. 626
14. 04	−1. 508	−1. 485	−1. 421	−1. 325	1. 209	−1. 085	−. 963	−. 849	−. 746	−. 656	−. 615
26. 56	−1. 156	−1. 146	−1. 118	−1. 073	−1. 011	−. 937	−. 856	−. 773	−. 693	−. 618	
45. 00	−. 597	−. 596	−. 595	−. 593	−. 587	−. 578	−. 564	−. 545	−. 519	−. 489	−. 472
63. 43	−. 296	−. 295	−. 293	−. 289	−. 284	−. 279	−. 273	−. 267	−. 261	−. 255	−. 252
75. 97	−. 244	−. 243	−. 240	−. 235	−. 229	−. 221	−. 213	−. 204	−. 194	−. 185	−. 180
84. 29	−. 239	−. 238	−. 235	−. 230	−. 224	−. 216	−. 208	−. 199	−. 189	−. 179	−. 175
90. 00	−. 239	−. 238	−. 235	−. 230	−. 224	−. 216	−. 208	−. 199	−. 189	−. 179	−. 175

TABLE III.—Concluded

JET-BOUNDARY-CORRECTION FACTORS δ_w FOR WIND-TUNNEL FLOOR ONLY

(c) $\gamma = 1.0$

Skew angle, χ, deg	Correction factor for σ of —						
	0	0.2	0.4	0.6	0.8	0.9	0.95
0	—1.114	—1.078	—0.984	—0.859	—0.730	—0.669	—0.639
14.04	—1.005	—.978	—.907	—.806	—.696	—.642	—.616
26.56	—.770	—.759	—.727	—.674	—.607	—.571	—.552
45.00	—.398	—.397	—.396	—.391	—.383	—.376	—.372
63.43	—.197	—.196	—.194	—.190	—.185	—.182	—.181
75.97	—.163	—.161	—.158	—.153	—.146	—.142	—.140
84.29	—.159	—.158	—.155	—.149	—.142	—.139	—.137
90.00	—.159	—.158	—.155	—.149	—.142	—.138	—.136

(d) $\gamma = 0.5$

Skew angle, χ, deg	Correction factor for σ of —						
	0	0.2	0.4	0.6	0.8	0.9	0.95
0	—0.557	—0.553	—0.539	—0.513	—0.492	—0.477	—0.469
14.04	—.503	—.499	—.489	—.473	—.453	—.442	—.435
26.56	—.385	—.384	—.380	—.373	—.363	—.358	—.354
45.00	—.199	—.199	—.199	—.193	—.198	—.197	—.197
63.43	—.099	—.099	—.098	—.093	—.097	—.096	—.096
75.97	—.081	—.081	—.081	—.080	—.079	—.078	—.078
84.29	—.080	—.080	—.079	—.073	—.077	—.077	—.076
90.00	—.080	—.080	—.079	—.073	—.077	—.077	—.076

TABLE IV

JET-BOUNDARY-CORRECTION FACTORS FOR A WAKE OF HORIZONTAL DOUBLETS IN A RECTANGULAR WIND TUNNEL

(a) Closed wind tunnel

Skew angle, χ, deg	Correction factor for γ of			
	0.5	1.0	1.5	2.0
0	−1.012	−1.329	−1.811	−2.380
14.04	−.959	−1.088	−1.400	−1.877
26.56	−.841	−.811	−1.005	−1.316
45.00	−.645	−.477	−.541	−.676
63.43	−.443	−.274	−.283	−.341
75.97	−.253	−.141	−.142	−.172
84.29	−.108	−.056	−.057	−.069
90.00	0	0	0	0

(b) Wind tunnel closed on bottom only

Skew angle, χ, deg	Correction factor for γ of			
	0.5	1.0	1.5	2.0
0	−0.307	−1.114	−1.836	−2.636
14.04	−.142	−.864	−1.496	−2.211
26.56	.018	−.589	−1.112	−1.656
45.00	.165	−.264	−.650	−.986
63.43	.161	−.129	−.403	−.683
75.97	.109	−.111	−.351	−.589
84.29	.045	−.121	−.338	−.548
90.00	−.008	−.136	−.335	−.526

(c) Wind-tunnel floor only

Skew angle, χ, deg	Correction factor for γ of			
	0.5	1.0	1.5	2.0
0	−0.637	−1.273	−1.910	−2.546
14.04	−.523	−1.046	−1.568	−2.091
26.56	−.384	−.769	−1.153	−1.537
45.00	−.218	−.437	−.655	−.873
63.43	−.131	−.262	−.394	−.525
75.97	−.102	−.204	−.306	−.408
84.29	−.088	−.176	−.264	−.352
90.00	−.080	−.159	−.239	−.318

TABLE V

COMPARISON OF JET-BOUNDARY-CORRECTION FACTORS δ_w FOR A SMALL ROTOR ($\chi=90°$) AND FOR A SMALL WING (REF. 3)

(a) Closed wind tunnel

γ	δ_w for	
	Wing	Rotor
0.5	−1.048	−1.046
1.0	−.548	−.545
2.0	−.548	−.545

(b) Wind tunnel closed on bottom only

γ	δ_w for—	
	Wing	Rotor
0.5	0.524	0.524
1.0	.250	.250
2.0	0	0

TABLE VI

COMPARISON OF JET-BOUNDARY-CORRECTION FACTORS δ_w FOR A ROTOR ($\chi=90°$) AND FOR A WING (REF. 11) IN CLOSED WIND TUNNELS

(a) $\gamma=2.0$

σ	δ_w for—		
	Wing		Rotor
	Elliptic loading	Uniform loading	
0	−0.548	−0.548	−0.545
.2	−.516	−.508	−.523
.4	−.450	−.424	−.480
.5	−.416	−.374	−.454
.6	−.388	−.370	−.427
.7	−.370	−.362	−.401
.8	−.366	−.370	−.377
.9	−.378	−.438	−.355

(b) $\gamma=1.0$

σ	δ_w for—		
	Wing		Rotor
	Elliptic loading	Uniform loading	
0	−0.548	−0.543	−0.545
.2	−.550	−.552	−.533
.4	−.562	−.563	−.543
.6	−.590	−.610	−.552
.8	−.654	−.724	−.569
.9	−.718	−.870	−.582

U.S. GOVERNMENT PRINTING OFFICE: 1961